Insulin Receptor Loss Impairs Mammary Tumorigenesis in Mice

Lauren Podmore[1,‡], Yekaterina Poloz[2,3,‡], Catherine Iorio[2], Samar Mouaaz[2], Kevin Nixon[2], Petr Smirnov[1], Brianna McDonnell[1], Sonya Lam[2], Bowen Zhang[1], Pirashaanthy Tharmapalan[1], Foram Vyas[1], Marguerite Ennis[4], Ryan Dowling[2,3], Vuk Stambolic[1,2,*].

Affiliations:

1: Department of Medical Biophysics, University of Toronto, Princess Margaret Cancer Research Tower, Toronto, Ontario, Canada M5G 1L7.

2: Princess Margaret Cancer Centre, University Health Network, Princess Margaret Cancer Research Tower, Toronto, Ontario, Canada M5G 1L7.

3: Current address: F. Hoffmann-La Roche Ltd, Mississauga, Ontario, Canada L5N 5M8.

4: Applied Statistician, Markham, Ontario, Canada, L3R 6H9.

‡These authors contributed equally to this work

*Corresponding Author:

Vuk Stambolic

Princess Margaret Cancer Centre, University Health Network, Princess Margaret Cancer Research Tower, Room 13-313, 101 College Street, Toronto, Ontario, Canada M5G 1L7.

E-mail: vuks@uhnresearch.ca

Summary

Breast cancer (BC) prognosis and outcome are adversely affected by increased body weight, obesity, and the obesity-associated type 2 diabetes. Hyperinsulinemia, common in the obese state, has been associated with higher risk of death and recurrence in BC. Up to 80% of breast cancers overexpress the insulin receptor (INSR), which correlates with worse prognosis. To directly probe the role of insulin signaling in mammary tumorigenesis, we generated the MMTV-driven polyoma middle T (PyMT) and ErbB2/Her2 BC mouse models, respectively, with coordinate mammary epithelium-restricted deletion of the *INSR*. In both models, deletion of either one or both copies of the *INSR* in the mammary gland led to a marked delay in tumor onset and burden, including in mice fed to mimic conditions of human obesity. Phenotypic characterization and longitudinal monitoring of mouse tumours, and *ex vivo* analysis of mammary cells from the generated mouse models revealed that tumor initiation, rather than progression and metastasis, were impacted by *INSR* deletion. Mechanistically, INSR deficiency in non-transformed mammary epithelial cells led to diminished bioenergetic fitness. The similarity of phenotypes elicited by the deletion of one or both copies of *INSR* indicates that there is a dose-dependent threshold for the contribution of INSR to mammary tumorigenesis.

Running Title: Investigating the function of INSR in mammary tumourigenesis

Keywords: insulin receptor, BC, mammary tumourigenesis, genetically engineered mouse model, bioenergetic fitness

Introduction

Obesity is a global epidemic, with over 650 million obese and further 1.3 billion overweight individuals worldwide (World Health Organization, 2021). 5% and 10% of all US cancer cases in men and women, respectively, can be attributed to excess body weight (Islami et al., 2019). Estimates from two decades ago attribute obesity to approximately 14% of the deaths from cancer in men and 20% of the deaths from cancer in women (Calle et al., 2003). In breast cancer (BC), for each 5 kg/m^2 increase in body mass index (BMI), risk of BC–specific mortality increased by 17-29% (D. S. M. Chan et al., 2014). Importantly, sustained weight loss is associated with lower BC risk in women 50 or older, indicating that the effects of excess body weight on BC are reversible (Teras et al., 2020).

Elevated levels of circulating insulin, or hyperinsulinemia, a condition that parallels obesity (Lazarus et al., 1998), has an adverse effect on a patient's prognosis and risk in operable BC (Dankner et al., 2012; Goodwin et al., 2002; Gunter et al., 2009; Kabat et al., 2009). Further, there is a positive association between cancer incidence and insulin dose in persons with type 2 diabetes treated by either human insulin or synthetic insulin analogues (Hemkens et al., 2009). Adverse effects of insulin and benefits of insulin deprivation in a rat model of mammary tumorigenesis were observed half a century ago (Heuson et al., 1972; Heuson & Legros, 1972). More recently, excess insulin was found to accelerate mammary tumorigenesis in mouse models, whereas insulin reducing agents counter it (Fierz et al., 2010; Novosyadlyy et al., 2010). Importantly, in a pancreatic cancer mouse model, hyperinsulinemia accelerated tumorigenesis, whereas genetically-mediated insulin reduction decelerated tumorigenesis, separating the impact of elevated insulin on tumor growth from the accompanying hyperglycemia seen in metabolic disease (A. M. Y. Zhang et al., 2019).

Clinical studies have revealed that 48-92% of breast tumours express insulin's preferred cell surface receptor, the insulin receptor (INSR) (Dowling et al., 2015; Law et al., 2008; Mulligan et al., 2007), while others have shown that breast cancers overexpress INSR protein relative to normal breast tissue (Frasca et al., 1999; Papa et al., 1990). INSR is a heterotetrameric receptor tyrosine kinase typically found in muscle, fat, and liver cells, where it propagates metabolic signalling (White & Kahn, 2021). There is evidence from a number of mammalian cell lines on the regulation of INSR transcription, including involvement of hormonal and environmental factors (reviewed in (Payankaulam et al., 2019)). While metabolic tissues express the INSR-B isoform, cancers predominantly express INSR-A, the foetal INSR isoform capable of mediating mitogenic signaling (Vella et al., 2018). Engagement of insulin with INSR results in activation of the PI3K-Akt signaling pathway, an anabolic cascade central to the control of glucose transport across cell membranes, glycolysis, lipolysis, mRNA translation and cell growth, survival, and migration (Hopkins et al., 2020). Hyperactivation of PI3K-Akt signaling is found in many human tumours, largely owing to the activating mutations in PIK3CA, the catalytic subunit of PI3K, and loss of function of the tumor suppressor PTEN, which counters PI3K signaling via its lipid phosphatase activity against phosphatidylinositol second messengers produced by PI3K (Yuan & Cantley, 2008). Moreover, insulin stimulation of INSR-A also activates the pro-mitogenic Ras-MAPK signaling cascade (Saltiel, 2021).

Preclinical studies in mouse models of type 2 diabetes mellitus (T2DM) have shown that hyperinsulinemia promoted breast cancer growth and metastasis through activation of INSR and its receptor tyrosine kinase family member insulin-like growth factor receptor 1 (IGF1R), specifically through hyperactivation of the PI3K-Akt and Ras-MAPK pathways (Ferguson et al., 2012; Novosyadlyy et al., 2010). IGF1R shares structural homology, ligands, and downstream signaling effectors with INSR, and is similarly overexpressed in human breast cancer (Pandini et al., 1999). Moreover, INSR and IGF1R have been found to form hybrid receptors with unique affinities for binding the ligands insulin, IGF1, and IGF2 (Pandini et al., 2002), and activation of these hybrid receptors may promote tumourigenesis (Vigneri et al., 2016). Finally, it is thought that increased insulin levels found in hyperinsulinemic individuals might be capable of overcoming IGF1R's lower affinity for binding insulin and activating this pro-mitogenic receptor (Novosyadlyy et al., 2010).

Despite their distinct biological impacts in normal tissues, the individual contributions of INSR and IGF1R to insulin-mediated mammary tumourigenesis remain poorly understood (Nagao et al., 2021). Owing to the fact that the detection method for the activated state of INSR and IGF1R is based on the recognition of a shared amino acid sequence within their respective tyrosine kinase domains, their activation cannot be uncoupled *in situ* (Slaaby, 2015). Nevertheless, clinical studies have found that increased INSR expression and activation of INSR and/or IGF1R, but not increased IGF1R expression alone, associated with enhanced tumourigenesis and worse survival outcomes in human breast cancer (Gallagher et al., 2020; Law et al., 2008). Given that the mitogenic INSR-A is the predominantly expressed INSR isoform in cancer, these data indicate that INSR alone may be capable of conferring the pro-tumourigenic effects of hyperinsulinemia.

To better understand how INSR individually contributes to the function of insulin signaling in mammary tumorigenesis, we genetically disrupted the *INSR* gene in mammary tissues of two mouse models of BC, driven by the polyoma middle T (*PyMT*) and *HER2/ErbB2/neu* oncogenes, respectively. Our data demonstrate that *INSR* loss impairs mammary tumor initiation, but not progression or metastasis, and suggest the existence of a dose-dependent threshold for the contribution of INSR to mammary tumorigenesis. We further show that *INSR* loss in non-transformed murine mammary epithelial cell line COMMA1D lowers mRNA expression of many components of the mitochondrial respiratory chain and impairs their energetic capacity, implicating bioenergetic fitness as a mechanism by which INSR mediates breast tumour initiation, likely facilitated through non-canonical INSR signaling.

Results

INSR is broadly expressed in human cancer and regulates PI3K-Akt and Ras-MAPK signaling pathways in mammary epithelial cells

To expand on the previous analyses detecting prevalent INSR protein expression in BC (**Figure 1A**) (Chang et al., 2016; Dowling et al., 2015; Frasca et al., 1999; Mulligan et al., 2007; Papa et al., 1990), we analyzed gene expression by RNAseq of *INSR* from The Cancer Genome Pan-Cancer Atlas (TCGA PANCAN) dataset (Weinstein et al., 2013). Levels of *INSR* mRNA expression in BC were increased relative to more than half of other obesity-linked cancers (**Figure 1B**), and to three-quarters of all cancer types (**Supplementary Figure 1A**). While *INSR* mRNA expression varied amongst BC molecular subtypes in the BC subset of TCGA PANCAN (TCGA Breast) (**Figure 1C**) (Koboldt et al., 2012), it appeared equal amongst BC molecular subtypes in samples from the Molecular Taxonomy of Breast Cancer International Consortium (METABRIC) dataset (**Figure 1D**) (Curtis et al., 2012), reflecting variability between patient datasets.

Further indicative of variability were survival comparisons within these two datasets, as high *INSR* expression did not correlate with overall survival (OS) in TCGA Breast patients (**Supplementary Figure 2A**), whereas high *INSR* associated with worse OS in METABRIC patients (**Supplementary Figure 2B**). This pattern of discrepancy between datasets repeated within the Luminal A subtype (**Supplementary Figures 2C-D**) and Luminal B subtype (**Supplementary Figures 2E-F**), although high *INSR* expression associated with better OS in METABRIC Luminal A subtype samples. Of note, high *INSR* expression did associate with worse OS in the HER2 subtype in both

TCGA Breast and METABRIC datasets (**Supplementary Figures 3A-B**). *INSR* expression had no impact on OS outcomes in Basal subtype (**Supplementary Figures 3C-D**) or Normal-Like subtype (**Supplementary Figures 3E-F**) in either dataset. Curiously, high *INSR* expression did associate with better disease-specific survival (DSS) in TCGA breast cancer samples (**Supplementary Figure 4A**), likely reflective of its high proportion of Luminal B subtype samples, in which high *INSR* also associated with better DSS (**Supplementary Figure 4C**). Moreover, high *INSR* expression associated with a larger disease-free interval (DFI) in the TCGA Breast dataset (**Supplementary Figure 5A**), as well as within the Luminal A and Basal subtypes (**Supplementary Figures 5B**, **E**) of these patients.

INSR mRNA expression was also analyzed in cell lines from the Cancer Cell Line Encyclopedia dataset (Barretina et al., 2012). Relative to all cancer lines, as classified by primary site, BC-derived cell lines rank within the top third by *INSR* mRNA expression (**Supplementary Figure 1B**). *INSR* mRNA expression appeared equal among BC cell lines grouped by molecular subtype (**Figure 1E**), as classified by the Cancer Dependency Map Project at Broad Institute (DepMap.org) (Tsherniak et al., 2017). We analyzed *INSR* isoform mRNA expression by RT-qPCR within a select group of cell lines (**Figure 1F**). All cell lines expressed both *INSR* isoforms, but at differing ratios of *INSR-A*:*INSR-B*, respectively; 40:60 in untransformed mammary epithelial MCF-10A cells, 80:20 in breast cancer cell lines MCF-7 and MDA-MB-231, and 60:40 in kidney cancer-derived HEK-293T cells. On protein level, INSR abundance in MCF-7 and MDA-MB-231 was comparable to that of HEK-293T cells, whereas MCF-10A cells displayed relatively lower INSR expression (**Figure 1G**).

To probe whether expressed INSR is responsive to ligand stimulation in mammary epithelia, MCF-10A cells were starved of serum and growth factors and short-term stimulated with insulin. Judging by stimulation-dependent increase in phosphorylation of INSR, AKT, S6 and ERK, insulin led to activation of both the metabolic and mitogenic arms of INSR signaling, reflective of their INSR-A expression (**Figure 1H**). The effect was INSR-dependent, as S6 and ERK phosphorylation in response to insulin stimulation were attenuated by *INSR* knockdown (**Supplementary Figure 6**).

INSR contributes to mammary tumourigenesis in BC model mice

To directly investigate the role of INSR in mammary tumorigenesis *in vivo*, we generated two genetically engineered mouse models with conditional mammary tissue-specific deletion of *INSR,* concomitant with expression of either oncogenic *HER2* (*MMTV-neu-IRES-Cre*, or *NIC*) or the polyoma middle-T (*PyMT*) antigen (*MMTV-rtTA;TetO-PyMT-IRES-Cre*, or *MTB:MIC*), respectively (**Figures 2A**-**B**) (Gunther et al., 2002; Rao et al., 2014; Ursini-Siegel et al., 2008). In *NIC INSR* animals, *HER2* expression and *INSR* deletion are coordinated by the activity of the MMTV promoter, whereas in the *MTB:MIC INSR* model, MMTV promoter-dependent *PyMT* expression/*INSR* deletion are induced through treatment with doxycycline in the drinking water. Predicted allele and oncogene representation was monitored by genomic PCR (**Figures 2C**-**E**). Mammary tumours that developed in both models expressed INSR protein (**Figures 2F**-**G**), while, consistent with their genotype, INSR was undetectable in mammary tumours of 10-week old *MTB:MIC INSR* and *NIC INSR* mice homozygous for the conditional *INSR* allele (F/F) compared to those wild-type for *INSR* (+/+). Metabolic

INSR expressing tissues, such as liver, muscle, and fat, displayed unchanged INSR levels (**Figure 2F**), and maintained normal glucose homeostasis (**Figure 2H**), validating specificity of the mammary tissue *INSR* deficiency.

Following validation of oncogene expression and coordinate *INSR* deficiency in pilot transgenic experiments, cohorts were established of female mice carrying the respective oncogenes which were wild-type for *INSR*(+/+), *INSR* heterozygous-null (F/+), or *INSR* homozygous-null (F/F) , and mice in both groups were monitored weekly for presence of tumours by palpation. In *NIC* mice, loss of *INSR* delayed tumour appearance in a deleted *INSR* allele-dependent manner, with *NIC INSR* (+/+) tumours emerging at 133 days, *NIC INSR* (F/+) at 158 days and *NIC INSR* (F/F) at 172 days (**Figure 3A**). Consistently, all *NIC INSR* (+/+) animals developed tumours within 172 days, while it took 294 days for all *NIC INSR* (F/F) mice to show signs of disease. In *MTB:MIC INSR* mice, where PyMT-Cre expression was induced at 10-12 weeks of age through doxycycline in the drinking water, PyMT induction rapidly led to appearance of tumours (~8 days post induction) in all three *INSR* genotypes. While all *MTB:MIC INSR* (+/+) mice presented with tumours within 30 days post induction, at the 8-week monitoring endpoint, set due to the severity of the tumour phenotypes found in *MTB:MIC INSR* (+/+) mice, a considerable proportion of *MTB:MIC INSR* (F/F) and *MTB:MIC INSR* (F/+) mice either did not show signs of disease or had delayed tumour onset (**Figure 3B**). Reduction in tumours followed the number of deleted *INSR* copies, with >20% of *MTB:MIC INSR* (F/+) and >40% of *MTB:MIC INSR* (F/F) mice remaining tumour-free at endpoint.

Delayed tumour onset due to *INSR* deletion was also reflected in the time it took mice to reach the humane endpoint, as determined by overall tumour volume, with *NIC INSR* (F/+) and *NIC INSR* (F/F) mice displaying substantial survival benefit compared to their *NIC INSR* (+/+) counterparts (**Figure 3C**). Moreover, deletion of a single copy or both copies of *INSR* also led to remarkably lowered tumour burden in both models, reflected in the number and total weight of mammary tumours at endpoint. *NIC INSR* (+/+) mice developed up to 15 tumours per mouse, whereas *NIC INSR* (F/+) and *NIC INSR* (F/F) mice averaged around 5 lesions per mouse (**Figure 3D**). Similarly, *MTB:MIC INSR* (+/+) mice had >20 tumours per mouse on average, while both *MTB:MIC INSR* (F/+) and *MTB:MIC INSR (F/F)* mice featured ~5 tumors per mouse at endpoint (**Figure 3E**). Reduced tumour count paralleled lower total tumour weights in *INSR*-deficient *MTB:MIC* mice at endpoint (**Figure 3F**).

Loss of *INSR* reduces mammary tumourigenesis in the obese state

To investigate INSR contribution to mammary tumorigenesis in the obese/hyperinsulinemic state, we placed our *MTB:MIC INSR* mice on a high fat content diet, which, in several mouse strains, including *FVB*, causes metabolic disease (Hu et al., 2018). Compared to mice fed a regular-fat diet (RFD; 17% of daily caloric intake from fat), *FVB/NJ* mice fed a high-fat diet (HFD; 45% of daily caloric intake from fat) for 10 weeks fared poorer in a glucose tolerance test (**Supplementary Figure 7A**), despite insignificant weight gain (**Supplementary Figure 7B**). To induce metabolic disease before tumour initiation, a cohort of *MTB:MIC INSR* mice aged 10 weeks were fed either RFD or HFD for additional 10 weeks, prior to induction of *PyMT* expression/*INSR* deletion with doxycycline, and throughout to endpoint.

Fasting blood glucose levels of *MTB:MIC INSR* mice on HFD increased relative to their RFD counterparts, without reaching statistical significance (**Supplementary Figure 7C**). In this mouse model, exposure to HFD did not lead to increased tumorigenicity, judged by the number and weight of mammary tumors (**Figures 3G**-**H**) as well as the time to tumour onset (**Supplementary Figures 7D**-**F**). Nevertheless, under conditions of caloric excess caused by HFD, deletion of one or both copies of *INSR* resulted in reduction of tumour burden (**Figures 3G**-**H**) and delayed onset (**Figure 3I**) in *MTB:MIC INSR* mice, comparable to that seen in the same mice on a normal diet.

INSR deletion does not impact mammary tumour progression or metastasis

While *MTB:MIC INSR* tumours that escaped the impact of *INSR* loss appeared to, on average, weigh less at endpoint (**Figure 4A**), this reduction was not statistically significant and the extent of disease in this model precluded further comparisons of the impact on tumour progression. Nevertheless, slower tumour development in *NIC INSR* mice afforded a more detailed assessment of the impact of INSR on tumour progression. Diameters/volumes of individual tumors and total tumors per mouse in the three *NIC INSR* genotypes were recorded weekly by caliper measurements. Plotting of the growth of individual tumours and cumulative tumour volume per mouse over time suggested non-linear, exponential growth (**Figures 4B**, **E**). Data were log10 transformed (**Figures 4C**, **F**) and fit of the linear mixed models to both the original and log-transformed data were compared (see Methods). Comparison of percent growth per day values for each tumour calculated from the models (>10 per genotype) showed that there was no difference in progression of individual tumors between the genotypes (**Figure 4D**).

To estimate the impact of *INSR* deletion on metastatic spread, number of lung metastases in both models were compared. In both the moderately metastatic *NIC INSR* and the highly metastatic *MIC:MTB INSR* models, deletion of either single or both copies of *INSR* had no effect on metastatic dissemination (**Figures 4G**, **H**). This lack of effect on metastasis persisted in *MTB:MIC INSR* mice fed HFD (**Figure 4I**).

***INSR* loss impairs mammary tumour initiation**

Despite *INSR*-deficiency delaying tumour onset and reducing endpoint tumour burden, the lack of effect of *INSR* loss on progression and metastasis points to the possibility that the functional contribution of INSR to BC occurs at an earlier time point in tumorigenesis. To directly probe the impact of *INSR* deletion on tumor initiation, mouse mammary epithelial cells from *MIC:MTB INSR* (+/+) and *MIC:MTB INSR* (F/F) not treated with Dox, and thus equivalent, were isolated and grown in Matrigel (**Figure 4J**). Tumour sphere formation was induced by continuous treatment with Dox (0.1 µg/mL) for 11 days and the appearance of tumour spheres were quantified. PyMT induction led to abundant tumor sphere formation by *MIC:MTB INSR* (+/+) mammary cells compared to those from parental *FVB* mice, or Dox-untreated controls (**Figure 4K**). By contrast, *INSR* deletion led to significantly lower tumor sphere development, supporting the notion that *INSR* loss reduces tumour initiation.

INSR-deficient tumours maintain canonical pathway signaling activity

To gain better insight into the lack of impact of INSR signaling on progressing mammary tumours *in vivo*, immunoblotting of tumor lysates and immunohistochemistry of tumor tissue sections collected at endpoint were performed in both models (**Figure 5**; **Supplementary Figures 8-11**). Immunoblotting for signaling pathway activity in tumour lysates failed to yield consistent output (**Supplementary Figure 8**), thought to be affected by the presence of stromal and other non-tumour tissue content in tumour isolates.

To quantitatively assess the tumour-specific biology of collected tissues, immunohistochemically stained sections of endpoint tumours were digitized (**Supplementary Figure 9**) and analyzed (**Figure 5**; **Supplementary Figures 10-11**). In agreement with their genotype, QuPath analysis(Bankhead et al., 2017) revealed that tumour-specific cells of *NIC INSR* (F/F) and *MTB:MIC INSR* (F/F) mice had greatly diminished INSR staining relative to their *INSR* (+/+) counterparts, with the tumour cells of mice heterozygous for *INSR* loss (F/+) exhibiting intermediary but non-statistically significant reduction (**Figures 5A-C**; **Supplementary Figures 10A-C**). Consistent with no impact on tumour progression, Ki67 staining, a marker of active proliferation in tumour cells, remained comparable at endpoint across *INSR* genotypes of both models (**Figures 5D-F**; **Supplementary Figures 10D-F**). This was paralleled by analogous lack of significant change in levels of phosphorylated AKT (**Figures 5G-I**; **Supplementary Figures 10G-I**) and phosphorylated ERK (**Figures 5J-L**; **Supplementary Figures 10J-L**). Potential compensatory changes in IGF1R levels in response to genetic *INSR* disruption were also tested by IHC to reveal no difference between genotypes (**Figures**

5M-**O**; **Supplementary Figures 10M**-**O**). Of note, *NIC INSR* (F/+) tumours displayed statistically significant reduction of both p-AKT (**Figure 5G**; **Supplementary Figure 10G**) and IGF1R (**Figure 5M**; **Supplementary Figure 10M**), an observation that was not accompanied by decreased proliferative signal (**Figure 5D**; **Supplementary Figure 10D**), nor with further reduction tracking with INSR levels in *NIC INSR* (F/F) tumours (**Figure 5A**; **Supplementary Figure 10A**). Judging by immunohistochemistry for the pan-immune marker CD45, there was no difference between *INSR* genotypes in the general immune infiltrates of *MTB:MIC INSR* tumours collected at 10 weeks post-doxycycline induction (**Supplementary Figure 11**).

INSR loss in murine mammary epithelial cells impairs their bioenergetic potential

To gain further insight into the mechanism(s) behind reduced tumour initiation upon *INSR* deletion, we generated two independent *INSR*-deficient luminal COMMA1D mouse mammary cell lines (COMMA1D INSR (-/-)) and two accompanying wild-type controls (COMMA1D INSR (+/+)) using CRISPR/Cas9 (**Supplementary Figure 12A**) (Ran et al., 2013). COMMA1D cells are immortalized but not transformed mammary epithelial cells isolated from *Balb/C* mice in mid-pregnancy and have been used to study oncogenic mammary transformation (Danielson et al., 1984; Werner et al., 2022). *INSR* deletion in COMMA1D cells did not affect net activation of the PI3K-Akt (**Supplementary Figures 12B**, **C**) and Ras-MAPK (**Supplementary Figures 12B**, **D**) signaling pathway components in response to insulin stimulation. This is likely due to the presence of IGF1R, as evidenced by a reduced but not depleted phospho-INSR/IGF1R signal in *INSR*-deficient cells (**Supplementary Figures 12B**, **E**).

COMMA1D INSR cells were further characterized using RNAseq. Based on GSEA, mRNA expression of genes associated with DNA replication, cell cycle regulation and mRNA translation/protein synthesis were affected by *INSR* deletion (**Supplementary Figures 13A**). Notably, we also observed INSR-dependent differential expression of a number of genes involved in mitochondrial respiratory electron transport (**Figure 6A**; **Supplementary Figures 13B**-**D**). More specifically, expression of many genes encoding components of respiratory complexes I-IV and complex V (ATP synthase) were lowered in *INSR*-deficient cells compared to their wild-type counterparts (**Supplementary Figure 13D**). Differential mRNA expression was corroborated by RT-qPCR of the select components of each respiratory complex (**Figure 6B**). To further validate these observations, equivalent analysis was performed in the independent GSE206565 RNAseq dataset (Nagao et al., 2023), in which mouse preadipocytes lacking both *INSR* and *IGF1R* (double knock-out, DKO) were reconstituted with either wild-type INSR (IR), a kinase-dead INSR mutant (KD), a truncated INSR lacking the C-terminus (CT), or a truncated INSR lacking the majority of the intracellular domain (juxtamembrane-domain only, JMO). Similar to the observations in our COMMA1D cells, dual *INSR*/*IGF1R* loss in these cells resulted in reduced expression of mitochondrial respiratory chain complex components, particularly in complexes I and IV (**Supplementary Figure 14**). Markedly, downregulation of subunits of these respiratory chain complex components in DKO cells was rescued by reconstitution of the kinase-dead INSR mutant, implicating non-canonical/ligand-and-tyrosine-kinase-independent (LYK-I) INSR signaling in mediating this effect.

We tested whether the deletion of *INSR* in COMMA1D cells resulted in alterations in cellular mitochondrial content. qPCR-DNA analysis of mitochondrial genome-encoded *COX2* gene levels relative to that of nuclear encoded b-globin indicated no differences in mitochondrial content between the *INSR*-deficient and -proficient cells (**Figure 6C**). We next investigated whether *INSR* deletion-dependent changes in mRNA abundance of respiratory chain components affect cellular bioenergetics by performing respirometry analysis (**Figures 6D**; **Supplementary Figure 15**). Monitoring of oxygen consumption rate (OCR) revealed diminished mitochondrial respiration in COMMA1D INSR (-/-) cells relative to their wild-type counterparts (**Supplementary Figure 15A**), evidenced by reduced basal and maximal respiration rates and ATP generated by oxidative phosphorylation (J-ATP ox) (**Figure 6D**; **Supplementary Figure 15C-D**). Parallel measurements of extracellular acidification rates (ECAR) (**Supplementary Figure 15B**) revealed reduced maximal glycolysis and ATP generated by glycolysis (J-ATP glyc) in *INSR* knockout cells compared to controls (**Figure 6D; Supplementary Figure 15C**, **E**). Together, *INSR* loss led to a major reduction of total bioenergetic capacity of COMMA1D cells (**Figure 6D**, **E**).

To further explore the biological significance of the bioenergetic impairment of *INSR*-deficient cells, glucose was replaced by galactose as the carbohydrate source in the growth media, forcing cells to rely on mitochondrial oxidative phosphorylation for ATP production (Crabtree, 1928; Rodríguez-Enríquez et al., 2001). Monitored over 3 days, COMMA1D INSR (-/-) cells failed to proliferate in galactose-containing media (**Figure 6F**), further corroborating gene expression (**Figure 6A**; **Supplementary Figure 13**) and respirometry findings **(Figure 6D**, **E**; **Supplementary Figure 15**).

Discussion

Human epidemiological and observational studies have defined a strong correlation between excess body weight and incidence and burden of many cancers, including BC. Obesity is a key driver in cardiovascular, musculoskeletal and kidney diseases, as well as a causal factor in the development of T2D (Blüher, 2019). The rapidly rising global prevalence of obesity makes it one of the greatest threats to human health in the 21st century. There are a number of systemic and molecular mechanisms implicated in mediating the harmful effects of obesity on human health, including the development of cancers (Heymsfield & Wadden, 2017). Coupled with broad expression of INSR in human cancers (**Figure 1B**; **Supplementary Figure 1A**), hyperinsulinemia, which correlates with worse BC outcomes (Bruning' et al., 1992; Cowey & Hardy, 2006; Goodwin et al., 2002), is one of the strongest obesity corollaries thought to contribute to cancer burden (reviewed in (Poloz & Stambolic, 2015)). The relationship between obesity, hyperinsulinemia, T2D, menopausal status and BC is complex (Giovannucci et al., 2010; Rose et al., 2007). While increased adiposity in postmenopausal women associates with an increase in BC risk, obesity and T2DM appear to have either no effect or even some protective effect in premenopausal women (Boyle et al., 2012; Lu et al., 2022; Schoemaker et al., 2018).

Using two well-defined genetically engineered mouse models of BC driven by the *PyMT* and *HER2* oncogenes, respectively, we directly probed the importance of the INSR to the development of mammary tumours by its coordinate genetic deletion in tumour tissue. Transcriptional profiling classifies PyMT mammary tumors with the human BC luminal B subtype (Pfefferle et al., 2013), whereas mammary tumours in the HER2 transgene model recapitulate many of the features of HER2-positive human BCs

(Simond & Muller, 2020). Control tumours from both models express INSR (**Figures 2F**, **G**), a feature found in >80% of human BC (Law et al., 2008; Mulligan et al., 2007).

In both models, deletion of a single or both *INSR* copies dramatically attenuated tumor onset, leading to reduced tumor burden at endpoint (**Figures 3A**-**F**). Comparable outcome was also reached in the PyMT model under conditions mimicking human obesity leading to hyperglycemia and hyperinsulinemia (**Figures 3G**-**H**). Longitudinal monitoring of individual tumours in the HER2 model revealed that once tumours appeared, *INSR* deficiency had no impact on progression or metastasis (**Figures 4A**-**I**), indicating that INSR likely participates in the tumour initiation phases. Indeed, when tumor spheres were initiated by PyMT *ex vivo*, *INSR* deletion significantly impaired their formation (**Figures 4J**-**K**), further corroborating the importance of INSR at the earliest stages of mammary tumorigenesis.

Mechanistically, mammary tumours driven by PyMT result from association-dependent activation of RTK-proximal effectors of mitogenic PI3K-Akt and Ras-MAPK signaling pathways (Attalla et al., 2021; Schaffhausen & Roberts, 2009) and the same pathways are also activated by superphysiological transgenesis of HER2 (Simond & Muller, 2020). From the tumour analysis at endpoint, *INSR* loss did not affect measures of proliferation, nor the PI3K-Akt and Ras-MAPK signaling throughput, highly representative of a tumour's stage of progression rather than *INSR* deficiency (**Figure 5**; **Supplementary Figure 10**). Complementary studies explored the effects of hyperinsulinemia without obesity on PyMT-driven mouse xenograft growth and found increased insulin-dependent acceleration of the development and progression of tumours (Novosyadlyy et al., 2010), whereas the same conditions augmented tumor development and metastasis of HER2-driven xenografts (Ferguson et al., 2013), accompanied by hyperactivation of Akt signaling in both models. Moreover, shRNA-mediated interference with *INSR* in BC cells in culture led to reduced proliferation and Akt signaling (J. Y. Chan et al., 2016; H. Zhang et al., 2010). Thus, while hyperinsulinemia can accelerate mammary tumour progression and metastasis in the context of PyMT and HER2 transgenesis in xenografts and *INSR* deletion can reduce *in vitro* BC cell line growth, presumed diminution of insulin signaling via reduction of INSR levels in mouse mammary gland tumours does not translate to effects on proliferation nor PI3K-Akt/Ras-MAPK pathway control at later stages of tumorigenesis. The differences between models might be a reflection of a developed insulin/INSR dependence of cultured and xenografted cells while grown *in vitro* and subcutaneously, or distinct tumor heterogeneity in the absence or reduced INSR since inception in the mouse genetically engineered models.

There is evidence that IGF1R and INSR can compensate for each other under conditions of pharmacological intervention or deficiency (Buck et al., 2010; H. Zhang et al., 2010), as well as during mouse embryonic development (Louvi et al., 1997). In our *MTB:MIC INSR* mouse models, levels of IGF1R remained unchanged following *INSR* loss (**Figures 5N-O**; **Supplementary Figures 10N-O**), suggesting lack of possible compensatory function of IGF1R in maintaining tumour proliferation and Erk/Akt signaling when *INSR* is reduced/deleted in PyMT-driven models. However, in *NIC INSR* mice, heterozygous *INSR* loss resulted in significantly reduced IGF1R expression (**Figure 5M**; **Supplementary Figure 10M**) and Akt signaling (**Figure 5G**; **Supplementary Figure 10G**), an effect not observed with homozygous *INSR* loss.

Given that INSR and IGF1R can also form hybrid receptors (Pandini et al., 2002), AKT signaling in endpoint HER2-driven tumours may be dependent on INSR under normal conditions, but this dependency shifts to hybrid receptors or IGF1R holo-receptors under conditions of reduced INSR or complete INSR deficiency, respectively. Regardless, high proliferation rates and Erk/Akt activity-associated phosphorylation upon *INSR* loss were paralleled by the unchanged progression indicators in *INSR*-deficient tumours, with both likely originating from the *PyMT* and *HER2* transgenes. Thus, *INSR* deletion impacts the early PyMT- and HER2-driven steps towards mammary epithelial transformation and initiation of primary tumours, but not the later phases of progression and metastasis.

Bioenergetic plasticity of cancer cells has long been recognized as one of neoplastic hallmarks (reviewed in (Martínez-Reyes & Chandel, 2021)). While proliferating cancer cell's carbon and energy hunger that accompany new biomass production, and reliance on aerobic glycolysis for energy production (the Warburg effect) (Warburg, 1925; Warburg et al., 1927) have been well studied, less is known about the energetic landscape of pre-cancerous cells during tumour initiation. Our mRNA expression analyses in *INSR*-deficient non-transformed mammary epithelial cells indicates that *INSR* loss leads to reduced expression of many subunits of the mitochondrial respiratory chain (MCR) complexes (**Figure 6A**; **Supplementary Figure 13**), an observation validated by analysis of the data from a complementary study in mouse preadipocytes (**Supplementary Figure 14**). Further analyses of the INSR-deficient COMMA1D cells revealed *INSR* loss-dependent breakdown in bioenergetic capacity (**Figure 6E**), through diminished ATP production via both OXPHOS and glycolysis (**Figures 6C**, **E**). Indeed, when challenged to grow in galactose as a carbohydrate source, which necessitates the use of OXPHOS for energy production, *INSR*-deficient cells failed to thrive (**Figure 6J**). The same cells upregulated mRNA expression of genes belonging to GO terms defining carbohydrate starvation and transport, as well as amino acid starvation, consistent with their bioenergetic deficiency (**Supplementary Figures 13B**-**C**). Remarkably, reduced MCR complex expression seen in mouse preadipocytes lacking both *INSR* and *IGF1R* could be reconstituted by re-expression of a kinase-dead INSR mutant, implicating ligand-and-tyrosine-kinase independent (i.e., non-canonical) INSR signaling mechanism(s) in mediating the metabolic effects. Taken together, these findings highlight INSR-upheld bioenergetic fitness as a major feature of non-transformed mammary epithelial cells and implicate INSR as an anabolic enabler of neoplastic transformation.

Several lines of evidence suggest that insulin/INSR contribution to tumorigenesis might be particularly prominent in cells/tissues sensitized to insulin action by acquisition of mutations impacting the PI3K-Akt and Ras-MAPK signaling pathways (reviewed in (Hopkins et al., 2020)). In our model systems, interference with INSR did not alter progression or metastasis of tumours caused by major drivers of these pathways, PyMT and HER2. Nevertheless, our work has revealed a parallel, likely kinase activity-independent mechanism of INSR-mediated tumour initiation. The comparable reduction in tumour burden by deletion of a single or both copies of *INSR* in our models indicates that there is a threshold for the contribution of INSR to tumour initiation. Further work aimed at reconciling the distinct mechanistic paths of INSR function in tumorigenesis will inform prevention and therapeutic strategies aimed at cancers featuring INSR expression and/or hyperinsulinemia.

Limitations of Study

Our work reveals a previously unrecognized INSR function in mammary tumour initiation and tumorigenesis but presents with certain limitations. Tumor initiation is one of the least explored aspects of tumorigenesis. Paucity of what can be defined as cancer initiating cell(s) limits the experimental approaches that can be applied towards understanding of the molecular mechanisms, an area that can be advanced through precision genetics and single cell analysis of early lesions. We employed two mammary tumour models that recapitulate features of the majority of human BC, but not the triple-negative subtype (10-15% of all BC). Existing triple-negative BC models require conditional deletion of 2 tumour suppressor genes, often BRCA1 and p53 (Liu et al., 2007), which combined with coordinate tissue specific Cre-recombinase expression and INSR deletion, renders the desired genotype in female mice scarce, and any subsequent study currently prohibitively resource- and time-intensive.

While previous observational and animal/cell model work firmly considered insulin/INSR as an “axis”, we found that INSR might be impacting early tumorigenesis acting independently of its kinase activity, and possibly distinct from insulin. This concept needs further testing, through retrospective and prospective observational studies of early human breast metaplastic and neoplastic lesions, including ductal carcinoma *in situ*, from normal and hyperinsulinemic individuals. The existence of an INSR threshold for contribution to cancer requires further probing of the relevance of the insulin/INSR relationship in tumorigenesis, via genetic manipulation of epithelial INSR levels in healthy and tumour models, with parallel reduction or increase in systemic insulin levels (A. M. Y. Zhang et al., 2019). Moreover, precision genetic animal model approaches aimed at uncoupling kinase activity-dependent and -independent INSR functions will further advance the underlying mechanistic details. Finally, recognition of the newly discovered INSR-upheld bioenergetic fitness in mammary epithelial cells, previously seen in metabolic insulin-target cells and tissues (Cheng et al., 2010), as a potential rate limiting feature of neoplastic transformation, requires consideration when designing lifestyle and therapeutic interventions aimed at improving metabolic health as a cancer prevention measure.

Acknowledgements

We would like to thank the staff in the Animal Research Center at the University Health Network (UHN) for help with animal husbandry, UHN's Applied Molecular Profiling Laboratory for assistance with immunohistochemistry and Soumili Sarkar for help with image acquisition. We are indebted to Drs. David Papadopoli and Ivan Topisirovic for their help with bioenergetic analyses. This work was supported by the Canadian Institutes of Health Research Project Grant (162296) and the Canadian Cancer Society Grant (i2I16-2 grant #704786) to V.S. L.P. is a recipient of The Princess Margaret Hospital Foundation Graduate Fellowships in Cancer Research. Y. P was a recipient of the Canadian BC Foundation postdoctoral fellowship and R. D. of the Banting Postdoctoral Fellowship from the Government of Canada.

Author Contributions

Experiments were designed by Y.P., L.P. and V.S. and performed by Y.P., L.P., and C.I. S.M and S.L. helped with animal husbandry. Data, gene expression and statistical analyses was performed by L.P, M.E., P.S., and K.N. B.Z. and B.M. participated in data acquisition. R.D, F.V. and P.T. provided conceptual and technical input. L.P., Y.P. and V.S. wrote the manuscript. All authors discussed the results and commented on the manuscript.

Declaration of Interests

The authors have no conflicts of interests to declare.

Figure Titles and Legends

Figure 1: *INSR expression in human breast cancer.*

(**A**)Table summarizing INSR expression data from previous clinical studies. (**B**) Boxplot of *INSR* mRNA expression in obesity-linked cancer types from the TCGA PANCAN dataset (Weinstein et al., 2013) in UCSC Xena Functional Genomics Explorer (Goldman et al., 2020). Breast cancer (BRCA) is highlighted in bold; see Supplementary Table 1 for other cancer type abbreviations. (**C**) Boxplot of *INSR* mRNA expression by molecular subtype from the Breast Invasive Carcinoma (TCGA, PanCancer Atlas; "TCGA Breast") (Koboldt et al., 2012) dataset in cBioPortal (Cerami et al., 2012; Gao et al., 2013). (**D**) Boxplot of *INSR* mRNA expression by molecular subtype from the Breast Cancer (METABRIC, Nature 2012 & Nat Commun 2016; "METABRIC") (Curtis et al., 2012; Pereira et al., 2016) dataset in cBioPortal. (**E**) Scatterplot of *INSR* mRNA expression in BC cell lines, grouped by molecular subtype, from the Cancer Cell Line Encyclopedia (Broad, 2019; "CCLE") (Ghandi et al., 2019) dataset in cBioPortal. (**F**) Bar graph showing RT-qPCR analysis of relative mRNA expression of *INSR-A* and *INSR-B* isoforms in HEK-293T, MCF-10A, MCF-7 and MDA-MB-231 cell lines. (**G**) Western blot analysis of INSR protein expression in HEK-293T, MCF-7 and MDA-MB-231 and MCF-10A cell lines. MDA-MB-231 cells were transduced with an shRNA targeting *INSR* to demonstrate specificity. Blots were probed for INSR, with GAPDH probed for as a loading control. (**H**) Western blot analysis of MCF-10A cells grown in supplemented DMEM/HAM (Basal) or starved overnight in the absence of insulin and FBS (Starved), and then either stimulated with 100 nM insulin for 5 minutes (Starved+Ins) or pre-treated with 1 μM OSI-906 for 2 hours before stimulation with 100 nM insulin for 5 minutes

(Starved+OSI+Ins). Blots were probed to determine both total and phosphorylated levels of INSR, AKT, ERK and S6. GAPDH was probed for a loading control. Boxplots show the median and interquartile range, with Tukey style whiskers. Scatterplot shows the median and interquartile range. ** $p < 0.01$, *** $p < 0.001$, **** $p < 0.0001$; Student's t-test.

Figure 2: *Generation of genetic mouse models of breast cancer with conditional deletion of INSR.*

(**A**) Breeding schematic for *NIC* mice that are either wild-type (+/+), heterozygous (F/+) or homozygous (F/F) for the conditional *INSR* allele. Tumour measurements were performed weekly, and mice were sacrificed at humane endpoint. (**B**) Breeding schematic for *MTB:MIC* mice that are either wild-type (+/+), heterozygous (F/+) or homozygous (F/F) for the conditional *INSR* allele. 10-week-old mice were fed either regular fat (RFD) or high fat (HFD) diets for an additional 10 weeks, followed by treatment with 2 mg/ml doxycycline to induce mammary tissue-specific expression of the PyMT oncogene with coordinate deletion of *INSR*. (**C**) Agarose gel image of PCR showing the genotyping of *NIC* positive (+) and negative (-) mice. (**D**) Agarose gel image of PCR showing tissue-specific Cre and PyMT expression upon doxycycline administration in the mammary tumours of *MTB:MIC* mice. (**E**) Agarose gel showing *INSR* exon 4 excision in $INSR^{F/+}$ (F/+) and $INSR^{F/F}$ (F/F) mice, followed by the schematic of the PCR strategy. Mice that are wild-type for *INSR* (+/+) are included as a control. (**F**) Immunohistochemical analysis of INSR expression in the mammary gland of *NIC* mice that are either wild-type (+/+) or homozygous (F/F) for the conditional *INSR* allele. (**G**) Immunohistochemical analysis of INSR expression in mammary gland, liver, muscle and fat tissues of *MTB:MIC* mice that are either wild-type (+/+) or homozygous (F/F) for the conditional *INSR* allele. (**H**) Scatterplot of fasting blood glucose levels in *FVB* (+/+, n = 3), *MTB:MIC INSR* (F/+) (n = 4) and *MTB:MIC INSR* (F/F) (n = 3) model mice. Scatterplot shows the median and interquartile range. n.s = non-significant; Student's t-test.

Figure 3: ***Loss of INSR delays mammary tumour onset, prolongs survival and reduces tumour burden in vivo.***

(**A**) Reverse Kaplan-Meier analysis of mammary tumour onset in *NIC* mice with wild-type *INSR* alleles (+/+*,* n = 5) and mice heterozygous (F/+, n = 9) and homozygous (F/F, n = 9) for the conditional *INSR* allele. (**B**) Reverse Kaplan-Meier analysis of mammary tumour onset (post-doxycycline regimen initiation) in *MTB:MIC* mice with wild-type *INSR* alleles (+/+*,* n = 9) and mice heterozygous (F/+, n = 20) and homozygous (F/F, n = 12) for the conditional *INSR* allele. (**C**) Kaplan-Meier analysis of overall survival (i.e. total tumour volume less than 1000 mm^3) in *NIC* mice with wild-type *INSR* alleles (+/+*,* n = 5) and mice heterozygous (F/+, n = 9) and homozygous (F/F, n = 9) for the conditional *INSR* allele. (**D**) Scatterplot of endpoint tumour burden in *NIC INSR* mice (+/+, n = 5; F/+, n = 9; F/F, n = 9). Mice were sacrificed at humane endpoint (tumour volume exceeding 1000 mm^3), followed by quantification of total tumour number. (**E**-**D**) Scatterplots of endpoint tumour burden in *MTB:MIC INSR* mice (+/+, n = 9; F/+, n = 18; F/F, n =12). Mice were sacrificed at 8 weeks post-doxycycline treatment regimen initiation, followed by quantification of total tumour (**E**) numbers and (**F**) weights. (**G**-**H**) Scatterplots of endpoint tumour burden in *MTB:MIC INSR* mice treated with regular-fat diet (RFD; +/+, n = 9; F/+, n = 18; F/F, n = 12) or high-fat diet (HFD; +/+, n = 9; F/+, n =

12; F/F, n = 9) for 10 weeks prior to 8-week doxycycline regimen initiation followed by sacrifice. Endpoint total tumour (**G**) numbers and (**H**) weights were quantified. (**I**) Reverse Kaplan-Meier analysis of mammary tumour onset (post-doxycycline regimen initiation) in HFD-fed *MTB:MIC* mice with wild-type *INSR* alleles (+/+, n = 9) and mice heterozygous (F/+, n = 12) and homozygous (F/F, n = 9) for the conditional *INSR* allele. Scatterplots show the median and interquartile range. * $p < 0.05$, ** $p < 0.01$, *** $p < 0.001$, **** $p < 0.0001$; log-rank test (**A**-**C, I**), Student's t-test (**D**-**H**).

Figure 4: *Loss of INSR impairs tumour initiation but does not impact tumour progression or metastasis.*

(**A**) Scatterplot of average weights of tumours at endpoint in *MTB:MIC INSR* mice which developed tumours by 8 weeks post-doxycycline induction. (**B**-**C**) Time-resolved plots for individual tumour growth in *NIC INSR* mice (+/+, n = 21; F/+, n = 24; F/F, n = 18) as a function of the age of the mouse in days, with tumour volume measurements displayed on (**B**) linear and (**C**) logarithmic scale. (**D**) Boxplot of estimated average % tumour growth per day for each *NIC INSR* mouse (+/+, n = 5; F/+, n = 9; F/F, n = 9). Estimates were calculated by adding together average growth rate for each genotype, and any estimated random variation from this average for each mouse. Values for each individual mouse are plotted over the boxplots. (**E**-**F**) Time-resolved plots for total tumour burden (as measured by summing total volume of each tumour per mouse) for *NIC INSR* mice (+/+, n = 5; F/+, n = 9; F/F, n = 9) as a function of the age of the mouse in days, with tumour volume measurements displayed on (**E**) linear and (**F**) logarithmic scale. (**G**-**I**) Scatterplots of metastatic burden in (**G**) *NIC INSR* mice (+/+, n = 5; F/+, n = 9; F/F, n = 9) and *MTB:MIC INSR* mice fed with (**H**) RFD (+/+, n = 8; F/+, n = 7; F/F, n =

9), or (**I**) either RFD or HFD (*for RFD*, +/+, n = 8; F/+, n = 7; F/F, n = 9; *for HFD*, +/+, n = 7; F/+, n = 7; F/F, n = 5). Mice were sacrificed at their respective endpoints and metastatic burden was assessed through quantification of the number of lung metastases as determined by H&E staining of FFPE lung sections, averaged across 5 sections. (**J**-**K**) Cells isolated from mammary glands of FVB, *MTB:MIC INSR* (+/+) *and MTB:MIC INSR* (F/F) mice were resuspended in Matrigel, cultured for 11 days in Epicult-B medium +/- 0.1 μg/mL doxycycline, followed by imaging using Cytation 5 live cell plate reader. (**J**) Representative Z-stack image projections of Matrigel domes. (**K**) Scatterplot of number of mammary tumour spheres per Matrigel dome as quantified using Gen 5 digital image analysis. Scatterplots show the median and interquartile range. Boxplots show the median and interquartile range, with Tukey style whiskers. * $p < 0.05$, **** $p < 0.0001$, n.s = non-significant; Student's t-test (**A, G**-**I, K**), ANOVA (**D**).

Figure 5: *INSR-deficient tumours display no difference in canonical signaling downstream of INSR.*

Scatterplots of digital pathological analysis using QuPath software of immunohistochemically stained sections of paraffin embedded tumours collected at endpoint from (**A**, **D**, **G**, **J**, **M**) *NIC INSR* mice (+/+, n = 5; F/+, n = 9; F/F, n = 9), (**B**, **E**, **H**, **K**, **N**) *MTB:MIC INSR* mice fed RFD (+/+, n = 9; F/+, n = 6; F/F, n = 4), and (**C**, **F**, **I**, **L**, **O**) *MTB:MIC INSR* mice fed either RFD (+/+, n = 9; F/F, n = 4) or HFD (+/+, n = 3; F/F, n = 3). H-scores for scanned images of stained tumour sections were determined by QuPath using *Simple Tissue Detection* followed by *Positive Cell Detection* and tissue classification, which selectively scored individual tumour cells as positive (1+, 2+ or 3+) or negative (0) for staining of (**A**-**C**) INSR, (**D**-**F**) Ki67, (**G**-**I**) p-AKT, (**J**-**L**) p-ERK, and (**M**-

O) IGF1R. Scatterplots show the median and interquartile range. * $p < 0.05$, ** $p < 0.01$, *** $p < 0.001$, **** $p < 0.0001$, n.s. = not significant; Student's t-test.

Figure 6: *INSR loss in mammary epithelial cells reduces bioenergetic capacity.*

(**A**) Heatmap of mean z-score normalized expression by RNAseq for replicates of COMMA1D INSR (+/+) cells (n = 6) and COMMA1D INSR (-/-) cells (n = 6) for genes associated with mitochondrial respiratory chain complexes. Genes differentially expressed (FDR < 0.05) between genotypes are highlighted in bold. (**B**) Bar graph showing relative mRNA expression by RT-qPCR of *INSR* and select components of the mitochondrial respiratory chain shown to be differentially expressed in COMMA1D INSR cells in **A**. Gene expression levels were normalized to *HPRT* expression. (**C**) Bar graph showing the relative mitochondrial DNA content in COMMA1D cells, as measured by qPCR of MT-genome encoded *COX2* (mitochondrial gene) normalized to nuclear genome-encoded β-globin. (**D**-**E**) Seahorse Mito Stress Test Assay of COMMA1D INSR (+/+) (n = 39) and COMMA1D INSR (-/-) (n = 40) cells seeded onto 96-well Seahorse assay plates. Compounds were loaded into a hydrated cartridge in the following order: Port A 1 μM Oligomycin, Port B 2μM FCCP, Port C 1 μM Rotenone/ Antimycin A, and Port D 20 μM Monensin. Measurements were determined by WAVE software. (**D**) Bioenergetic plot representing the average glycolytic ATP production rate (J ATP-glyc; x-axis) plotted against the average mitochondrial respiratory ATP production rate (J ATP-ox; y-axis) of COMMA1D INSR cells under basal, maximal OXPHOS (FCCP), and maximal glycolytic (Monensin) conditions. Areas under the boxes represent average bioenergetic capacity. (**E**) Bar graph representing bioenergetic capacities from **D**. (**F**)

Glucose/Galactose assay of COMMA1D INSR (+/+) (n = 6) and COMMA1D INSR (-/-) (n = 6) cells seeded into 6-well plates with DMEM/F12 glucose-free media supplemented with glucose and counted the following day, as well as counted the next three days following media replenishment using DMEM/F12 glucose-free media supplemented with either 17 mM glucose (permits either oxidative phosphorylation or glycolysis) or 17 mM galactose (permits oxidative phosphorylation only). Bar graphs show mean with error bars representing SEM. Time-resolved plot shows mean with error bars representing SEM. * $p < 0.05$, ** $p < 0.01$, *** $p < 0.001$, **** $p < 0.0001$, n.s. = non-significant; Student's t-test.

Materials & Methods

Gene expression analyses from published datasets of human samples and cell lines

RNAseq gene expression data from The Cancer Genome Atlas PanCancer study (TCGA PANCAN) (Weinstein et al., 2013) was obtained from the web-based program xenabrowser (Goldman et al., 2020). Microarray gene expression data from the Molecular Taxonomy of Breast Cancer International Consortium project (METABRIC, Nature 2012 & Nat Commun 2016; “METABRIC”) (Curtis et al., 2012; Pereira et al., 2016), as well as RNA-seq gene expression data from the Breast Invasive Carcinoma (TCGA, PanCancer Atlas; “TCGA Breast”) (Koboldt et al., 2012) dataset and from the Cancer Cell Line Encyclopedia (Broad, 2019; “CCLE”) (Ghandi et al., 2019) dataset were all obtained from the web-based program cBioPortal (Cerami et al., 2012; Gao et al., 2013). Boxplots, scatterplots, and p-values of these data were visualized and calculated using GraphPad Prism 9.

Survival analyses of breast cancer samples from published datasets

Gene expression in transcripts per million (TPM) was downloaded from the TCGA PANCAN study in xenabrowser and converted to gene-level TPM in R. Additionally, normalized microarray expression for BRCA samples from the METABRIC project were downloaded from cBioPortal. Samples belonging to the TGCA Breast project were then subset and assigned a PAM50 subtype and claudin status using the genefu Bioconductor package (v. 2.28.0) (Deena M.A. Gendoo et al., 2022). TCGA Breast or METABRIC samples were then stratified into *INSR*-high or *INSR*-low expressed samples using the surv_cutpoint() function from the survminer Bioconductor package (v. 0.4.9) (Kassambara A et al., 2021) to determine an optimized expression threshold for each dataset. Kaplan-Meier curves and log-rank scores were generated using the survival Bioconductor package (v. 3.3-1) (Terry M. Therneau & Patricia M. Grambsch, 2000; Therneau T, 2022).

Culture of human cell lines

MCF-10A cells were cultured in DMEM/F12 (Invitrogen #11330-032) supplemented with 5% fetal bovine serum (FBS), 20 ng/mL epidermal growth factor, 0.5 mg/mL hydrocortisone, 100 ng/mL cholera toxin, 10 µg/mL insulin and 1% penicillin/streptomycin (Soule et al., 1990). HEK-293T, MCF-7 and MDA-MB-231 cells were cultured in DMEM (Invitrogen #D5796-500ML) supplemented with 10% FBS and 1% penicillin/streptomycin. For immunoblot signalling analyses, MCF-10A cells were seeded in above culture medium (Basal), followed by either basal medium replenishment or overnight starvation with DMEM/F12 supplemented with only 0.5 mg/mL hydrocortisone, 100 ng/mL cholera toxin and 1% penicillin/streptomycin (Starved). These cells were then stimulated with 10 µg/mL insulin in either the absence (Starved + Ins) or presence (Starved + OSI + Ins) of pre-treatment with 1 µM linsitinib (OSI-906) for 2 hours. For shRNA analyses, MCF-10A cells were transduced with lentiviral pLKO.1 puromycin shRNA vectors (RNAi Consortium, Broad Institute) to target expression of either *INSR* (shRNA 80 = 5’-GTG-CTG-TAT-GAA-GTG-AGT-TAT-3’, shRNA 82 = 5’-CTC-GTT-TGG-TTA-CCA-ATT-TAA-3’) or a non-targeting control (*shGFP*, 5'-GCA-AGC-TGA-CCC-TGA-AGT-TCA-T-3'), followed by growth in either Basal, Starved or Starved + Ins conditions outlined above.

PCR of human breast cancer cell lines

Cells were grown under normal culture conditions followed by lysis with TRIzol Reagent (Invitrogen # 15596026), phase separation with chloroform, and RNA precipitation with isopropanol. RNA was then washed with 70% ethanol and re-dissolved with DEPC-treated water. First-strand cDNA synthesis from isolated mRNA was performed as outlined in the protocol for Superscript III Reverse Transcriptase (Invitrogen #18080051). For cDNA isolated from HEK-293T, MCF-10A, MCF-7 and MDA-MB-231 cells, polymerase chain reaction (PCR) was performed using primers spanning *INSR* exon 11 (Fwd: 5’-AAC-CAG-AGT-GAG-TAT-GAG-GAT-3’; Rev: 5’-CCG-TTC-CAG-AGC-GAA-GTG-CTT-3’) to specifically detect *INSR* isoforms as previously described (Belfiore et al., 2009). PCR products (*INSR-A* (exon 11-) = 600 bp; *INSR-B* (exon 11+) = 636 bp) were separated by agarose gel electrophoresis, allowing for relative *INSR* isoform expression levels to be calculated by densitometry analysis using ImageJ software, with visualization of relative *INSR* isoform expression performed in GraphPad Prism 9.

For shRNA knockdown experiments in MCF-10A cells, cells were lysed and first-strand cDNA synthesis was performed as described above, with real-time quantitative PCR (RT-qPCR) performed using primers targeting *INSR* (Fwd: 5’-AAC-CAG-AGT-GAG-TAT-GAG-GAT-3’; Rev: 5’-CGT-TCC-AGA-GCG-AAG-TGC-TT-3’) and *RPLPO* (Fwd: 5’- CAA-CCC-TGA-AGT-GCT-TGA-CAT-3’, Rev: 5’-AGG-CAG-ATG-GAT-CAG-CCA-3’). Fold change in mRNA expression between shRNA-treated and untreated cells was calculated using the $2^{-\Delta\Delta Cq}$ method as previously described (Livak & Schmittgen,

2001) with *RPLPO* expression used as a reference for normalization. Calculated results were visualized in GraphPad Prism 9.

Immunoblotting

To prepare total protein lysates, cells were homogenized in CHAPS lysis buffer (0.3% CHAPS, 120 mM NaCl, 1x protease inhibitor cocktail in 1.5 mM HEPES buffer pH 7.5). To detect relative protein and phosphorylated protein levels, immunoblots were probed with antibodies against INSR (Millipore Sigma #07-724), phospho-INSR/IGF1R (Y1135/1136, Cell Signaling #3024), Akt (Cell Signaling #4691), phospho-AKT (S^{473}) (Cell Signaling #4058), ERK (Cell Signaling #9102), phospho-p44/42 MAPK (Erk1/2) (T^{202}/Y^{204}) (Cell Signaling #9101), S6 (Cell Signaling #2217), and phospho-S6 (S235/S236, Cell Signaling #). GAPDH (Santa Cruz #sc-25778) was probed for as a loading control.

Conditional INSR deletion in *MTB:MIC* or *NIC* mouse models

The animals used in these experiments were housed in the UHN animal facilities accredited by the Canadian Council on Animal Care and treated in accordance with the institutional guidelines and the UHN Animal Care Committee-approved protocols. *MMTV-rtTA* (*MTB*) mice were a generous gift of Dr. Lewis A. Chodosh from the University of Pennsylvania School of Medicine (Gunther et al., 2002). *PyMT-IRES-Cre* (*MIC*) mice were a generous gift of Dr. William Muller from the Rosalind and Morris Goodman Cancer Research Centre at McGill University (Rao et al., 2014). *MMTV-NIC* (*NIC*) mice were a generous gift of Dr. Giuseppina Ursini-Siegel from the Lady Davis Institute for Medical Research at McGill University (Ursini-Siegel et al., 2008). $INSR^{F/F}$ (B6.129S4(FVB)-$Insr^{tm1Khn}$/J; stock #006955) and *FVB/NJ* mice (stock #001800) were purchased from the Jackson Laboratory. *INSR*$^{F/F}$ were backcrossed onto the *FVB/NJ* background for 6 generations. Mice were genotyped using the following primers: *MMTV-rtTA* (Fwd: 5' ACC GTA CTC GTC AAT TCC AAG GG 3', Rev: 5' CGC CAT TAT TAC GAC AAG 3'), *PyMT-IRES-Cre* (Fwd: 5' GGA AGC AAG TAC TTC ACA AGG G 3', Rev: 5' GGA AAG TCA CTA GGA GCA GGG 3'), *neu* (Fwd: 5′-CCT CTG ACG TCC ATC GTC TC-3′, Rev: 5′-CGG ATC TTC TGC TGC CGT CG-3′), and the conditional *INSR* allele (Fwd: 5' GAT GTG CAC CCC ATG TCT G 3', Rev: 5' CTG AAT AGC TGA GAC CAC AG 3'). Regular chow-fed (#7012, Teklad Diets) *MMTV-rtTA/PyMT-IRES-Cre/INSR*$^{+/+,\ F/+\ or\ F/F}$ (*MTB:MIC INSR* (+/+), (F/+) or (F/F)) mice were administered 2 mg/mL doxycycline hyclate (Sigma-Aldrich #D9891) in their drinking water at 10-12 weeks of age. Alternatively, *MTB:MIC:INSR*$^{+/+,\ F/+\ or\ F/F}$ mice were fed a high-fat diet (#TD-01435, Teklad Diets) for 10 weeks before the doxycycline administration. *MTB:MIC INSR* (+/+), (F/+) or (F/F) mice were sacrificed at a fixed end-point of 8 weeks or 10 weeks post doxycycline administration. *NIC INSR* (+/+), (F/+) or (F/F) mice were fed regular chow and monitored weekly for palpable tumours; upon detection, weekly caliper measurements were performed until a humane endpoint was reached (total tumour volume ≥ 1000 mm^3), followed immediately by sacrifice. For both mouse models, mammary tumours, lungs, and other tissues were excised, weighed (tumours only), counted (tumours only) and fixed in 5% formalin for 48 hr at 4° C. Post-fixation, tumours and tissues were rinsed with PBS and stored in 70% ethanol at 4°C. Visualization and statistical analysis of all measurements were performed in GraphPad Prism 9.

Blood glucose concentrations in INSR knockout mice

To ensure that INSR signaling was intact in the metabolic tissues of INSR knockout mice, their blood glucose and plasma insulin concentrations were measured. Mice were deprived of food for 6 hours, at which time blood glucose concentrations were measured using Accu-Chek Performa test strips and meter (Roche). The mice were then bled and euthanized according to ethics guidelines of UHN, plasma insulin concentrations were determined by rodent-specific insulin ELISA kit (Millipore #EZRMI-13K). For the glucose tolerance test, mice were deprived of food for 6 hours, then injected with 2 g/Kg glucose into the intraperitoneal cavity. Blood glucose concentrations were measured as described previously (Dowling et al., 2016) at 0, 15, 30, 60, and 120 minutes post-injection. Visualization and statistical analysis of all measurements were performed in GraphPad Prism 9.

Statistical modeling and analysis of tumour growth data

Tumour growth data from *NIC INSR* mice was filtered to ensure that all tumours considered had at least two measurements before the mouse was sacrificed. Visual examination of the data suggested an exponential growth pattern for the tumours. To directly test for this, both linear and log-linear mixed models were fit to the measured tumour volume data over time to estimate the average tumour growth rate for each mouse. The measured volume of each tumour was modelled as a function of the tumour age, including fixed effect terms for the interaction between the genotype and the age of the tumour, as well as a fixed effect intercept for each genotype. Random effects were included for the mouse-to-mouse variation in the slope of the model, and for the tumour-to-tumour variation in the intercept. The model estimated an average tumour growth rate (linear or exponential) for each genotype, allowing for random variation in the growth rates between mice. The relationships between the residual and fitted values for the linear and log-linear models were visually examined, with the linear model displaying a pronounced dependency between the residuals and the fitted volume, suggesting a biased fit to the observed data, validating the use of the log-linear model. Estimated percent growth per day values were calculated from the coefficients estimated by the model for each mouse, adding together the average genotype growth rate and the random mouse-specific deviation from the average.

The significance of differences between groups was assessed using a nested-model ANOVA, comparing the full model described to a restricted model which excludes the fixed and random effects of genotype on growth rate (but retains the effect of genotype on the intercept). The tested null hypothesis was that a single average growth rate explains the observed data, as well as an average growth rate fit to each genotype separately. Two group comparisons were done by first refitting both models to the subset of the data belonging to the two compared groups.

The same data were also analysed after summing the tumour volumes for each mouse, calculating total tumour volume per mouse. Note that the previous analysis estimated an intercept term for each tumour, meaning the slopes were fit after adjusting for the different time of tumour onset. In per mouse analysis, the volume of tumours arising from the same mouse is added to the mouse total as they arise. For modelling these data, the models described above were modified to fit one random intercept per mouse. The same approach was taken for this analysis: after visual examination, linear and log-linear mixed models were fit to the data and compared based on a bias of residuals based on fitted total tumour volumes. As in per tumour analysis, the log-linear model was found to be a better fit than the linear model. Significance testing was done as above, comparing the explanatory power of models fit using the genotype information to those fitting a single slope for mice from all genotypes.

All models were estimated using the afex (1.0-1) (CRAN.R-project.org/package=afex) and lme4 (1.1-27.1) (Bates et al., 2015) packages, as implemented in the R Statistical Computing Environment (4.1.2) (R-project.org/). Plots were generated using the ggprism (1.0.3) (CRAN.R-project.org/package=ggprism) and ggplot2 (3.3.5) (ggplot2.tidyverse.org) packages.

Immunohistochemistry and semi-automated digital image analysis

For histopathological and signaling analyses, FFPE tumours of *MTB:MIC INSR* and *NIC INSR* mice collected at endpoint were sectioned and stained with hematoxylin and eosin (H&E), or probed with antibodies against INSR (Upstate #05-1104), IGF1R (Cell Signalling #3027), HER2 (Santa Cruz #284), phospho-AKT (S^{473}) (p-AKT; Cell Signaling #4058), phospho-p44/42 MAPK (Erk1/2) (T^{202}/Y^{204}) (p-ERK; Cell Signaling #9101), and Ki67 (Lab Vision #RM-9106-S1, clone SP6) by the Applied Molecular Profiling Laboratory and the Pathology Research Program at UHN. All slides were digitized for subsequent quantification by image analysis.

INSR, IGF1R, p-AKT, p-ERK and Ki67 stains were quantified using QuPath bioimage analysis software (Bankhead et al., 2017). Briefly, images of all slides of a given stain were loaded into a single project file where stain vector and background estimates for each antibody were used to improve stain separation using colour deconvolution. *Simple Tissue Detection* command was used to batch process the selection of tissue from tumour sections and exclusion of white space on all project slide images, followed by manual annotation of each tissue sample and exclusion of any stain artifact. The *Positive Cell Detection* command, which detects paired nuclei and cell boundaries within an annotation and scores each cell for staining intensity, was run with its parameters manually set and intensity thresholds optimized for each stain based upon mean nuclear (Ki67), cytoplasm (INSR, IGF1R, p-AKT) and cell (p-ERK) DAB optical densities of positive and negative control annotations. All project annotations were then batch processed with the optimized *Positive Cell Detection* parameters, followed by tissue classification using a Random Forest Classifier trained on manual annotations of tumour or stomal cells which finally enumerated tumour tissue-specific cells that were either negative (0 < lowest intensity threshold parameter) or positive (weak (1+) ≥ lowest intensity threshold parameter; moderate (2+) ≥ 2-fold 1+; strong (3+) ≥ 3-fold 1+) for a stain. Tumour % Positivity and Tumour H-scores for each annotation were quantified by QuPath, with subsequent visualization and statistical analysis performed in GraphPad Prism 9. Representative images of stained sections were visualized in QuPath at 20X magnification.

To validate tissue-specificity of the INSR knockout, FFPE liver, muscle and adipose (fat) tissues in *MTB:MIC INSR* (+/+) and (F/F) mice were sectioned, stained with anti-INSR and digitized for image visualization. To count metastases for both *MTB:MIC INSR* and *NIC INSR* mice, FFPE lungs collected at endpoint were serially sectioned (5 µm sections, 100 µm apart) and stained with H&E, followed by digitization and analysis using Aperio ImageScope (Leica Biosystems). The number of metastases were averaged across 5 sections, with subsequent visualization and statistical analysis performed in GraphPad Prism 9.

Mammary tumour sphere forming assay

In vitro Matrigel colony forming assay was performed with adaptations from a method previously described (Joshi et al., 2010). Mammary glands of 6-12 week old *FVB* (control) mice, *MTB:MIC INSR* (+/+),and *MTB:MIC INSR* (F/F) mice were resected, minced and digested in 4 ml of DMEM/F12 medium supplemented with 750 U/ml collagenase and 250 U/ml hyaluronidase for 1.5 hours at 37^0C. Cell preparations were vortexed and mammary gland digestion halted with 10 mL of HF buffer (Hank's Buffered Salt Solution supplemented with 2% FBS), followed by centrifugation at 1200 rpm for 5 minutes at 4^0C. Red blood cells were lysed by resuspension of cell pellet in a 1:5 ratio of HF buffer to ammonium chloride, followed by centrifugation. Resulting cell pellet was gently resuspended for 2 minutes in 2 mL 0.25% trypsin, followed by dilution with HF buffer and centrifugation. Cell pellet was again gently resuspended for 2 minutes in 2 mL of 5 µg/mL dispase solution supplemented with 100 µL of 1 mg/mL DNAse I. After addition of 10 mL of HF buffer, cell suspension was filtered through a 40 µm cell strainer before centrifugation. Cell pellet was resuspended in HF buffer, and viable cell numbers determined using Trypan blue exclusion. 5000 cells were seeded per well in 50 µL Matrigel (Corning #356231) in 24 well plates and cultured in mouse Epicult-B medium (DMEM:F12 medium supplemented with 5 µg/mL insulin, 10 ng/mL EGF, 10 ng/ML cholera toxin, 180 µM adenine, 0.5 µg/mL hydrocortisone, 10% FBS, and 10 µM Rock inhibitor). Cells were treated daily with or without 0.1 µg/mL doxycycline hyclate for 11 days.

The Z-stack and montage functions of the Cytation 5 imaging multi-mode reader (BioTek) were used to image entire Matrigel domes containing mammary tumour spheres. The brightfield Z-stacks were converted to Z-projections and processed by digital phase contrast using the Gen5 software (Cytation 5). Tumour sphere morphometric data for each well was collected by performing image analysis on processed digital phase contrast images in Gen5. Briefly, all objects identified by Gen5 were filtered based on calculated metrics to identify all "spheres" in a well, and further filtering classified a subset of these as "tumour." The parameters for the "tumour" filter were based on the following calculated metrics: size > 250; perimeter < 5000; circularity ≥ 0.2; mean intensity ≥ 25,000; eccentricity ≥ 0.1. Eccentricity (or "spikiness") was used as a measure of sphere budding formation and was defined as: $1 - ((4\pi*\text{Sphere Area})/(\text{Sphere Perimeter}^2))$. Visualization and statistical analysis of counts of mammary tumour spheres were performed in GraphPad Prism 9.

INSR deletion by CRISPR/Cas9 in COMMA1D murine mammary epithelial cells

COMMA1D cells, a non-transformed murine mammary epithelial cell line, were cultured in COMMA1D media (DMEM/F12 media (Wisent Inc #319-005-CL) supplemented with 5% FBS (Wisent Inc #098150,), 20ng/ml EGF (Peprotech #AF-100-15), 0.5mg/ml Hydrocortisone (Sigma #H0888), 100ng/ml Cholera Toxin (Sigma C8052), 10ug/ml Insulin (Biogems #10-365), and 1% Penicillin/Streptomycin (Wisent Inc #450-201-EL)). Cells were stained with FITC anti-mouse Ly-6A/E (Sca-1; Biolegend #122504) and APC/Cy7 anti-mouse CD326 (Ep-CAM; Biolegend #118217) and sorted by FACS (Aria Fusion, BD Biosciences) to isolate the luminal (Ep-CAM high:Sca-1 low) and basal (Ep-CAM low:Sca-1 high) populations (Werner et al., 2022). Sorted luminal COMMA1D cells were then genetically modified to delete *INSR* using CRISPR/Cas9 as described in (Ran et al., 2013). Briefly, px458 (Addgene #62988), a plasmid containing a Cas9n D10A nickase mutant with a puromycin selection marker, was cloned to incorporate knock-out sgRNAs targeting *INSR* (Top: 5'-CAC-CGG-GTA-TAA-GTC-TCT-CAT-TTG-G-3', Bottom: 5'-AAA-CCC-AAA-TGA-GAG-ACT-TAT-ACC-C-3'). COMMA1D cells were then transfected with *INSR* knock-out plasmid using 15 µL PolyJet transfection reagent (SignaGen Laboratories #SL100688). Following transfection, cells were selected with 5 µg/ml puromycin (Sigma #P8833) for 48 hours, after which selection pressure was removed and cells allowed to proliferate until colonies formed (~4 days). Clones were picked, expanded in COMMA1D media, and screened for deletion of *INSR* by PCR (Fwd primer: 5'-CTC-ATG-TGC-AGC-TAG-CTT-TC-3', Rev primer: 5'-GAG-ATT-CCT-GCT-GCA-GAT-TG-3'). Two COMMA1D *INSR* knock-out (-/-) clones (#87, #160) and two control COMMA1D *INSR* wild-type (+/+) clones (#44, #65) were selected, expanded in COMMA1D media, and validated for INSR knock-out or expression by immunoblotting. Immunoblot analysis of canonical INSR signaling was performed as described above. Analysis of immunoblot signal by densitometry was performed in ImageJ, with visualization and statistical analysis performed in GraphPad Prism 9.

RNAseq of COMMA1D INSR cells

Cells derived from two clones each of COMMA1D INSR (+/+) (Clones #44 and #65) and COMMA1D INSR (-/-) (Clones #87 and #160) were cultured in triplicate using COMMA1D media in 10 cm plates. RNA was then isolated using the RNeasy mini kit

(Qiagen #74104) according to the manufacturer's protocol and using the RNase free DNase set. 2 µg of purified RNA (each) from the triplicate samples was then sent to Novogene Inc. for RNAseq analysis.

Paired-end RNAseq reads were trimmed for Illumina adapters and sequencing quality using Trim Galore! (v. 0.6.6; https://www.bioinformatics.babraham.ac.uk/projects/trim_galore/) and aligned to the mm10 genome using STAR (v. 2.7.9a) (Dobin et al., 2013). High-quality, single-mapping reads were counted to gene exons using FeatureCounts (subread v. 2.0.1) (Liao et al., 2014) and normalized and analyzed for differential expression between *INSR* wild-type (+/+) and knock-out (-/-) conditions using DESeq2 (v. 1.36.0) (Love et al., 2014). Gene ontology enrichment analysis was performed using the Bioconductor package gprofiler2 (v. 0.2.1)(Peterson et al., 2020) and gene set enrichment analysis was performed using the Bioconductor package fgsea (v. 1.22.0) (Korotkevich et al., 2021) and manually curated gene sets from http://download.baderlab.org/EM_Genesets/November_17_2022/Mouse/symbol/Mouse_GOBP_AllPathways_no_GO_iea_November_17_2022_symbol.gmt. Gene ontology cellular component gene sets related to mitochondrial respiratory chain complexes were obtained from g:profiler gene sets.

Analysis of published RNAseq data from mouse preadipocytes

Raw RNAseq gene-level counts for INSR/IGF1R-depleted cells reconstituted with various forms of human INSR were obtained from GEO (Accession: GSE206565) (Nagao et al., 2023). Counts were normalized using DESeq2 and mitochondrial respiratory chain complex gene sets were applied to z-score scaled gene expression.

RT-qPCR of murine mammary epithelial cells

Total RNA from COMMA1D INSR (+/+) (Clones #44 and #65) and COMMA1D INSR (-/-) (Clones #87 and #160) cultured in triplicate in COMMA1D media was isolated using the Qiagen RNeasy mini kit (Qiagen # 74104) according to the manufacturer's protocol. First-strand cDNA synthesis from isolated mRNA was performed as outlined in the protocol for Superscript III Reverse Transcriptase (Invitrogen #18080051). Real - time quantitative PCR (RT-qPCR) was performed using the BioRad SsoAdvanced Universal SYBR green Supermix according to the manufacterer's protocol (BioRad #172571). Briefly, 12.5ng cDNA was added to 5ul SsoAdvanced Universal SYBR Green Supermix in a skirted 96 well plate (BioRad #HSP9601) with the following primers: *INSR* (Fwd: 5'-AGA-TGA-GAG-GTG-CAG-TGT-GGC-T-3', Rev: 5-GGT-TCC-TTT-GGC-TCT-TGC-CAC-A-3'), *ATP5b* (Fwd: 5'-CTC-TGA-CTG-GTT-TGA-CCG-TTG-C-3', Rev: 5'-TGG-TAG-CCT-ACA-GCA-GAA-GGG-A-3'), *SHDA* (Fwd: 5'-GAG-ATA-CGC-ACC-TGT-TGC-CAA-G-3', Rev: 5'-GGT-AGA-CGT-GAT-CTT-TCT-CAG-GG-3'), *UQCRB* (Fwd: 5'-CCA-TAA-GAA-GGC-TTC-CTG-AGG-AC-3', Rev: 5'-TTT-GTC-CAC-TGA-TCC-TTA-GGC-AAG-3'), *Cox7c* (Fwd: 5'-ATG-TTG-GGC-CAG-AGT-ATC-CG-3', Rev: 5'-ACC-CAG-ATC-CAA-AGT-ACA-CGG-3'), *Ndusf6* (Fwd: 5'-CGG-GGA-AAA-GAT-CAC-GCA-TAC-C-3', Rev: 5'-TCC-ACC-TCG-TTC-ACA-GGC-TGT-T-3'), and *HPRT* (Fwd: 5'-CTG-GTG-AAA-AGG-ACC-TCT-CGA-AG-3', Rev: 5'-CCA-GTT-TCA-CTA-ATG-ACA-CAA-ACG-3'). The RT-qPCR amplification was performed in the CFX Connect PCR machine (BioRad) using the CFX Manager 3.0 software (BioRad) with the following parameters: 39 cycles of 98^0C for 5 seconds followed by 60^0C for 20 seconds. Data was exported and mRNA expression was calculated using the $2^{-\Delta\Delta Cq}$ method as previously described (Livak & Schmittgen, 2001). Calculated expression levels of *INSR*, *ATP5b*, *SHDA*, *UQCRB*, *Cox7c*, and *Ndusf6* were each normalized to mRNA expression of housekeeping gene *HPRT*. Visualization and statistical analysis of relative gene expression was performed in GraphPad Prism 9.

Determination of relative mtDNA content in murine mammary epithelial cells

Total cellular DNA of COMMA1D INSR (+/+) (Clones #44 and #65) and COMMA1D INSR (-/-) (Clones #87 and #160) was extracted using the Qiagen DNeasy Blood and Tissue kit (Qiagen #69504). Relative mitochondrial DNA content was evaluated by qPCR targeting the β-globin gene and the mitochondrial *COX2* (*MT-COX2*) as previously described (Ding et al., 2017) using the following primers: *MT-COX2* (Fwd: 5’-GCC-GAC-TAA-ATC-AAG-CAA-CA-3’, Rev: 5’-CAA-TGG-GCA-TAA-AGC-TAT-GG-3’) and β-globin (Fwd: 5’-GAA-GCG-ATT-CTA-GGG-AGC-AG-3’, Rev: 5’-GGA-GCA-GCG-ATT-CTG-AGT-AGA-3’). The reaction was conducted in a 10 uL system containing 12.5ng DNA, 5ul SsoAdvanced Universal SYBR Green Supermix (BioRad #172571) in a skirted 96 well plate (BioRad #HSP9601), and 2 nM forward and reverse primers. The PCR amplification was performed in the CFX Connect PCR machine (BioRad) using the CFX Manager 3.0 software (BioRad) with the following process: 39 cycles of 98 ^{0}C for 5 seconds followed by 60 ^{0}C for 20 seconds. The qPCR results were calculated using the $2^{-\Delta\Delta Cq}$ method as previously described (Livak & Schmittgen, 2001), and *MT-COX2* content was normalized to that of genomic β-globin. Visualization and statistical analysis of relative mtDNA content was performed in GraphPad Prism 9.

Seahorse Mito Stress Test assay

Cells derived from two clones each of COMMA1D INSR (+/+) (Clones #44 and #65) and COMMA1D INSR (-/-) (Clones #87 and #160) cultured in COMMA1D media were seeded in 22 wells of a Seahorse 96-well plate (Agilent #103792-100) at a density of 15,000 cells per well. The following day, cells were replenished with XF-Base media (Agilent #103334-100) containing 10 mM glucose, 1 mM pyruvate, and 2 mM glutamine. The following compounds were loaded into the Seahorse XFe 96 (Agilent #103792-100): Port A, 1 μM oligomycin (Sigma #O4876); Port B, 2 μM FCCP (Sigma #C2920); Port C, 1 μM rotenone/Antimycin A (Sigma #R8875 and #A8674); and Port D, 20 μM monensin (Sigma #M5273). Following calibration, culture plates containing wild-type and knock-out COMMA1D INSR cells were introduced into the Seahorse XFe 96 tray and the acquisition program was run. This program included an equilibration step followed by three measurements of basal oxygen consumption rates (OCR) and extracellular acidification rates (ECAR), as well as three OCR and ECAR measurements each post-oligomycin injection, post-FCCP injection, post-rotenone/Antimycin A injection, and post-monensin injection. Readings were collected approximately 5, 10, and 15 minutes following the initiation of each step. Data were collected and analysed using the Wave 2.6 software (Agilent Technologies), with calculations of ATP production rates by mitochondrial respiration (J-ATPox) and glycolysis(J-ATPglyc) under basal, maximal OXPHOS, and maximal glycolytic conditions performed as previously described (Mookerjee et al., 2017). Data visualization and statistical analyses were performed in GraphPad Prism 9.

Glucose/galactose growth assay

COMMA1D INSR (+/+) and COMMA1D INSR (-/-) cells were cultured in COMMA1D glucose-free media (glucose-free DMEM/F12 media (Wisent Inc #319-176-CL) supplemented with 5% FBS (Wisent Inc #098150), 20ng/ml EGF (Peprotech #AF-100-15), 0.5mg/ml Hydrocortisone (Sigma #H0888), 100ng/ml Cholera Toxin (Sigma #C8052), 10ug/ml Insulin (Biogems #10-365), 1% Penicillin/Streptomycin (Wisent Inc #450-201-EL) additionally supplemented with 17 mM glucose (Sigma #G5767). Cells were counted using Trypan blue exclusion, followed by seeding of 200,000 cells each in 4 wells of two 6-well plates (performed in triplicate). The following day (Day 0), cells from one well each of the duplicate plates were washed in 1X PBS (Wisent Inc #311-010-CL), treated with 0.5 mL 0.25% trypsin, and viable cell numbers were determined using Trypan blue exclusion. Media was then removed from the remaining wells and cells were washed in 1X PBS, followed by replenishment in COMMA1D glucose-free media supplemented with either 17 mM glucose or 17 mM galactose (Sigma #G0750). Viable cell numbers were then determined as described above from one of the remaining wells of each duplicate plate at 24, 48, and 72 hours following Day 0 replenishment with either glucose- or galactose-containing media. Visualization and statistical analysis of viable cell counts were performed in GraphPad Prism 9.

Supplemental Information

Supplementary Figure 1: *INSR expression across cancer types and cell lines.*

(**A**) Boxplot of *INSR* mRNA expression by RNAseq across various cancer types from the TCGA PANCAN dataset found in UCSC Xena Functional Genomics Explorer. Breast cancer (BRCA) is highlighted in bold; see Supplementary Table 1 for other cancer type abbreviations. (**B**) Boxplot of *INSR* mRNA expression by RNAseq across various cancer cell lines, grouped by primary site, from the CCLE dataset found in cBioPortal. Breast is highlighted in bold. (**C**) Scatterplot of RNAseq expression analysis of *INSR* in breast cancer cell lines from the CCLE dataset found in cBioPortal. Boxplots show the median and interquartile range, with Tukey style whiskers.

Supplementary Table 1: *Cancer type abbreviations in TCGA PANCAN study.*

Abbr.	Cancer Type		Abbr.	Cancer Type
ACC	adrenocortical cancer		LUSC	lung squamous cell carcinoma
BLCA	bladder urothelial carcinoma		MESO	mesothelioma
BRCA	breast invasive carcinoma		OV	ovarian serous cystadenocarcinoma
CESC	cervical & endocervical cancer		PAAD	pancreatic adenocarcinoma
CHOL	cholangiocarcinoma		PCPG	pheochromocytoma & paraganglioma
COAD	colon adenocarcinoma		PRAD	prostate adenocarcinoma
DLBC	diffuse large B-cell lymphoma		READ	rectum adenocarcinoma
ESCA	esophageal carcinoma		SARC	sarcoma
GBM	glioblastoma multiforme		SKCM	skin cutaneous melanoma
HNSC	head & neck squamous cell carcinoma		STAD	stomach adenocarcinoma
KICH	kidney chromophobe		TGCT	testicular germ cell tumor
KIRC	kidney clear cell carcinoma		THCA	thyroid carcinoma
KIRP	kidney papillary cell carcinoma		THYM	thymoma
LIHC	liver hepatocellular carcinoma		UCEC	uterine corpus endometrioid carcinoma
LAML	acute myeloid leukemia		UCS	uterine carcinosarcoma
LGG	brain lower grade glioma		UVM	uveal melanoma
LUAD	lung adenocarcinoma			

Supplementary Figure 2*: Impact of INSR expression on overall survival for all samples and luminal subtype samples in TCGA Breast and METABRIC.*

Kaplan-Meier curves of survival analyses of overall survival in BC samples stratified by *INSR* expression from (**A**, **C**, **E**) the TCGA Breast study and (**B**, **D**, **F**) the METABRIC project. Analyses were performed on (**A**-**B**) all BC samples, as well as the (**C**- **D**) Luminal A subtype and (**E**-**F**) Luminal B subtype subsets. Stratification of samples into *INSR* high or *INSR* low was performed using an optimized expression threshold for each dataset. * $p < 0.05$, ** $p < 0.01$, n.s. = non-significant; log-rank test.

Supplementary Figure 3*: Impact of INSR expression on overall survival for HER2, basal, and normal-like subtype samples in TCGA Breast and METABRIC.*

Kaplan-Meier curves of survival analyses of overall survival in BC samples stratified by *INSR* expression from (**A**, **C**, **E**) the TCGA Breast study and (**B**, **D**, **F**) the METABRIC project. Analyses were performed on the (**A**-**B**) HER2 subtype, (**C**-**D**) Basal subtype, and (**E**- **F**) Normal-Like subtype subsets. Stratification of samples into *INSR* high or *INSR* low was performed using an optimized expression threshold for each dataset. ** $p < 0.01$, n.s. = non-significant; log-rank test.

Supplementary Figure 4: *Impact of INSR expression on disease-specific survival in TCGA Breast.*

Kaplan-Meier curves of survival analyses of disease-specific survival in BC samples stratified by *INSR* expression from the TCGA Breast study. Analyses were performed on (**A**) all BC samples, as well as the (**B**) Luminal A subtype, (**C**) Luminal B subtype, (**D**) HER2 subtype, (**E**) Basal subtype, and (**F**) Normal-Like subtype subsets. Stratification of samples into *INSR* high or *INSR* low was performed using an optimized expression threshold for each dataset. * $p < 0.05$, ** $p < 0.01$, n.s. = non-significant; log-rank test.

Supplementary Figure 5: *Impact of INSR expression on disease-free interval in TCGA Breast.*

Kaplan-Meier curves of survival analyses of disease-free interval in BC samples stratified by *INSR* expression from the TCGA Breast study. Analyses were performed on (**A**) all BC samples, as well as the (**B**) Luminal A subtype, (**C**) Luminal B subtype, (**D**) HER2 subtype, (**E**) Basal subtype, and (**F**) Normal-Like subtype subsets. Stratification of samples into *INSR* high or *INSR* low was performed using an optimized expression threshold for each dataset. * $p < 0.05$, n.s. = non-significant; log-rank test.

Supplementary Figure 6: *INSR signalling in mammary epithelial cells.*

(**A**) Western blot of MCF-10A cells transduced with either two shRNAs against *INSR* or a non-targeting control (*shGFP*), followed by growth in either supplemented DMEM/HAM (Basal) or starved overnight in the absence of insulin (Starved), and then stimulated with 100 nM insulin for 5 min (Starved + Ins). Cell signaling was analyzed using antibodies against p-INSR/p-IGF1R, INSR, p-ERK, ERK, p-S6, S6 and GAPDH and performed on 25 μg total cell protein. (**B**) Bar graph showing quantification of change in mRNA expression of *INSR* after treatment of MCF-10A cells with indicated shRNA against *INSR*, relative to *INSR* mRNA expression in MCF-10A cells treated with shGFP, analyzed via qRT-PCR. Change in *RPLPO* expression was used as a reference. Bar graphs show the mean with error bars representing SEM.

Supplementary Figure 7: *High fat diet recapitulates obese conditions in mice.*

(**A**) Time-resolved plot of intraperitoneal glucose tolerance test (2 g/Kg) and (**B**) scatterplot of total body weight measurements performed on *FVB* mice fed either regular-fat diet (RFD; n = 5) or high-fat diet (HFD; n = 5), followed by fasting for 6 hours. (**C**) Scatterplots of blood glucose of *MTB:MIC INSR* mice treated with regular fat diet (RFD) or high fat diet (HFD) for 10 weeks prior to 8-week doxycycline regimen initiation followed by sacrifice. Endpoint basal blood glucose concentrations (*for RFD*, +/+, n = 4; F/+, n = 4; F/F, n = 6; *for HFD*, +/+, n = 10; F/+, n = 13; F/F, n = 9) were quantified. (**D**-**F**) Reverse Kaplan-Meier analyses of mammary tumour onset in RFD-fed or HFD-fed *MTB:MIC INSR* mice with either (**D**) wild-type *INSR* alleles (RFD*,* n = 9; HFD, n = 9) or (**E**) heterozygous (F/F) (RFD, n = 20; HFD, n = 12) or (**F**) homozygous (F/F) (RFD, n = 12; HFD, n = 9) for the conditional *INSR* allele. Time-resolved plot shows the mean with error bars representing SEM. Scatterplots show the median and interquartile range. * p < 0.05, ** p < 0.01, n.s. = not significant; Student's t-test.

Supplementary Figure 8: *Immunoblotting analysis of NIC INSR and MTB:MIC INSR tumour lysates.*

Western blot analysis of lysates of *NIC INSR* (+/+, n = 4; F/+, n = 4; F/F, n = 4) and *MTB:MIC INSR* (+/+, n = 1; F/F, n = 1) mammary tumours snap frozen at endpoint. Blots were probed with antibodies to determine total levels of INSR, HER2, AKT and ERK, and phosphorylated levels of AKT and ERK. GAPDH was probed for as a loading control.

Supplementary Figure 9: *Immunohistochemistry of NIC INSR and MTB:MIC INSR tumour sections.*

Representative images from digital scans of INSR, IGF1R, HER2, p-AKT, p-ERK, Ki67 or H&E stained sections from endpoint tumours of (**A**) *NIC INSR* mice, or *MTB:MIC INSR* mice fed with (**B**) RFD or (**C**) HFD. Images represent 20X magnification.

Supplementary Figure 10: *Semi-automated digital image analysis of NIC and MTB:MIC tumour sections.*

Scatterplots of digital pathological analysis using QuPath software of immunohistochemically stained sections of paraffin embedded tumours collected at endpoint from (**A**, **D**, **G**, **J**, **M**) *NIC INSR* mice (+/+, n = 5; F/+, n = 9; F/F, n = 9), (**B**, **E**, **H**, **K**, **N**) *MTB:MIC INSR* mice fed RFD (+/+, n = 9; F/+, n = 6; F/F, n = 4), and (**C**, **F**, **I**, **L**, **O**) *MTB:MIC INSR* mice fed either RFD (+/+, n = 9; F/F, n = 4) or HFD (+/+, n = 3; F/F, n = 3). The percentage of positive tumour cells (% Positive Tumour Cells) in scanned images of stained tumour sections were determined by QuPath using *Simple Tissue Detection* followed by *Positive Cell Detection* and tissue classification, which selectively scored individual tumour cells as positive (1+, 2+ or 3+) or negative (0) for staining of (**A**-**C**) INSR, (**D**-**F**) Ki67, (**G**-**I**) p-AKT, (**J**-**L**) p-ERK, and (**M**-**O**) IGF1R. Scatterplots show the median and interquartile range. * $p < 0.05$, ** $p < 0.01$, *** $p < 0.001$, **** $p < 0.0001$, n.s. = not significant; Student's t-test.

Supplementary Figure 11: *INSR loss does not impact immune infiltration in progressing mammary tumours.*

Scatterplot of CD45 infiltration score of tumours collected from *MTB:MIC INSR* mice (+/+, n = 6; F/+, n = 6; F/F, n = 3) following 10-week doxycycline induction. Scatterplot shows the median and interquartile range. n.s. = not significant; Student's t-test.

Supplementary Figure 12: *INSR loss in murine mammary epithelial cells does not impact canonical INSR signaling.*

Murine mammary epithelial cell line COMMA1D cells were sorted by FACS to isolate luminal population, which were then transfected with plasmids containing *Cas9* and sgRNAs designed to knock out *INSR*. (**A**) Western blot analysis of lysates of COMMA1D INSR wild-type (+/+) (n = 2) and COMMA1D INSR knockout (-/-) (n = 2) clones. Blots were probed with antibody against INSR. ERK1/2 was probed for as a loading control. (**B**) Western blot analysis of lysates of parental COMMA1D cells (n = 1) as well as COMMA1D INSR (+/+) (n = 2) and COMMA1D INSR (-/-) (n = 2) clones starved overnight, followed by stimulation with 100 nM insulin (ins). Lysates were collected immediately prior to stimulation (-), as well as 5 and 15 minutes post stimulation. Blots were probed with antibodies against p-INSR/IGF1R, INSR, IGF1R, p-AKT, AKT, p-ERK, and ERK2. GAPDH was probed as a loading control. (**C**-**E**) Time-resolved plots quantifying the relative optical density of the (**C**) p-AKT (normalized to AKT), (**D**) p-ERK (normalized to ERK2), and (**E**) p-INSR/IGF1R signal (normalized to the sum of INSR and IGF1R) of COMMA1D INSR (+/+) (n = 2) clones and COMMA1D INSR (-/-) (n = 2) clones, as measured by ImageJ software. Values were normalized to the optical density of GAPDH. Time-resolved plots show the mean value with error bars representing SEM. n.s. = non-significant; Student's t-test.

Supplementary Figure 13: *Loss of INSR in mammary epithelial cells reduces expression of mitochondrial respiratory chain complex components.*

(**A**) Enrichment map generated in Cytoscape of 358 significantly enriched pathways from gene set enrichment analysis (GSEA; FDR < 0.1) of COMMA1D INSR (-/-) cells (n

= 6), relative to COMMA1D INSR (+/+) cells (n = 6), as measured by RNAseq. Each node represents a pathway and each edge represents an overlap of shared genes between pathways of 0.5. All pathways in this analysis are downregulated in COMMA1D INSR (-/-). Related pathways are clustered. (**B**) Heatmap showing significance [-log10(FDR)] of gene ontology biological processes associated with oxidative phosphorylation/electron transport, glucose starvation and transport, and amino acid starvation enriched in down- or up-regulated genes differentially expressed between COMMA1D INSR (-/-) (n = 6) and COMMA1D INSR (+/+) (n = 6) cells, as measured by RNAseq. Dark-grey cells indicate no significant enrichment. (**C**) Boxplot of mean z-score normalized counts by RNAseq for COMMA1D INSR (+/+) (n = 6) and COMMA1D INSR (-/-) (n = 6) cells for genes associated with biological processes related to oxidative phosphorylation/electron transport (# of genes: 183), glucose starvation and transport (# of genes: 199), and amino acid starvation (# of genes: 51). (**D**) Boxplot of mean z-score normalized counts by RNAseq for COMMA1D INSR (+/+) cells (n = 6) and COMMA1D INSR (-/-) cells (n = 6) for genes associated with mitochondrial respiratory chain complexes. Boxplots show the median and interquartile range, with Tukey style whiskers. * $p < 0.05$; ** $p < 0.01$; **** $p < 0.0001$; Benjamini-Hochberg corrected Wilcoxon rank-sum test.

Supplementary Figure 14: *Impact of INSR and IGF1R loss on mitochondrial respiratory chain subunit expression in mouse preadipocytes is rescued by kinase-dead INSR.*

Boxplot of mean z-score normalized expression by RNAseq from GSE206565 (Nagao et al., 2023) in mouse preadipocytes with a double knockout for INSR and IGF1R (DKO; n = 3) and DKO cells expressing a rescue with the wild-type human INSR gene (IR; n =

3), a truncated human INSR missing the C-terminus (CT; n = 3), a human INSR juxtamembrane domain only (JMO; n = 3), and a kinase-dead human INSR (KD; n = 3). Genes shown are associated with mitochondrial respiratory chain complexes. Boxplots show the median and interquartile range, with Tukey style whiskers. * $p < 0.05$; **$p < 0.01$; ***$p < 0.001$; **** $p < 0.0001$; Benjamini-Hochberg corrected Wilcoxon rank-sum test.

Supplementary Figure 15: *Impact of INSR loss on bioenergetic fitness in mammary epithelial cells.*

Seahorse Mito Stress Test Assay of COMMA1D INSR (+/+) (n = 39) and COMMA1D INSR (-/-) (n = 40) cells seeded onto 96-well Seahorse assay plates. Compounds were loaded into a hydrated cartridge in the following order: Port A 1 µM Oligomycin, Port B 2µM FCCP, Port C 1 µM Rotenone/ Antimycin A, and Port D 20 µM Monensin. Measurements were determined by WAVE software. (**A**-**B**) Time-resolved plots showing (**A**) mitochondrial respiration (oxidative phosphorylation, OXPHOS) capacity as measured by oxygen consumption rate (OCR) and (**B**) glycolysis as measured by extracellular acidification rate (ECAR). (**C**) Stacked bar graph showing ATP production rates by glycolysis (J-ATP glyc) and mitochondrial respiration (J-ATP ox) of COMMA1D INSR cells under basal conditions. (**D**) Bar graph showing mitochondrial respiration ATP production rates (J-ATP ox) of COMMA1D INSR cells under maximal OXPHOS conditions (following FCCP injection). (**E**) Bar graph showing glycolytic ATP production rates (J-ATP glyc) of COMMA1D INSR cells under maximal glycolytic conditions (following Monensin injection). Time-resolved plots, bar graphs, and stacked bar graphs show mean with error bars representing SEM. * $p < 0.05$, **** $p < 0.0001$, n.s. = non-significant; Student's t-test.

References

Attalla, S., Taifour, T., Bui, T., & Muller, W. (2021). Insights from transgenic mouse models of PyMT-induced breast cancer: recapitulating human breast cancer progression in vivo. *Oncogene*, *40*(3), 475–491. https://doi.org/10.1038/s41388-020-01560-0

Bankhead, P., Loughrey, M. B., Fernández, J. A., Dombrowski, Y., McArt, D. G., Dunne, P. D., McQuaid, S., Gray, R. T., Murray, L. J., Coleman, H. G., James, J. A., Salto-Tellez, M., & Hamilton, P. W. (2017). QuPath: Open source software for digital pathology image analysis. *Scientific Reports*, *7*(1). https://doi.org/10.1038/S41598-017-17204-5

Barretina, J., Caponigro, G., Stransky, N., Venkatesan, K., Margolin, A. A., Kim, S., Wilson, C. J., Lehár, J., Kryukov, G. V, Sonkin, D., Reddy, A., Liu, M., Murray, L., Berger, M. F., Monahan, J. E., Morais, P., Meltzer, J., Korejwa, A., Jané-Valbuena, J., … Garraway, L. A. (2012). The Cancer Cell Line Encyclopedia enables predictive modelling of anticancer drug sensitivity. *Nature*, *483*(7391), 603–607. https://doi.org/10.1038/nature11003

Bates, D., Mächler, M., Bolker, B. M., & Walker, S. C. (2015). Fitting linear mixed-effects models using lme4. *Journal of Statistical Software*, *67*(1), 1–48. https://doi.org/10.18637/jss.v067.i01

Belfiore, A., Frasca, F., Pandini, G., Sciacca, L., & Vigneri, R. (2009). Insulin receptor isoforms and insulin receptor/insulin-like growth factor receptor hybrids in physiology and disease. *Endocr Rev*, *30*(6), 586–623.

Blüher, M. (2019). Obesity: global epidemiology and pathogenesis. In *Nature Reviews Endocrinology* (Vol. 15, Issue 5, pp. 288–298). Nature Publishing Group. https://doi.org/10.1038/s41574-019-0176-8

Boyle, P., Boniol, M., Koechlin, A., Robertson, C., Valentini, F., Coppens, K., Fairley, L. L., Boniol, M., Zheng, T., Zhang, Y., Pasterk, M., Smans, M., Curado, M. P., Mullie, P., Gandini, S., Bota, M., Bolli, G. B., Rosenstock, J., & Autier, P. (2012). Diabetes and breast cancer risk: a meta-analysis. *British Journal of Cancer 2012 107:9*, *107*(9), 1608–1617. https://doi.org/10.1038/bjc.2012.414

Bruning', P. F. ~, Bonfrer', J. M. G., Van Noord, P. A. H., Hart^, A. A. M., De Jong-Bakker!, M., & Nooijen', W. J. (1992). INSULIN RESISTANCE AND BREAST-CANCER RISK. In *Int. J. Cancer* (Vol. 52).

Buck, E., Gokhale, P. C., Koujak, S., Brown, E., Eyzaguirre, A., Tao, N., Rosenfeld-Franklin, M., Lerner, L., Chiu, M. I., Wild, R., Epstein, D., Pachter, J. A., & Miglarese, M. R. (2010). *Compensatory Insulin Receptor (IR) Activation on Inhibition of Insulin-Like Growth Factor-1 Receptor (IGF-1R): Rationale for Cotargeting IGF-1R and IR in Cancer*. https://doi.org/10.1158/1535-7163.MCT-10-0318

Calle, E. E., Rodriguez, C., Walker-Thurmond, K., & Thun, M. J. (2003). Overweight, Obesity, and Mortality from Cancer in a Prospectively Studied Cohort of U.S. Adults. *New England Journal of Medicine*, *348*(17), 1625–1638. https://doi.org/10.1056/nejmoa021423

Cerami, E., Gao, J., Dogrusoz, U., Gross, B. E., Sumer, S. O., Aksoy, B. A., Jacobsen, A., Byrne, C. J., Heuer, M. L., Larsson, E., Antipin, Y., Reva, B., Goldberg, A. P., Sander, C., & Schultz, N. (2012). The cBio cancer genomics portal: an open platform for exploring multidimensional cancer genomics data. *Cancer Discovery*, *2*(5), 401–404. https://doi.org/10.1158/2159-8290.CD-12-0095

Chan, D. S. M., Vieira, A. R., Aune, D., Bandera, E. V., Greenwood, D. C., McTiernan, A., Navarro Rosenblatt, D., Thune, I., Vieira, R., & Norat, T. (2014). Body mass index and survival in women with breast cancer—systematic literature review and meta-analysis of 82 follow-up studies. In *Annals of Oncology* (Vol. 25, Issue 10, pp. 1901–1914). https://doi.org/10.1093/annonc/mdu042

Chan, J. Y., Lapara, K., & Yee, D. (2016). Disruption of insulin receptor function inhibits proliferation in endocrine-resistant breast cancer cells. *Oncogene*, *35*(32), 4235–4243. https://doi.org/10.1038/onc.2015.488

Chang, M., Ennis, M., Dowling, R., Stambolic, V., & Goodwin, P. (2016). Leptin receptor in breast carcinoma tissue: ubiquitous expression and correlation with hormone-receptors and leptinmediated signaling, but not with systemic markers of obesity. *San Antonio Breast Cancer Symposium*.

Cheng, Z., Tseng, Y., & White, M. F. (2010). Insulin signaling meets mitochondria in metabolism. *Trends in Endocrinology & Metabolism*, *21*(10), 589–598. https://doi.org/10.1016/j.tem.2010.06.005

Cowey, S., & Hardy, R. W. (2006). The metabolic syndrome: A high-risk state for cancer? In *American Journal of Pathology* (Vol. 169, Issue 5, pp. 1505–1522). https://doi.org/10.2353/ajpath.2006.051090

Crabtree, H. G. (1928). The carbohydrate metabolism of certain pathological overgrowths. *Biochemical Journal*, *22*(5), 1289–1298. https://doi.org/10.1042/BJ0221289

Curtis, C., Shah, S. P., Chin, S. F., Turashvili, G., Rueda, O. M., Dunning, M. J., Speed, D., Lynch, A. G., Samarajiwa, S., Yuan, Y., Gräf, S., Ha, G., Haffari, G., Bashashati, A., Russell, R., McKinney, S., Aparicio, S., Brenton, J. D., Ellis, I., … Caldas, C. (2012). The genomic and transcriptomic architecture of 2,000 breast tumours reveals novel subgroups. *Nature 2012 486:7403*, *486*(7403), 346–352. https://doi.org/10.1038/nature10983

Danielson, K. G., Oborn, C. J., Durban, E. M., Butel, J. S., & Medina, D. (1984). Epithelial mouse mammary cell line exhibiting normal morphogenesis in vivo and functional differentiation in vitro. *Proceedings of the National Academy of Sciences*, *81*(12), 3756–3760. https://doi.org/10.1073/PNAS.81.12.3756

Dankner, R., Shanik, M. H., Keinan-Boker, L., Cohen, C., & Chetrit, A. (2012). Effect of elevated basal insulin on cancer incidence and mortality in cancer incident patients: The Israel GOH 29-year follow-up study. *Diabetes Care*, *35*(7), 1538–1543. https://doi.org/10.2337/dc11-1513

Deena M.A. Gendoo, Natchar Ratanasirigulchai, Markus S. Schroeder, Laia Pare, Joel S Parker, Aleix Prat, & Benjamin Haibe-Kains. (2022). *_genefu: Computation of Gene Expression-Based Signatures in Breast Cancer_.* (R package version 2.28.0). http://www.pmgenomics.ca/bhklab/software/genefu

Ding, Y., Xia, B. H., Zhang, C. J., & Zhuo, G. C. (2017). Mutations in mitochondrial tRNA genes may be related to insulin resistance in women with polycystic ovary syndrome. *American Journal of Translational Research*, *9*(6), 2984. /pmc/articles/PMC5489898/

Dobin, A., Davis, C. A., Schlesinger, F., Drenkow, J., Zaleski, C., Jha, S., Batut, P., Chaisson, M., & Gingeras, T. R. (2013). STAR: ultrafast universal RNA-seq aligner. *Bioinformatics (Oxford, England)*, *29*(1), 15–21. https://doi.org/10.1093/BIOINFORMATICS/BTS635

Dowling, R. J. O., Lam, S., Bassi, C., Mouaaz, S., Aman, A., Kiyota, T., Al-Awar, R., Goodwin, P. J., & Stambolic, V. (2016). Metformin Pharmacokinetics in Mouse Tumors: Implications for Human Therapy. *Cell Metabolism*, *23*(4), 567–568. https://doi.org/10.1016/j.cmet.2016.03.006

Dowling, R. J. O., Niraula, S., Chang, M. C., Done, S. J., Ennis, M., McCready, D. R., Leong, W. L., Escallon, J. M., Reedijk, M., Goodwin, P. J., & Stambolic, V. (2015). Changes in insulin receptor signaling underlie neoadjuvant metformin administration in breast cancer: A prospective window of opportunity neoadjuvant study. *Breast Cancer Research*, *17*(1), 1–12. https://doi.org/10.1186/S13058-015-0540-0/FIGURES/5

Ferguson, R. D., Gallagher, E. J., Cohen, D., Tobin-Hess, A., Alikhani, N., Novosyadlyy, R., Haddad, N., Yakar, S., & LeRoith, D. (2013). Hyperinsulinemia promotes metastasis to the lung in a mouse model of Her2-mediated breast cancer. *Endocrine-Related Cancer*, *20*(3), 391–401. https://doi.org/10.1530/ERC-12-0333

Ferguson, R. D., Novosyadlyy, R., Fierz, Y., Alikhani, N., Sun, H., Yakar, S., & LeRoith, D. (2012). Hyperinsulinemia enhances c-Myc-mediated mammary tumor development and advances metastatic progression to the lung in a mouse model of type 2 diabetes. *Breast Cancer Research*, *14*(1), 1–12. https://doi.org/10.1186/BCR3089/FIGURES/5

Fierz, Y., Novosyadlyy, R., Vijayakumar, A., Yakar, S., & LeRoith, D. (2010). Insulin-sensitizing therapy attenuates type 2 diabetes-mediated mammary tumor progression. *Diabetes*, *59*(3), 686–693. https://doi.org/10.2337/db09-1291

Frasca, F., Pandini, G., Scalia, P., Sciacca, L., Mineo, R., Costantino, A., Goldfine, I. D., Belfiore, A., & Vigneri, R. (1999). Insulin receptor isoform A, a newly recognized, high-affinity insulin-like growth factor II receptor in fetal and cancer cells. *Molecular and Cellular Biology*, *19*(5), 3278–3288. https://doi.org/10.1128/MCB.19.5.3278

Gallagher, E. J., Fei, K., Feldman, S. M., Port, E., Friedman, N. B., Boolbol, S. K., Killelea, B., Pilewskie, M., Choi, L., King, T., Nayak, A., Franco, R., Cruz, D., Antoniou, I. M., Leroith, D., & Bickell, N. A. (2020). Insulin resistance contributes to racial disparities in breast cancer prognosis in US women. *Breast Cancer Research*, *22*(1), 1–10. https://doi.org/10.1186/S13058-020-01281-Y/FIGURES/2

Gao, J., Aksoy, B. A., Dogrusoz, U., Dresdner, G., Gross, B., Sumer, S. O., Sun, Y., Jacobsen, A., Sinha, R., Larsson, E., Cerami, E., Sander, C., & Schultz, N. (2013). Integrative analysis of complex cancer genomics and clinical profiles using the cBioPortal. *Science Signaling*, *6*(269). https://doi.org/10.1126/SCISIGNAL.2004088

Ghandi, M., Huang, F. W., Jané-Valbuena, J., Kryukov, G. V., Lo, C. C., McDonald, E. R., Barretina, J., Gelfand, E. T., Bielski, C. M., Li, H., Hu, K., Andreev-Drakhlin, A. Y., Kim, J., Hess, J. M., Haas, B. J., Aguet, F., Weir, B. A., Rothberg, M. V., Paolella, B. R., … Sellers, W. R. (2019). Next-generation characterization of the

Cancer Cell Line Encyclopedia. *Nature*, *569*(7757), 503–508. https://doi.org/10.1038/S41586-019-1186-3

Giovannucci, E., Harlan, D. M., Archer, M. C., Bergenstal, R. M., Gapstur, S. M., Habel, L. A., Pollak, M., Regensteiner, J. G., & Yee, D. (2010). Diabetes and CancerA consensus report. *Diabetes Care*, *33*(7), 1674–1685. https://doi.org/10.2337/DC10-0666

Goldman, M. J., Craft, B., Hastie, M., Repečka, K., McDade, F., Kamath, A., Banerjee, A., Luo, Y., Rogers, D., Brooks, A. N., Zhu, J., & Haussler, D. (2020). Visualizing and interpreting cancer genomics data via the Xena platform. In *Nature Biotechnology* (Vol. 38, Issue 6, pp. 675–678). https://doi.org/10.1038/s41587-020-0546-8

Goodwin, P. J., Ennis, M., Pritchard, K. I., Trudeau, M. E., Koo, J., Madarnas, Y., Hartwick, W., Hoffman, B., & Hood, N. (2002). Fasting insulin and outcome in early-stage breast cancer: results of a prospective cohort study. *J Clin Oncol*, *20*(1), 42–51.

Gunter, M. J., Hoover, D. R., Yu, H., Wassertheil-Smoller, S., Rohan, T. E., Manson, J. E., Li, J., Ho, G. Y. F., Xue, X., Anderson, G. L., Kaplan, R. C., Harris, T. G., Howard, B. V., Wylie-Rosett, J., Burk, R. D., & Strickler, H. D. (2009). Insulin, insulin-like growth factor-I, and risk of breast cancer in postmenopausal women. *Journal of the National Cancer Institute*, *101*(1), 48–60. https://doi.org/10.1093/jnci/djn415

Gunther, E. J., Belka, G. K., Wertheim, G. B. W., Wang, J., Hartman, J. L., Boxer, R. B., & Chodosh, L. A. (2002). A novel doxycycline-inducible system for the transgenic analysis of mammary gland biology. *The FASEB Journal*, *16*(3), 283–292. https://doi.org/10.1096/fj.01-0551com

Hemkens, L. G., Grouven, U., Bender, R., Günster, C., Gutschmidt, S., Selke, G. W., & Sawicki, P. T. (2009). Risk of malignancies in patients with diabetes treated with human insulin or insulin analogues: A cohort study. *Diabetologia*, *52*(9), 1732–1744. https://doi.org/10.1007/s00125-009-1418-4

Heuson, J. C., & Legros, N. (1972). Influence of Insulin Deprivation on Growth of the 7,12-Dimethylbenz(a)anthracene-induced Mammary Carcinoma in Rats Subjected to Alloxan Diabetes and Food Restriction. *Cancer Research*, *32*(2), 226–232.

Heuson, J. C., Legros, N., & Heimann, R. (1972). Influence of insulin administration on growth of the 7,12-dimethylbenz(a)anthracene-induced mammary carcinoma in intact, oophorectomized, and hypophysectomized rats. *Cancer Research*, *32*(2), 233–238.

Heymsfield, S. B., & Wadden, T. A. (2017). Mechanisms, Pathophysiology, and Management of Obesity. *New England Journal of Medicine*, *376*(3), 254–266. https://doi.org/10.1056/nejmra1514009

Hopkins, B. D., Goncalves, M. D., & Cantley, L. C. (2020). Insulin–PI3K signalling: an evolutionarily insulated metabolic driver of cancer. In *Nature Reviews Endocrinology* (Vol. 16, Issue 5, pp. 276–283). https://doi.org/10.1038/s41574-020-0329-9

Hu, S., Wang, L., Yang, D., Li, L., Togo, J., Wu, Y., Liu, Q., Li, B., Li, M., Wang, G., Zhang, X., Niu, C., Li, J., Xu, Y., Couper, E., Whittington-Davies, A., Mazidi, M., Luo, L., Wang, S., … Speakman, J. R. (2018). Dietary Fat, but Not Protein or Carbohydrate, Regulates Energy Intake and Causes Adiposity in Mice. *Cell Metabolism*, *28*(3), 415-431.e4. https://doi.org/10.1016/j.cmet.2018.06.010

Islami, F., Goding Sauer, A., Gapstur, S. M., & Jemal, A. (2019). Proportion of Cancer Cases Attributable to Excess Body Weight by US State, 2011-2015. *JAMA Oncology*, *5*(3), 384–392. https://doi.org/10.1001/jamaoncol.2018.5639

Joshi, P. A., Jackson, H. W., Beristain, A. G., Di Grappa, M. A., Mote, P. A., Clarke, C. L., Stingl, J., Waterhouse, P. D., & Khokha, R. (2010). Progesterone induces adult mammary stem cell expansion. *Nature*, *465*(7299), 803–807. https://doi.org/10.1038/nature09091

Kabat, G. C., Kim, M., Caan, B. J., Chlebowski, R. T., Gunter, M. J., Ho, G. Y. F., Rodriguez, B. L., Shikany, J. M., Strickler, H. D., Vitolins, M. Z., & Rohan, T. E. (2009). Repeated measures of serum glucose and insulin in relation to postmenopausal breast cancer. *International Journal of Cancer*, *125*(11), 2704–2710. https://doi.org/10.1002/ijc.24609

Kassambara A, Kosinski M, & Biecek P. (2021). _*survminer: Drawing Survival Curves using 'ggplot2'_.* (R package version 0.4.9). https://CRAN.R-project.org/package=survminer

Koboldt, D. C., Fulton, R. S., McLellan, M. D., Schmidt, H., Kalicki-Veizer, J., McMichael, J. F., Fulton, L. L., Dooling, D. J., Ding, L., Mardis, E. R., Wilson, R. K., Ally, A., Balasundaram, M., Butterfield, Y. S. N., Carlsen, R., Carter, C., Chu, A., Chuah, E., Chun, H. J. E., … Palchik, J. D. (2012). Comprehensive molecular portraits of human breast tumours. *Nature 2012 490:7418*, *490*(7418), 61–70. https://doi.org/10.1038/nature11412

Korotkevich, G., Sukhov, V., Budin, N., Shpak, B., Artyomov, M. N., & Sergushichev, A. (2021). Fast gene set enrichment analysis. *BioRxiv*, 060012. https://doi.org/10.1101/060012

Law, J. H., Habibi, G., Hu, K., Masoudi, H., Wang, M. Y. C., Stratford, A. L., Park, E., Gee, J. M. W., Finlay, P., Jones, H. E., Nicholson, R. I., Carboni, J., Gottardis, M., Pollak, M., & Dunn, S. E. (2008). Phosphorylated insulin-like growth factor-i/insulin receptor is present in all breast cancer subtypes and is related to poor survival. *Cancer Research*, *68*(24), 10238–10246. https://doi.org/10.1158/0008-5472.CAN-08-2755

Lazarus, R., Sparrow, D., & Weiss, S. (1998). Temporal relations between obesity and insulin: Longitudinal data from the normative aging study. *American Journal of Epidemiology*, *147*(2), 173–179. https://doi.org/10.1093/oxfordjournals.aje.a009431

Liao, Y., Smyth, G. K., & Shi, W. (2014). featureCounts: an efficient general purpose program for assigning sequence reads to genomic features. *Bioinformatics (Oxford, England)*, *30*(7), 923–930. https://doi.org/10.1093/BIOINFORMATICS/BTT656

Liu, X., Holstege, H., van der Gulden, H., Treur-Mulder, M., Zevenhoven, J., Velds, A., Kerkhoven, R. M., van Vliet, M. H., Wessels, L. F. A., Peterse, J. L., Berns, A., & Jonkers, J. (2007). Somatic loss of BRCA1 and p53 in mice induces mammary tumors with features of human BRCA1-mutated basal-like breast cancer. *Proc Natl Acad Sci U S A* ., *104*(29), 12111–12116. https://doi.org/https://doi.org/10.1073/pnas.0702969104

Livak, K. J., & Schmittgen, T. D. (2001). Analysis of Relative Gene Expression Data Using Real-Time Quantitative PCR and the 2−ΔΔCT Method. *Methods*, *25*(4), 402–408. https://doi.org/10.1006/METH.2001.1262

Louvi, A., Accili, D., & Efstratiadis, A. (1997). Growth-promoting interaction of IGF-II with the insulin receptor during mouse embryonic development. *Developmental Biology*, *189*(1), 33–48. https://doi.org/10.1006/dbio.1997.8666

Love, M. I., Huber, W., & Anders, S. (2014). Moderated estimation of fold change and dispersion for RNA-seq data with DESeq2. *Genome Biology*, *15*(12). https://doi.org/10.1186/S13059-014-0550-8

Lu, Y., Hajjar, A., Cryns, V. L., Trentham-Dietz, A., Gangnon, R. E., Heckman-Stoddard, B. M., & Alagoz, O. (2022). Breast cancer risk for women with diabetes and the impact of metformin: A meta-analysis. *Cancer Medicine*, *00*, 1–16. https://doi.org/10.1002/CAM4.5545

Martínez-Reyes, I., & Chandel, N. S. (2021). Cancer metabolism: looking forward. *Nature Reviews Cancer 2021 21:10*, *21*(10), 669–680. https://doi.org/10.1038/s41568-021-00378-6

Mookerjee, S. A., Gerencser, A. A., Nicholls, D. G., & Brand, M. D. (2017). Quantifying intracellular rates of glycolytic and oxidative ATP production and consumption using extracellular flux measurements. *Journal of Biological Chemistry*, *292*(17), 7189–7207. https://doi.org/10.1074/jbc.M116.774471

Mulligan, A. M., O'Malley, F. P., Ennis, M., Fantus, I. G., & Goodwin, P. J. (2007). Insulin receptor is an independent predictor of a favorable outcome in early stage breast cancer. *Breast Cancer Research and Treatment*, *106*(1), 39–47. https://doi.org/10.1007/S10549-006-9471-X/TABLES/5

Nagao, H., Cai, W., Wewer Albrechtsen, N. J., Steger, M., Batista, T. M., Pan, H., Dreyfuss, J. M., Mann, M., & Ronald Kahn, C. (2021). Distinct signaling by insulin and IGF-1 receptors and their extra- And intracellular domains. *Proceedings of the National Academy of Sciences of the United States of America*, *118*(17), e2019474118. https://doi.org/10.1073/PNAS.2019474118/SUPPL_FILE/PNAS.2019474118.SD01.XLSX

Nagao, H., Jayavelu, A. K., Cai, W., Pan, H., Dreyfuss, J. M., Batista, T. M., Brandão, B. B., Mann, M., & Kahn, C. R. (2023). Unique ligand and kinase-independent roles of the insulin receptor in regulation of cell cycle, senescence and apoptosis. *Nature Communications 2023 14:1*, *14*(1), 1–18. https://doi.org/10.1038/s41467-022-35693-5

Novosyadlyy, R., Lann, D. E., Vijayakumar, A., Rowzee, A., Lazzarino, D. A., Fierz, Y., Carboni, J. M., Gottardis, M. M., Pennisi, P. A., Molinolo, A. A., Kurshan, N., Mejia, W., Santopietro, S., Yakar, S., Wood, T. L., & LeRoith, D. (2010). Insulin-mediated acceleration of breast cancer development and progression in a nonobese model of type 2 diabetes. *Cancer Research*, *70*(2), 741–751. https://doi.org/10.1158/0008-5472.CAN-09-2141/655532/P/INSULIN-MEDIATED-ACCELERATION-OF-BREAST-CANCER

Pandini, G., Frasca, F., Mineo, R., Sciacca, L., Vigneri, R., & Belfiore, A. (2002). Insulin/insulin-like growth factor I hybrid receptors have different biological characteristics depending on the insulin receptor isoform involved. *Journal of*

Biological Chemistry, *277*(42), 39684–39695. https://doi.org/10.1074/jbc.M202766200

Pandini, G., Vigneri, R., Costantino, A., Frasca, F., Ippolito, A., Fujita-Yamaguchi, Y., Siddle, K., Goldfine, I. D., & Belifiore, A. (1999). Insulin and Insulin-like Growth Factor-I (IGF-I) Receptor Overexpression in Breast Cancers Leads to Insulin/IGF-I Hybrid Receptor Overexpression: Evidence for a Second Mechanism of IGF-I Signaling 1 . *Clinical Cancer Research*, *5*(7), 1935–1944. https://aacrjournals.org/clincancerres/article/5/7/1935/287640/Insulin-and-Insulin-like-Growth-Factor-I-IGF-I

Papa, V., Vincenzo Pezzino, I., Costantino, A., Belfiore, A., Giuffnda, D., Fnttitta, L., Vannelli, G. B., Brand, R., Goldfine, I. D., Vigneri, R., Trischitta, V., Brunetti, A., Goodman, P. A., Treutelaar, M. K., Williams, J. A., Maddux, B. A., Vigneri, R., & Goldfine, I. D. (1990). Elevated insulin receptor content in human breast cancer. *Journal of Clinical Investigation*, *86*(5), 1503. https://doi.org/10.1172/JCI114868

Payankaulam, S., Raicu, A. M., & Arnosti, D. N. (2019). Transcriptional Regulation of INSR, the Insulin Receptor Gene. *Genes*, *10*(12). https://doi.org/10.3390/GENES10120984

Pereira, B., Chin, S. F., Rueda, O. M., Vollan, H. K. M., Provenzano, E., Bardwell, H. A., Pugh, M., Jones, L., Russell, R., Sammut, S. J., Tsui, D. W. Y., Liu, B., Dawson, S. J., Abraham, J., Northen, H., Peden, J. F., Mukherjee, A., Turashvili, G., Green, A. R., … Caldas, C. (2016). The somatic mutation profiles of 2,433 breast cancers refine their genomic and transcriptomic landscapes. *Nature Communications 2016 7:1*, *7*(1), 1–16. https://doi.org/10.1038/ncomms11479

Peterson, H., Kolberg, L., Raudvere, U., Kuzmin, I., & Vilo, J. (2020). gprofiler2 -- an R package for gene list functional enrichment analysis and namespace conversion toolset g: Profiler. *F1000Research*, *9*. https://doi.org/10.12688/F1000RESEARCH.24956.2/DOI

Pfefferle, A. D., Herschkowitz, J. I., Usary, J., Harrell, J. C., Spike, B. T., Adams, J. R., Torres-Arzayus, M. I., Brown, M., Egan, S. E., Wahl, G. M., Rosen, J. M., & Perou, C. M. (2013). Transcriptomic classification of genetically engineered mouse models of breast cancer identifies human subtype counterparts. *Genome Biology*, *14*(11). https://doi.org/10.1186/gb-2013-14-11-r125

Poloz, Y., & Stambolic, V. (2015). Obesity and cancer, a case for insulin signaling. *Cell Death & Disease*, *6*(12), e2037. https://doi.org/10.1038/cddis.2015.381

Ran, F. A., Hsu, P. D., Wright, J., Agarwala, V., Scott, D. A., & Zhang, F. (2013). Genome engineering using the CRISPR-Cas9 system. *Nature Protocols*, *8*(11), 2281–2308. https://doi.org/10.1038/NPROT.2013.143

Rao, T., Ranger, J. J., Smith, H. W., Lam, S. H., Chodosh, L., & Muller, W. J. (2014). Inducible and coupled expression of the polyomavirus middle T antigen and Cre recombinase in transgenic mice: An in vivo model for synthetic viability in mammary tumour progression. *Breast Cancer Research*, *16*(1). https://doi.org/10.1186/bcr3603

Rodríguez-Enríquez, S., Juárez, O., Rodríguez-Zavala, J. S., & Moreno-Sánchez, R. (2001). Multisite control of the Crabtree effect in ascites hepatoma cells. *European Journal of Biochemistry*, *268*(8), 2512–2519. https://doi.org/10.1046/J.1432-1327.2001.02140.X

Rose, D. P., Haffner, S. M., & Baillargeon, J. (2007). Adiposity, the Metabolic Syndrome, and Breast Cancer in African-American and White American Women. *Endocrine Reviews*, *28*(7), 763–777. https://doi.org/10.1210/ER.2006-0019

Saltiel, A. R. (2021). Insulin signaling in health and disease. In *Journal of Clinical Investigation* (Vol. 131, Issue 1). American Society for Clinical Investigation. https://doi.org/10.1172/JCI142241

Schaffhausen, B. S., & Roberts, T. M. (2009). Lessons from polyoma middle T antigen on signaling and transformation: A DNA tumor virus contribution to the war on cancer. In *Virology* (Vol. 384, Issue 2, pp. 304–316). https://doi.org/10.1016/j.virol.2008.09.042

Schoemaker, M. J., Nichols, H. B., Wright, L. B., Brook, M. N., Jones, M. E., O'Brien, K. M., Adami, H. O., Baglietto, L., Bernstein, L., Bertrand, K. A., Boutron-Ruault, M. C., Braaten, T., Chen, Y., Connor, A. E., Dorronsoro, M., Dossus, L., Eliassen, A. H., Giles, G. G., Hankinson, S. E., … Swerdlow, A. J. (2018). Association of Body Mass Index and Age With Subsequent Breast Cancer Risk in Premenopausal Women. *JAMA Oncology*, *4*(11), e181771–e181771. https://doi.org/10.1001/JAMAONCOL.2018.1771

Simond, A. M., & Muller, W. J. (2020). In vivo modeling of the EGFR family in breast cancer progression and therapeutic approaches. In *Advances in Cancer Research* (Vol. 147, pp. 189–228). Academic Press. https://doi.org/10.1016/bs.acr.2020.04.004

Slaaby, R. (2015). Specific insulin/IGF1 hybrid receptor activation assay reveals IGF1 as a more potent ligand than insulin. *Scientific Reports*, *5*. https://doi.org/10.1038/SREP07911

Soule, H. D., Maloney, T. M., Wolman, S. R., Brenz, R., Russo, J., Pauley, R. J., Jones, R. F., Brooks, S. C., & McGrath, C. M. (1990). Isolation and Characterization of a Spontaneously Immortalized Human Breast Epithelial Cell Line, MCF-10. *Cancer Research*, *50*(18), 6075–6086.

Teras, L. R., Patel, A. V, Wang, M., Yaun, S. S., Anderson, K., Brathwaite, R., Caan, B. J., Chen, Y., Connor, A. E., Eliassen, A. H., Gapstur, S. M., Gaudet, M. M., Genkinger, J. M., Giles, G. G., Lee, I. M., Milne, R. L., Robien, K., Sawada, N., Sesso, H. D., … Smith-Warner, S. A. (2020). Sustained Weight Loss and Risk of Breast Cancer in Women 50 Years and Older: A Pooled Analysis of Prospective Data. *Journal of the National Cancer Institute*, *112*(9), 929–937. https://doi.org/10.1093/jnci/djz226

Terry M. Therneau, & Patricia M. Grambsch. (2000). _*Modeling Survival Data: Extending the Cox Model*_. Springer.

Therneau T. (2022). _*A Package for Survival Analysis in R*_. (R package version 3.3-1). https://CRAN.R-project.org/package=survival

Tsherniak, A., Vazquez, F., Montgomery, P. G., Weir, B. A., Kryukov, G., Cowley, G. S., Gill, S., Harrington, W. F., Pantel, S., Krill-Burger, J. M., Meyers, R. M., Ali, L., Goodale, A., Lee, Y., Jiang, G., Hsiao, J., Gerath, W. F. J., Howell, S., Merkel, E., … Hahn, W. C. (2017). Defining a Cancer Dependency Map. *Cell*, *170*(3), 564-576.e16. https://doi.org/10.1016/j.cell.2017.06.010

Ursini-Siegel, J., Hardy, W. R., Zuo, D., Lam, S. H. L., Sanguin-Gendreau, V., Cardiff, R. D., Pawson, T., & Muller, W. J. (2008). ShcA signalling is essential for tumour progression in mouse models of human breast cancer. *EMBO Journal*, *27*(6), 910–920. https://doi.org/10.1038/emboj.2008.22

Vella, V., Milluzzo, A., Scalisi, N. M., Vigneri, P., & Sciacca, L. (2018). Insulin receptor isoforms in cancer. In *International Journal of Molecular Sciences* (Vol. 19, Issue 11). https://doi.org/10.3390/ijms19113615

Vigneri, R., Goldfine, I. D., & Frittitta, L. (2016). Insulin, insulin receptors, and cancer. *Journal of Endocrinological Investigation*, *39*(12), 1365–1376. https://doi.org/10.1007/S40618-016-0508-7/FIGURES/8

Warburg, O. (1925). The Metabolism of Carcinoma Cells. *The Journal of Cancer Research*, *9*(1), 148–163. https://doi.org/10.1158/JCR.1925.148

Warburg, O., Wind, F., & Negelein, E. (1927). THE METABOLISM OF TUMORS IN THE BODY. *Journal of General Physiology*, *8*(6), 519–530. https://doi.org/10.1085/JGP.8.6.519

Weinstein, J. N., Collisson, E. A., Mills, G. B., Shaw, K. R. M., Ozenberger, B. A., Ellrott, K., Sander, C., Stuart, J. M., Chang, K., Creighton, C. J., Davis, C., Donehower, L., Drummond, J., Wheeler, D., Ally, A., Balasundaram, M., Birol, I., Butterfield, Y. S.

N., Chu, A., … Kling, T. (2013). The cancer genome atlas pan-cancer analysis project. *Nature Genetics*, *45*(10), 1113–1120. https://doi.org/10.1038/ng.2764

Werner, R. L., Nekritz, E. A., Yan, K. K., Ju, B., Shaner, B., Easton, J., Yu, J., & Silva, J. (2022). Single-cell analysis reveals the Comma-1D cell line as a unique model for mammary gland development and breast cancer. *Journal of Cell Science*, *135*(10). https://doi.org/10.1242/JCS.259329

White, M. F., & Kahn, C. R. (2021). Insulin action at a molecular level – 100 years of progress. In *Molecular Metabolism* (Vol. 52). https://doi.org/10.1016/j.molmet.2021.101304

World Health Organization. (2021). *Obesity and Overweight*. https://www.who.int/news-room/fact-sheets/detail/obesity-and-overweight

Yuan, T. L., & Cantley, L. C. (2008). PI3K pathway alterations in cancer: variations on a theme. *Oncogene*, *27*(41), 5497–5510.

Zhang, A. M. Y., Magrill, J., de Winter, T. J. J., Hu, X., Skovsø, S., Schaeffer, D. F., Kopp, J. L., & Johnson, J. D. (2019). Endogenous Hyperinsulinemia Contributes to Pancreatic Cancer Development. In *Cell Metabolism* (Vol. 30, Issue 3, pp. 403–404). Cell Press. https://doi.org/10.1016/j.cmet.2019.07.003

Zhang, H., Fagan, D. H., Zeng, X., Freeman, K. T., Sachdev, D., & Yee, D. (2010). Inhibition of cancer cell proliferation and metastasis by insulin receptor downregulation. *Oncogene*, *29*(17), 2517–2527. https://doi.org/10.1038/onc.2010.17

A

Reference	Metric	Normal Breast	Breast Cancer
Papa et al., 1990	INSR content (ng/0.1 ug protein) [n]	0.95 ± 0.68 [27]	6.15 ± 3.69 [159]
Frasca et al., 1999	INSR content (ng/0.1 ug protein) [n]	0.5 ± 0.3 [12]	3.2 ± 1.8 [12]
Frasca et al., 1999	Proportion INSR-A in total INSR mRNA (Range % (Median %) [n])	30-50 (43) [12]	40-80 (73) [12]
Reference	**Metric**	**INSR low**	**INSR high**
Mulligan et al., 2007	Proportion (%) of BC samples [n]	12 [22]	88 [156]
Dowling et al., 2015	Proportion (%) of BC samples [n]	18 [7]	82 [32]
Chang et al., 2016	Proportion (%) of BC samples [n]	28 [36]	72 [93]

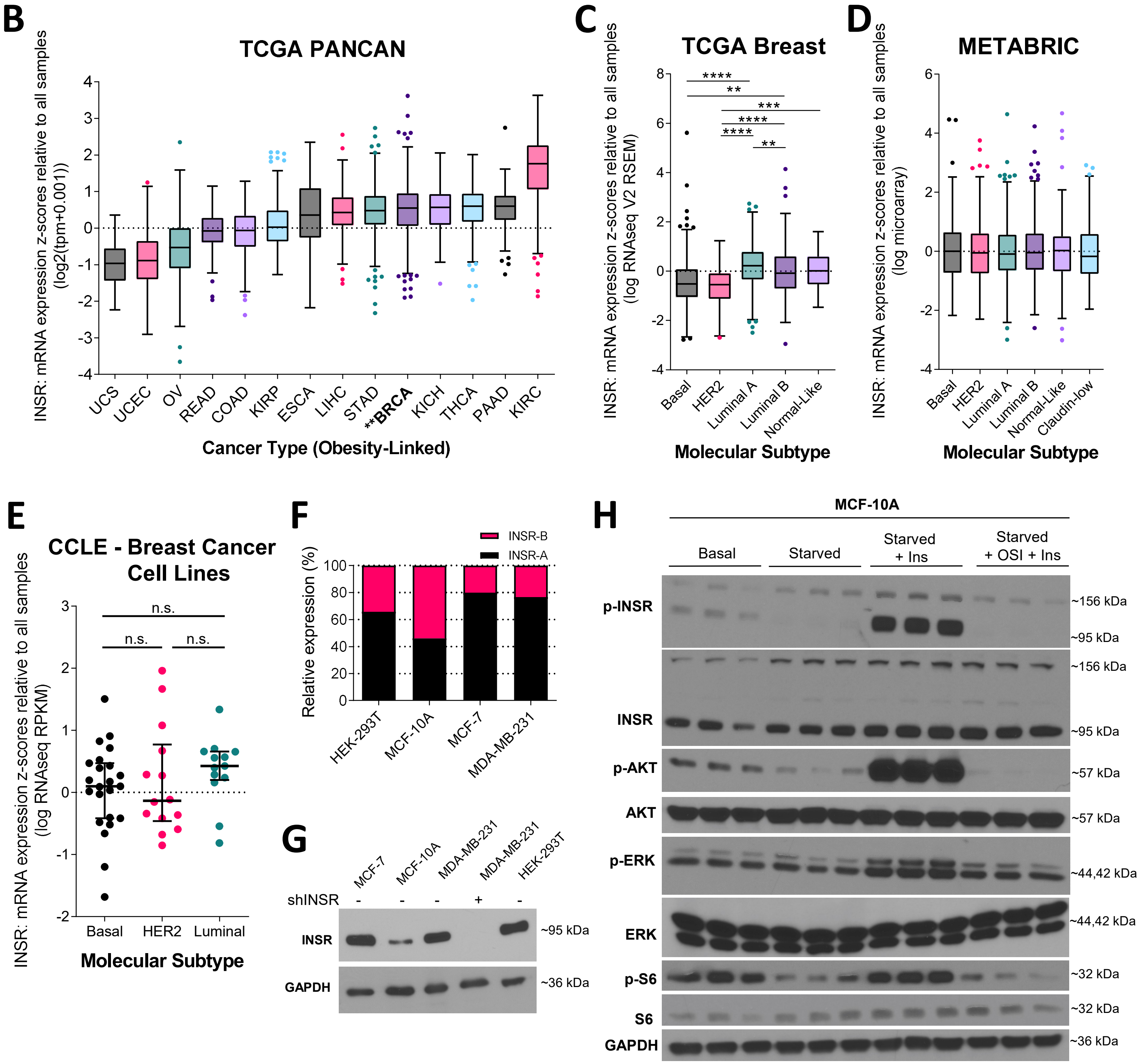

Figure 1: ***INSR expression in human breast cancer*.**

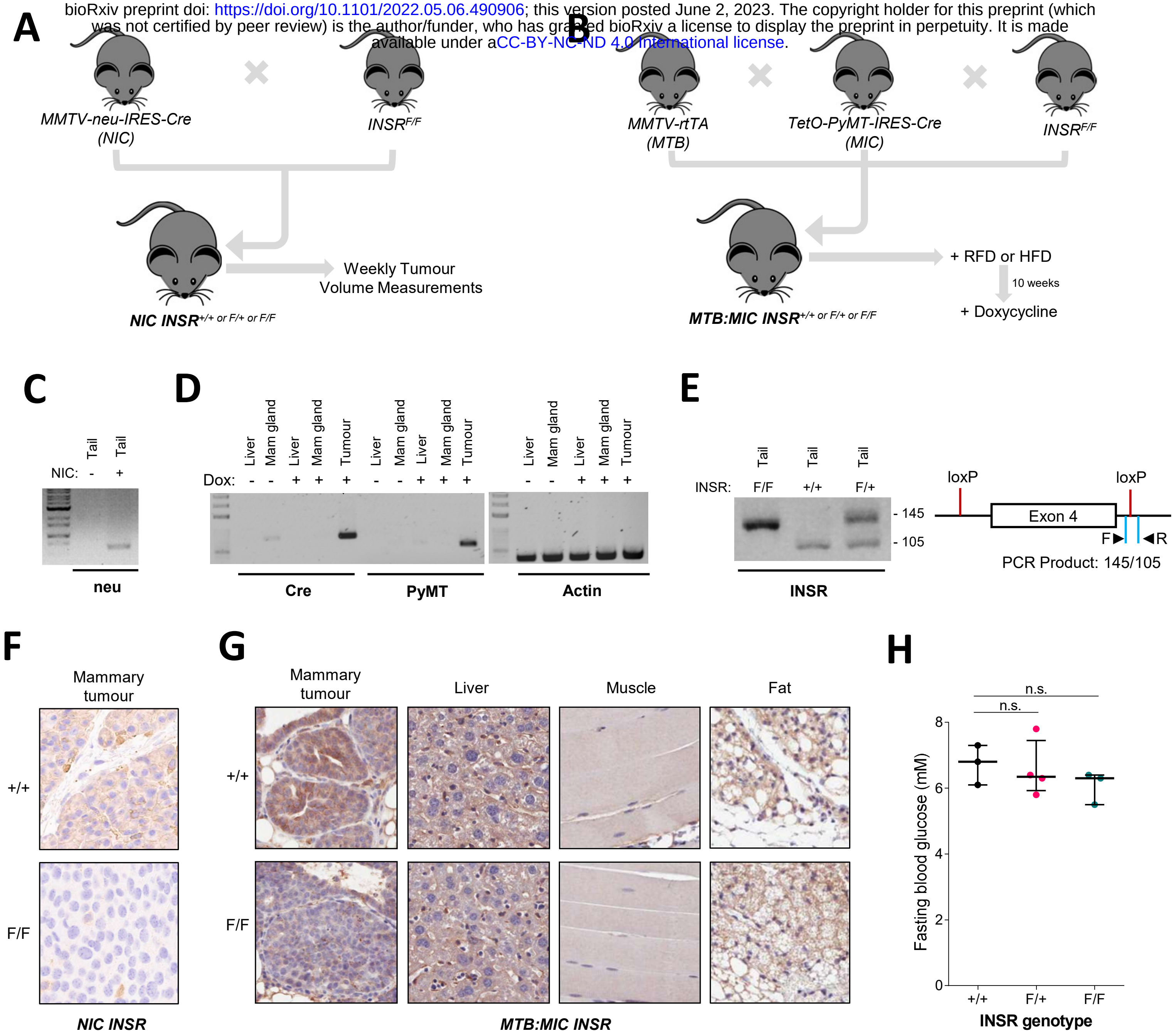

Figure 2: ***Generation of genetic mouse models of breast cancer with conditional deletion of INSR.***

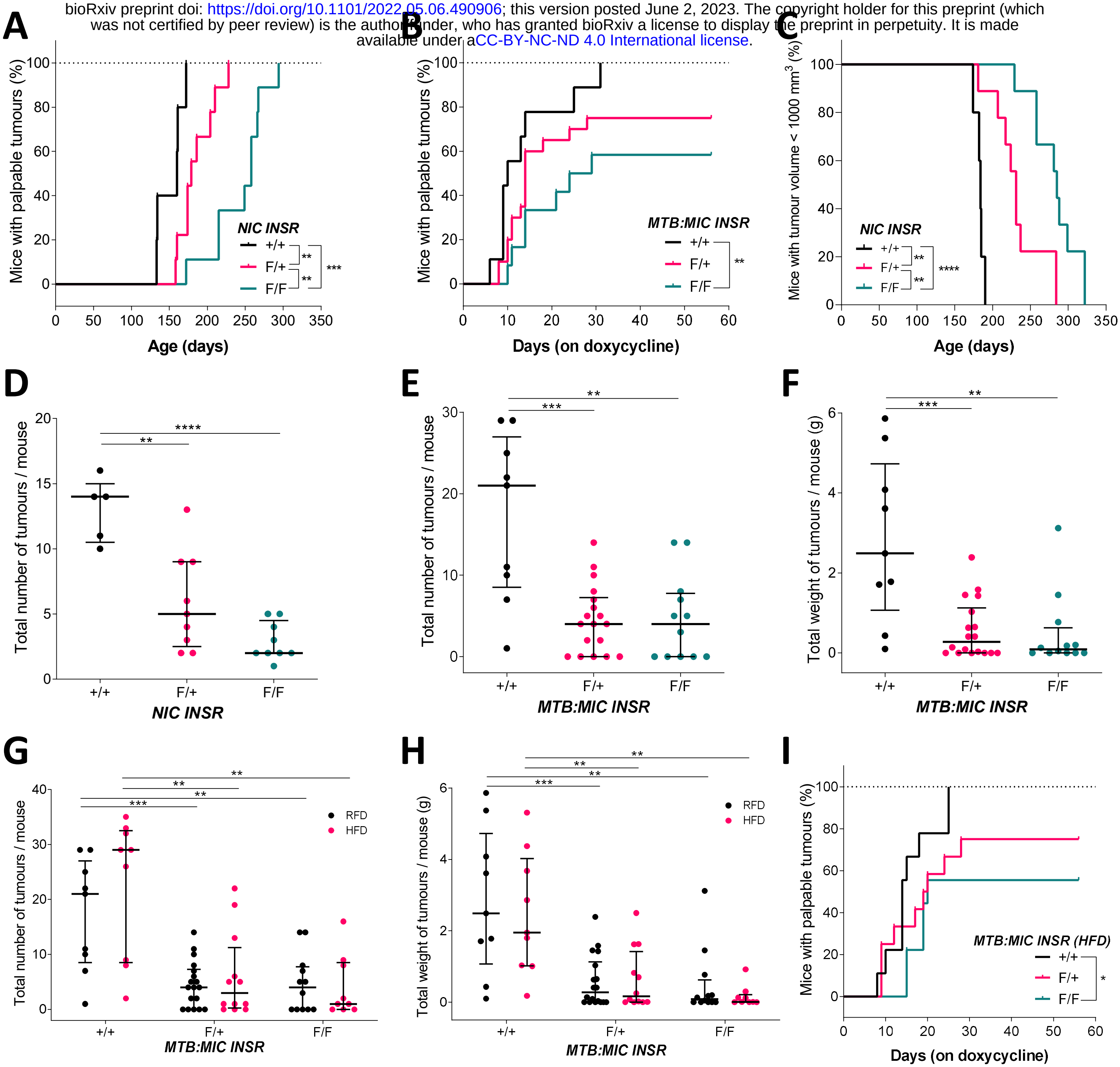

Figure 3*: Loss of INSR delays mammary tumour onset, prolongs survival and reduces tumour burden in vivo.*

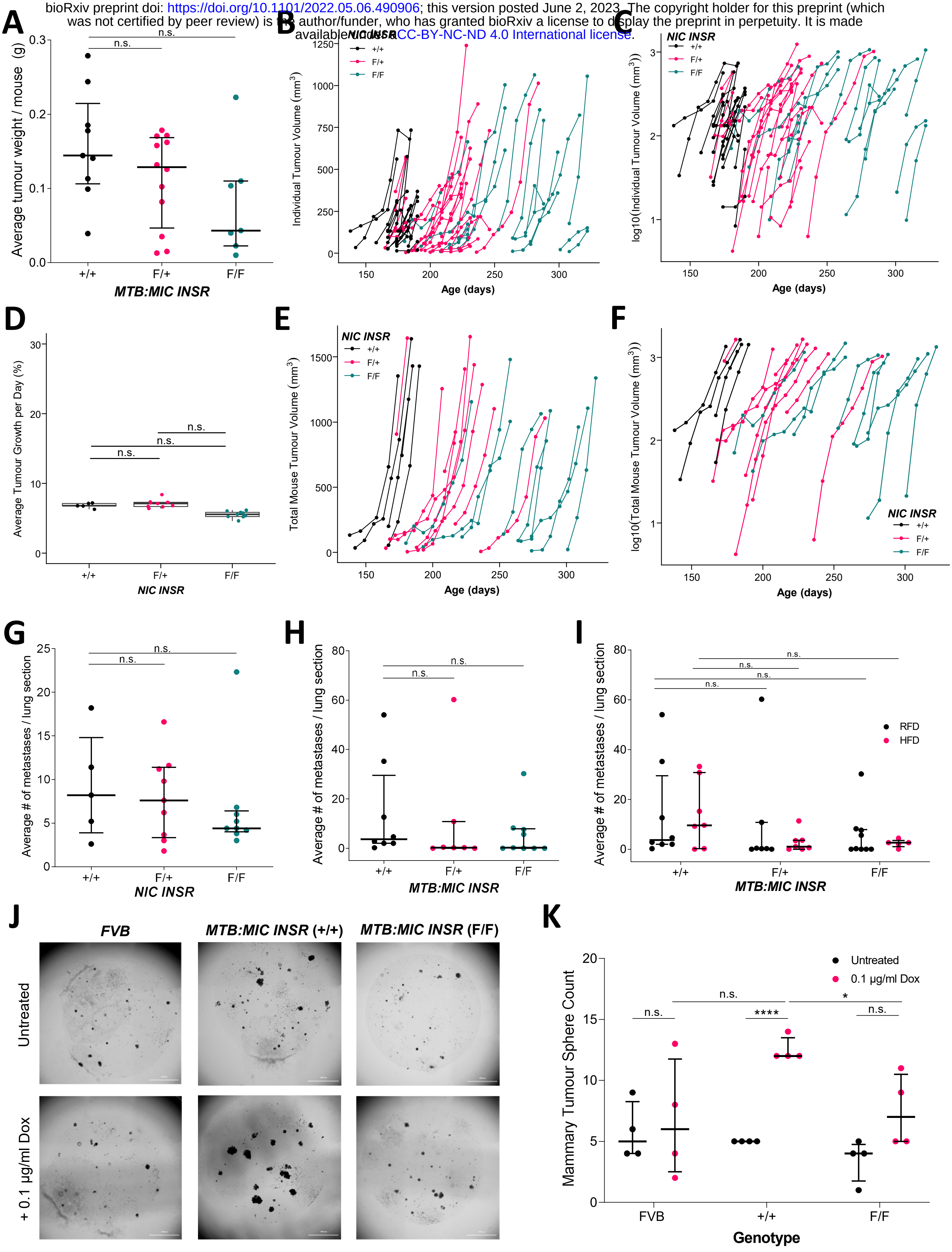

Figure 4: ***Loss of INSR impairs tumour initiation, but does not impact tumour progression or metastasis.***

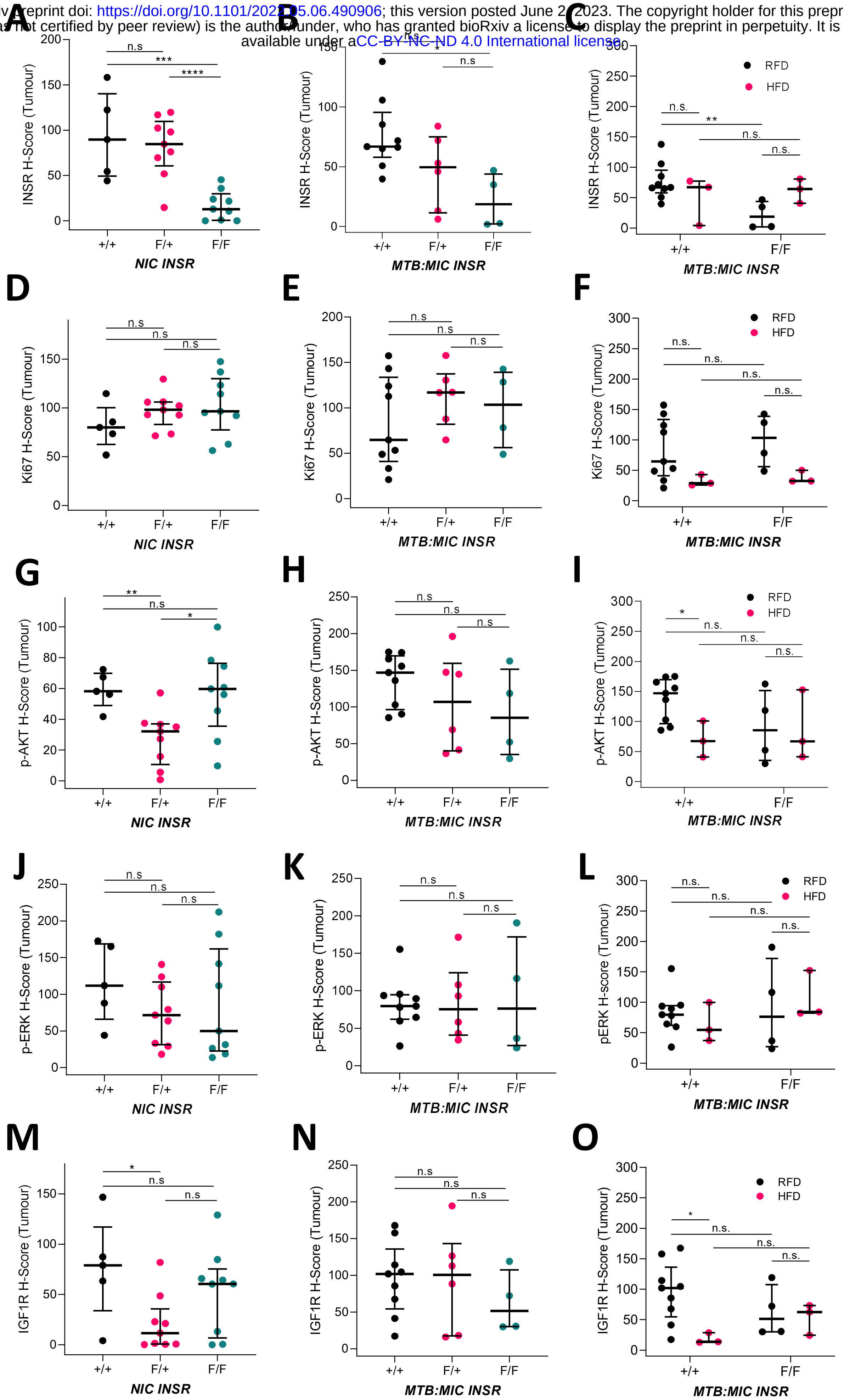

Figure 5: ***INSR-deficient tumours display no difference in canonical signaling downstream of INSR.***

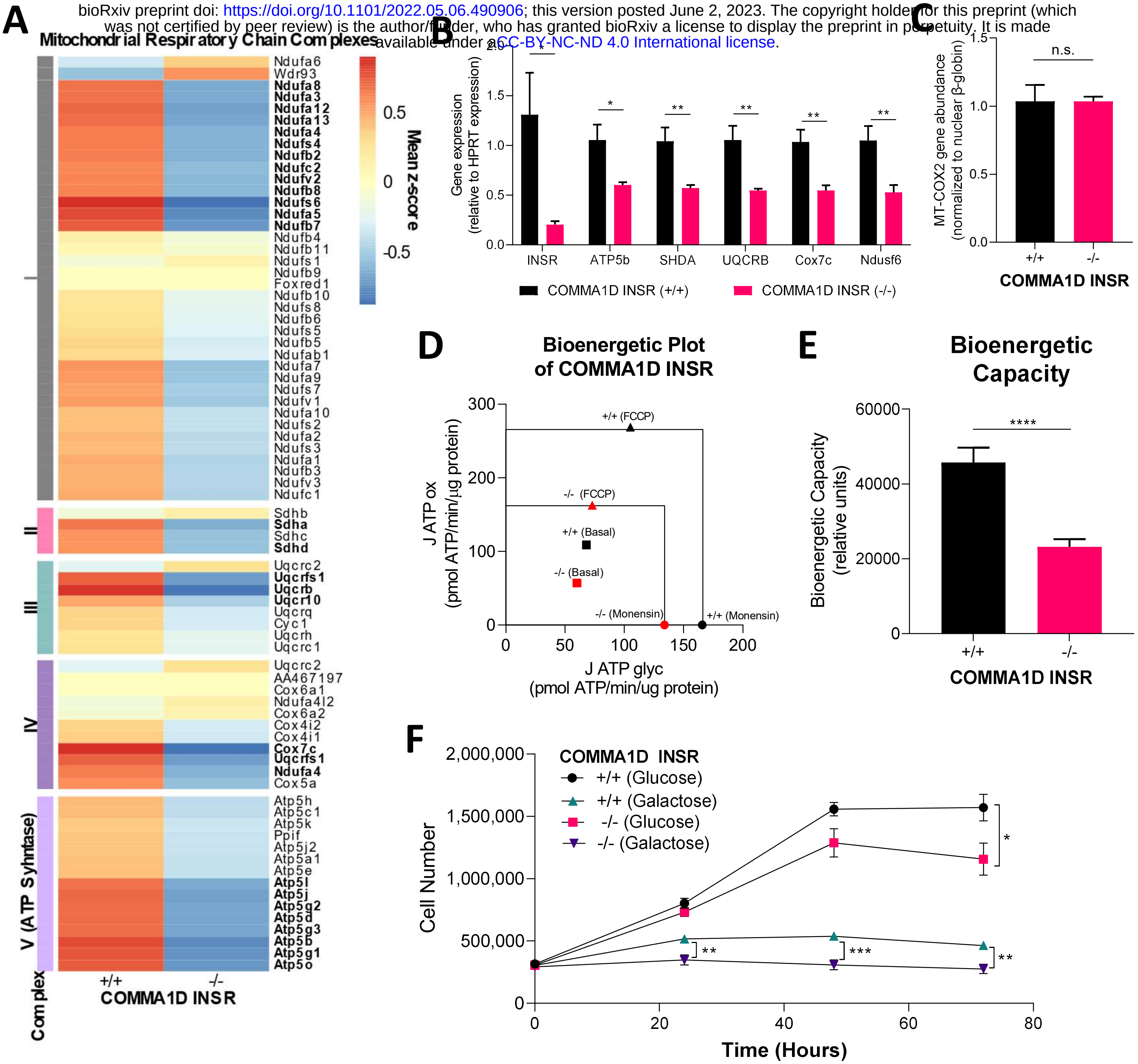

Figure 6: ***INSR loss in mammary epithelial cells reduces bioenergetic capacity.***

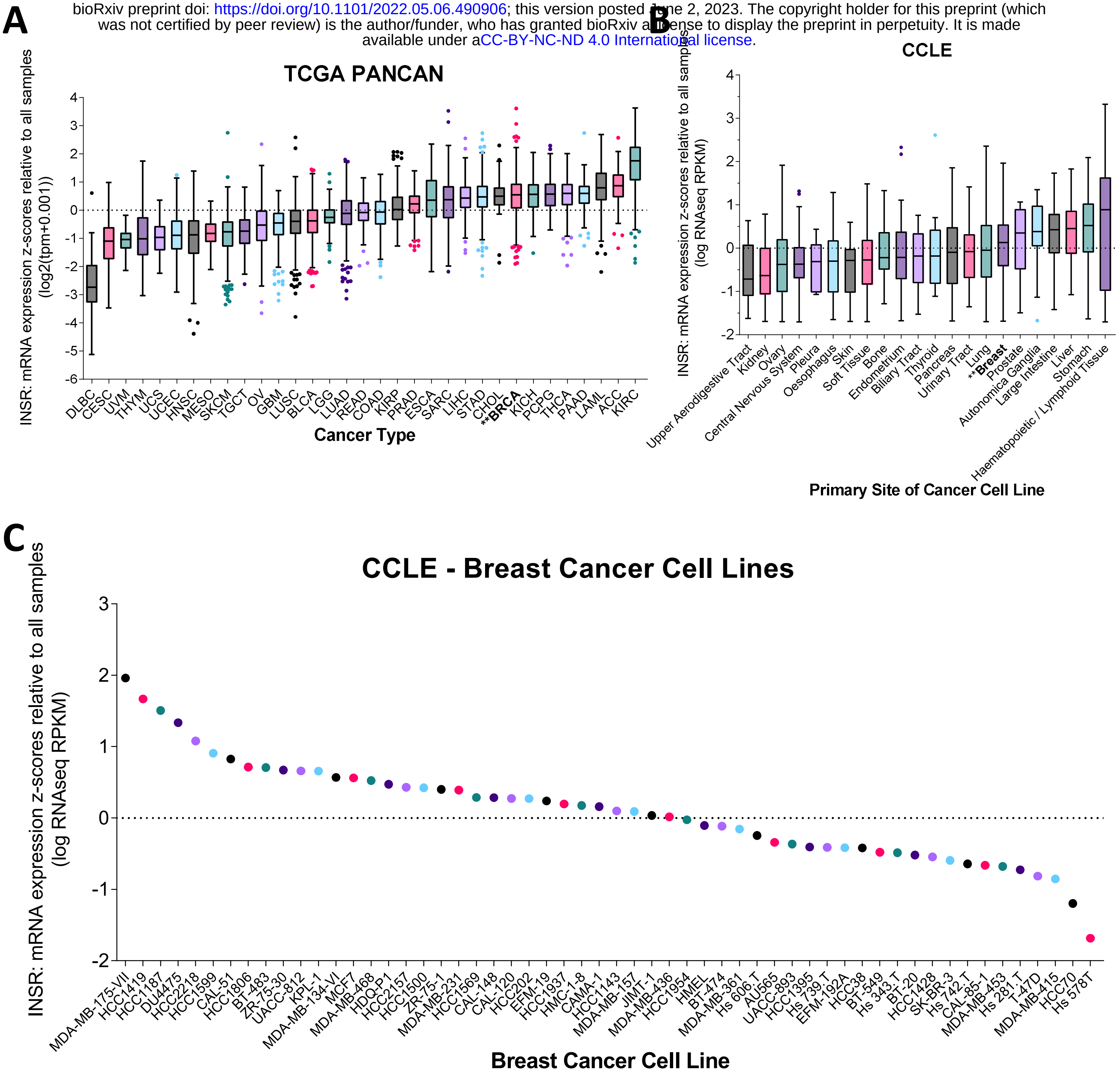

Supplementary Figure 1: ***INSR expression across cancer types and cell lines.***

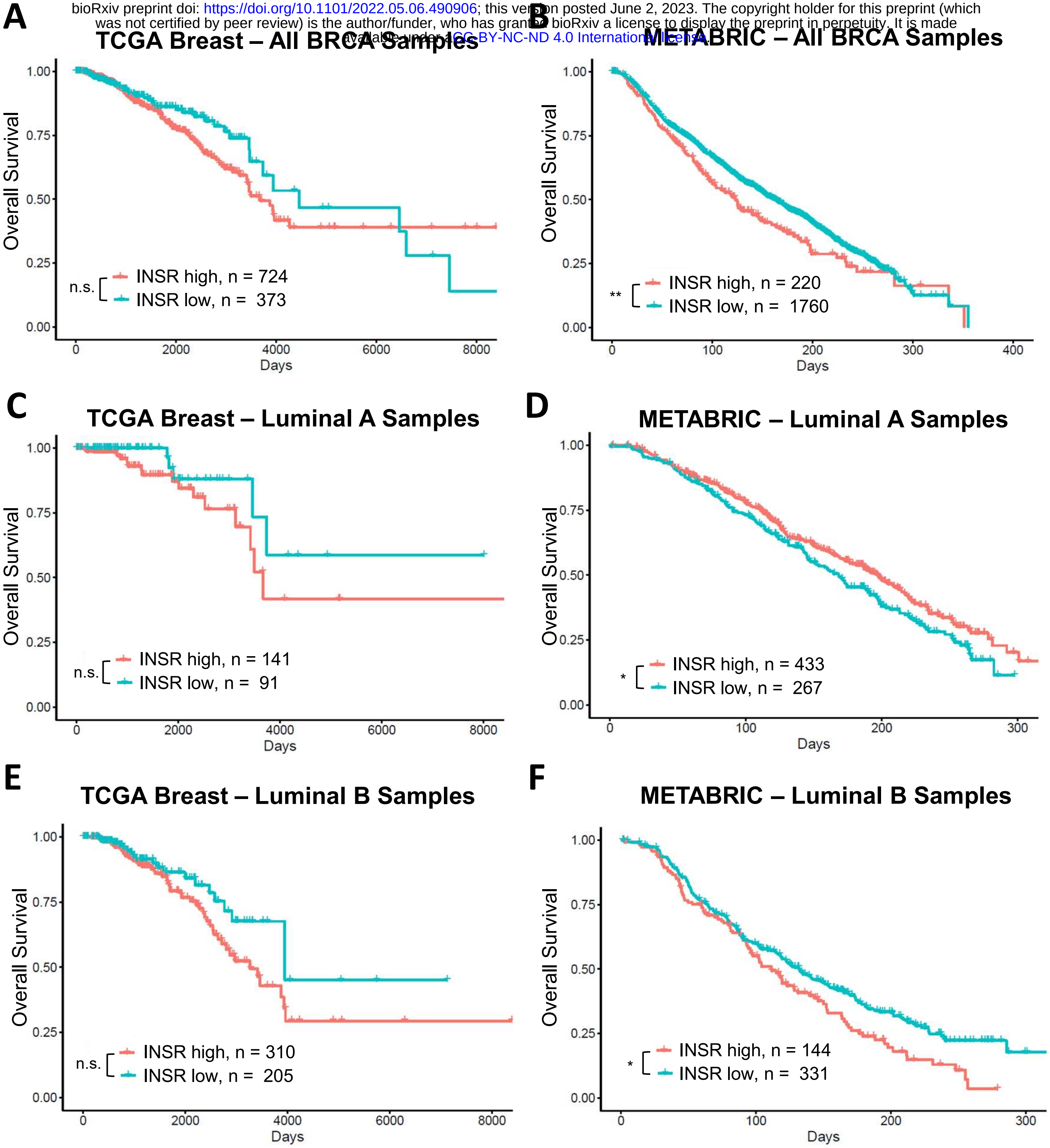

Supplementary Figure 2: ***Impact of INSR expression on overall survival for all samples and luminal subtype samples in TCGA Breast and METABRIC.***

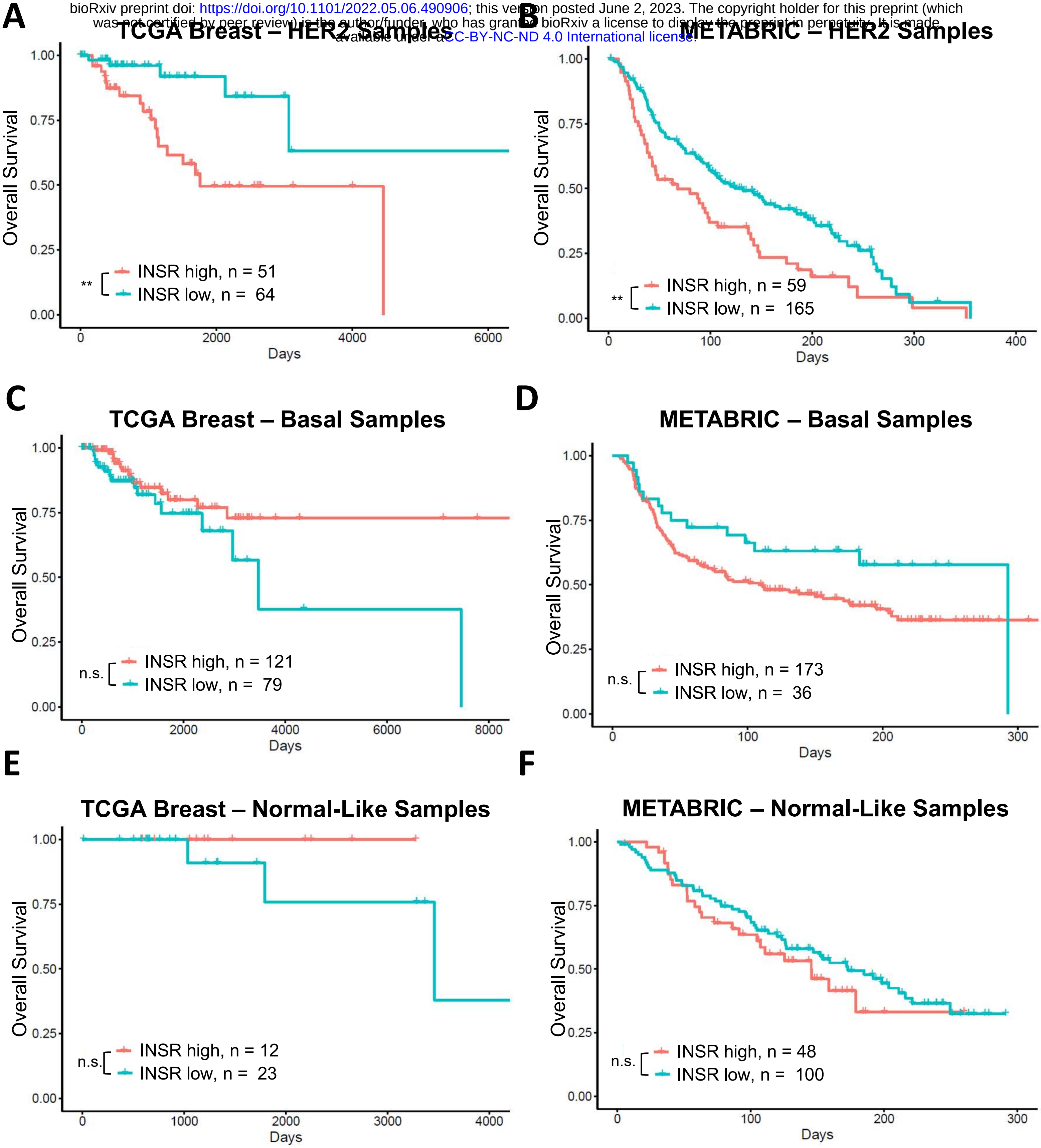

Supplementary Figure 3: ***Impact of INSR expression on overall survival for HER2, basal, and normal-like subtype samples in TCGA Breast and METABRIC.***

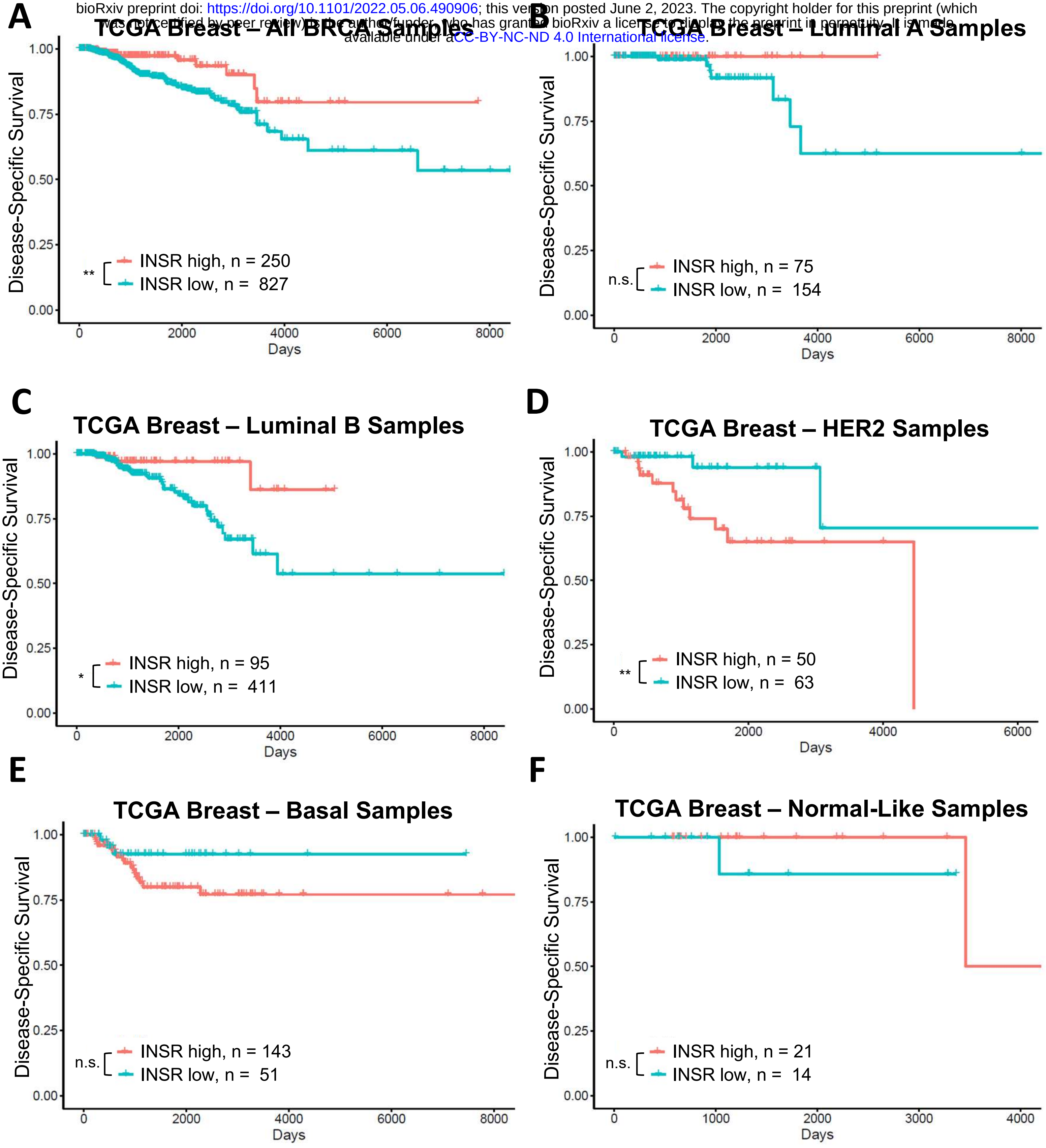

Supplementary Figure 4: ***Impact of INSR expression on disease-specific survival in TCGA Breast.***

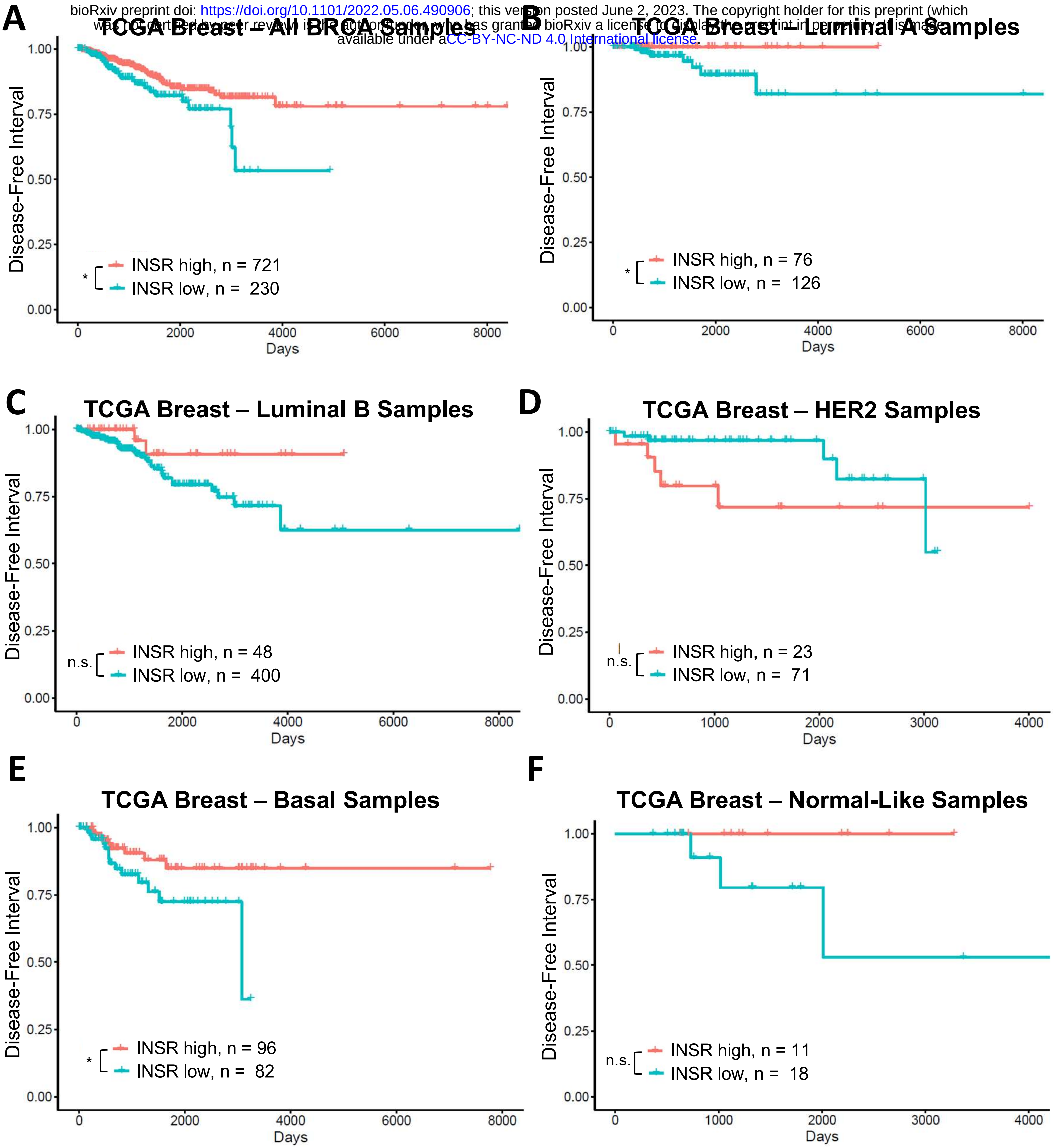
A TCGA Breast – All BRCA Samples

B TCGA Breast – Luminal A Samples

C TCGA Breast – Luminal B Samples

D TCGA Breast – HER2 Samples

E TCGA Breast – Basal Samples

F TCGA Breast – Normal-Like Samples

Supplementary Figure 5: ***Impact of INSR expression on disease-free interval in TCGA Breast.***

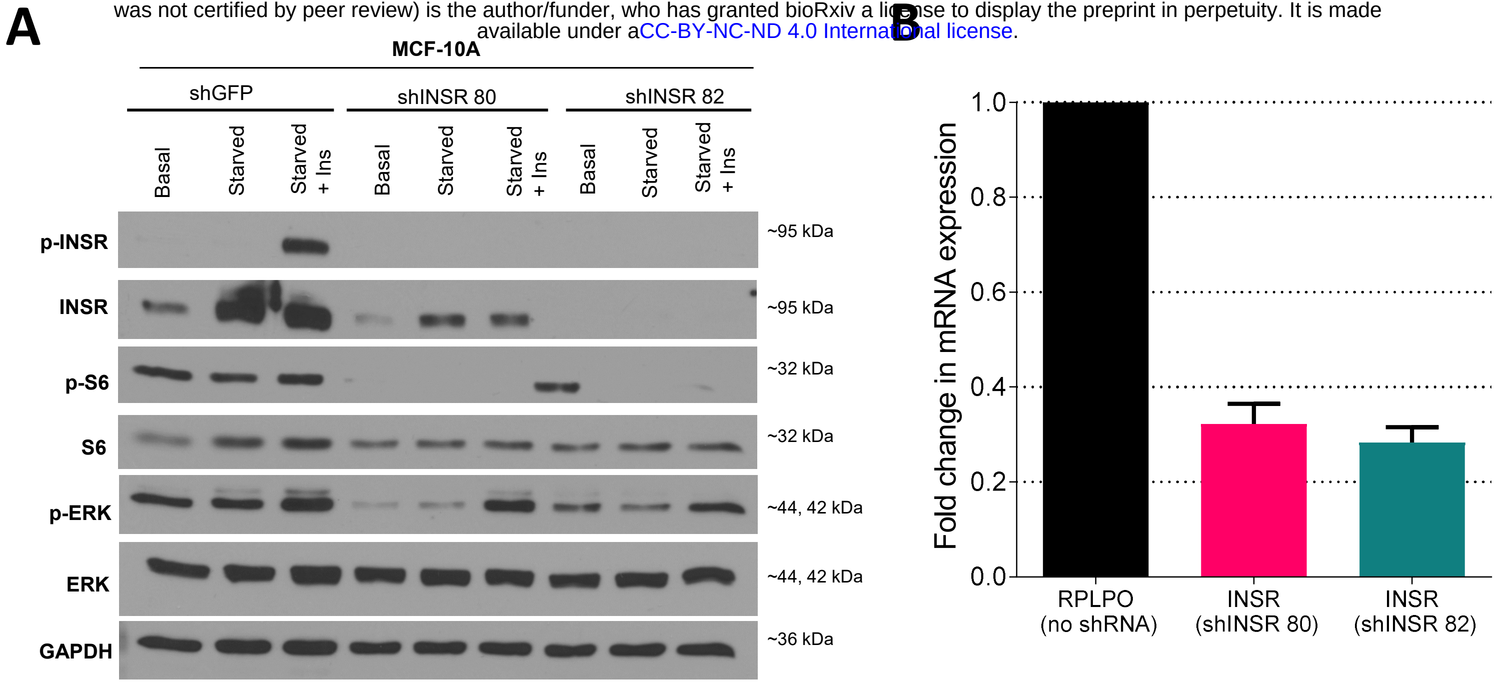

Supplementary Figure 6: ***INSR signalling in mammary epithelial cells.***

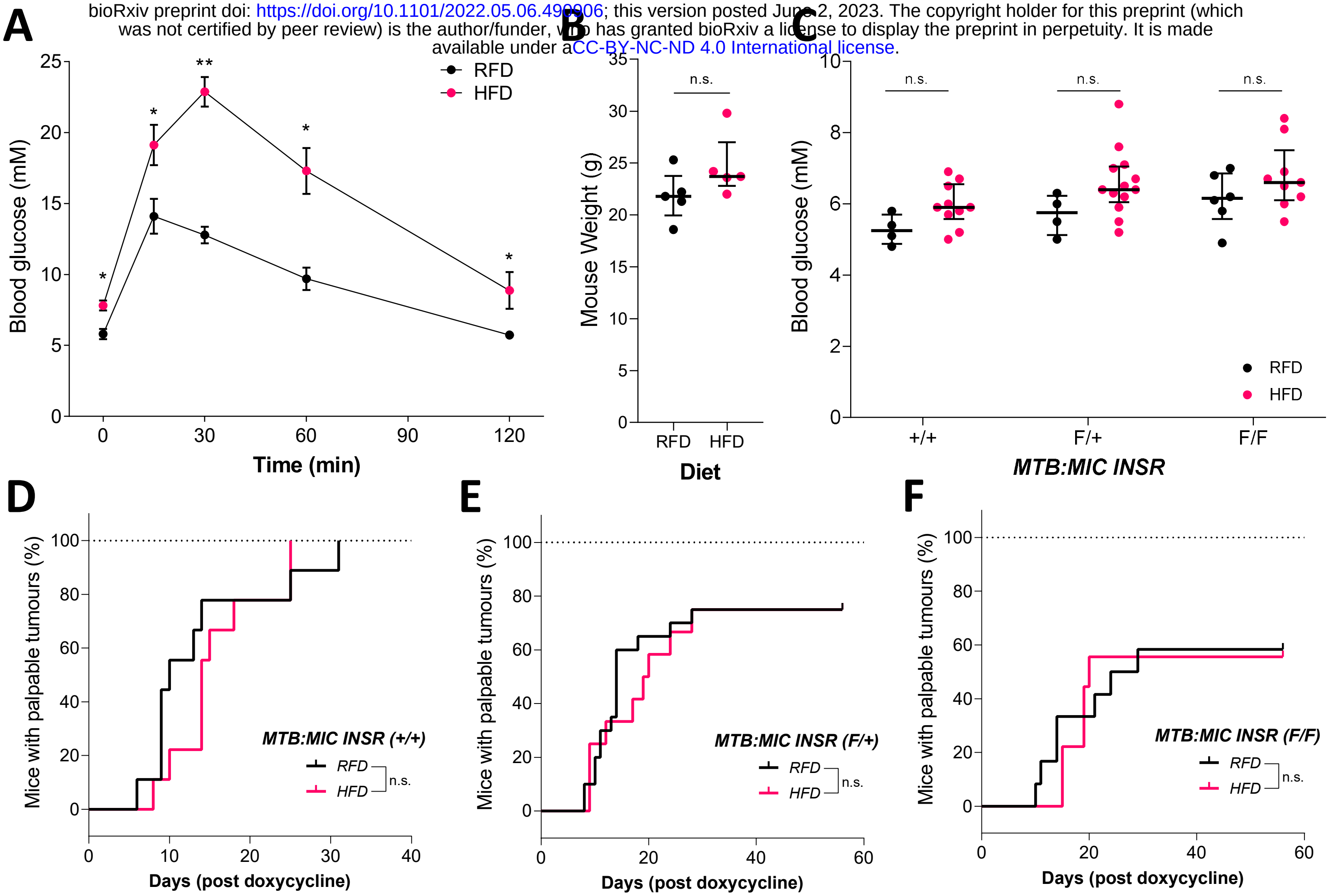

Supplementary Figure 7: ***High fat diet recapitulates obese conditions in mice.***

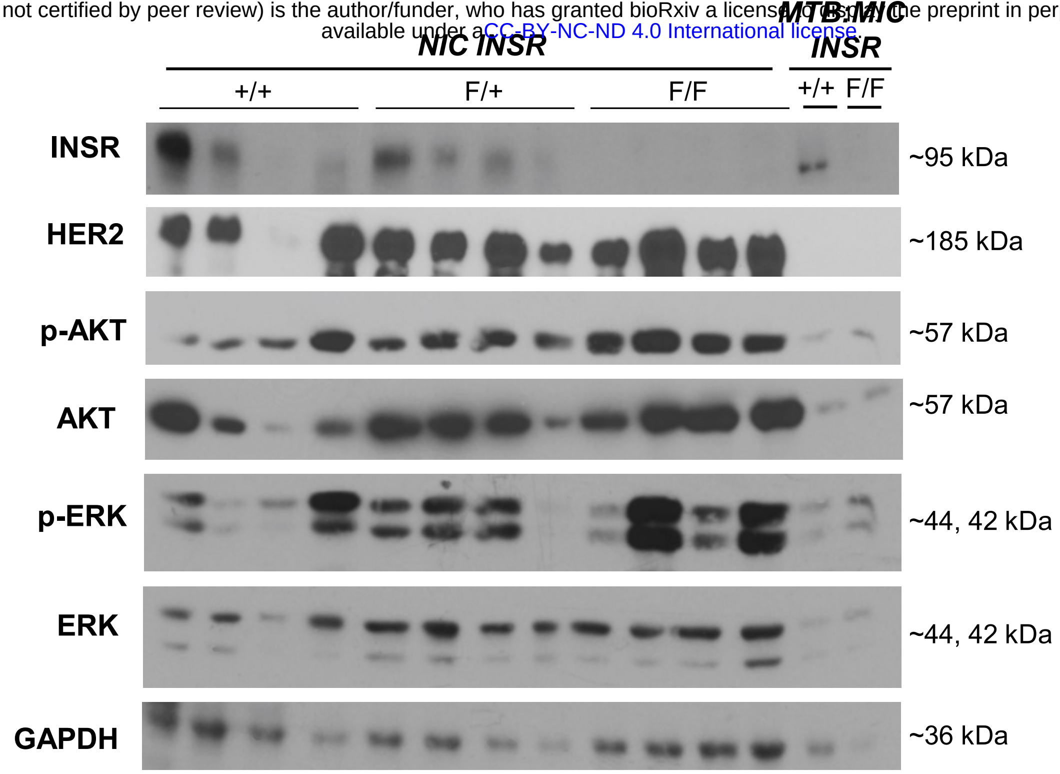

Supplementary Figure 8: *Immunoblotting analysis of NIC INSR and MTB:MIC INSR tumour lysates.*

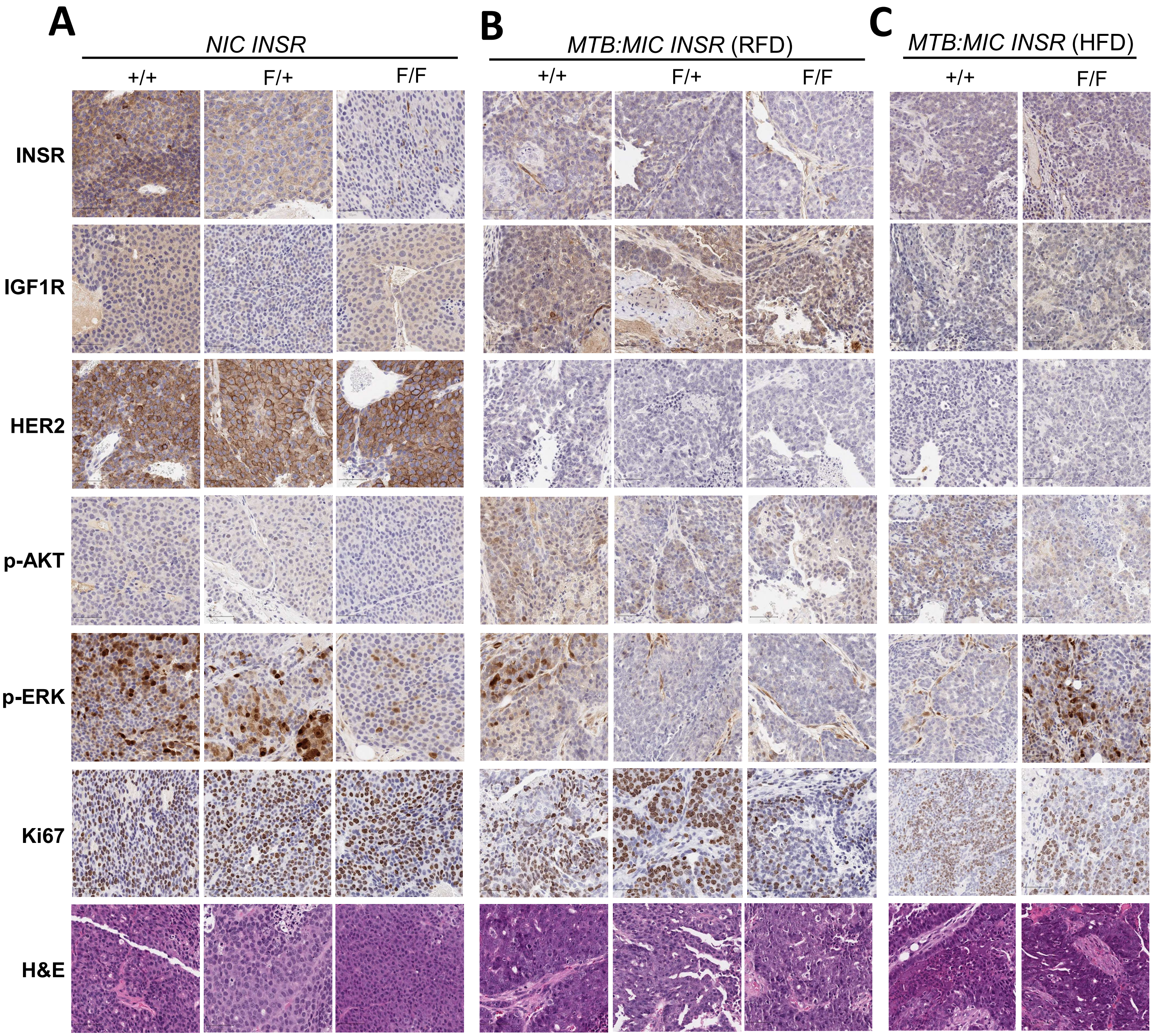

Supplementary Figure 9: ***Immunohistochemistry of NIC INSR and MTB:MIC INSR tumour sections.***

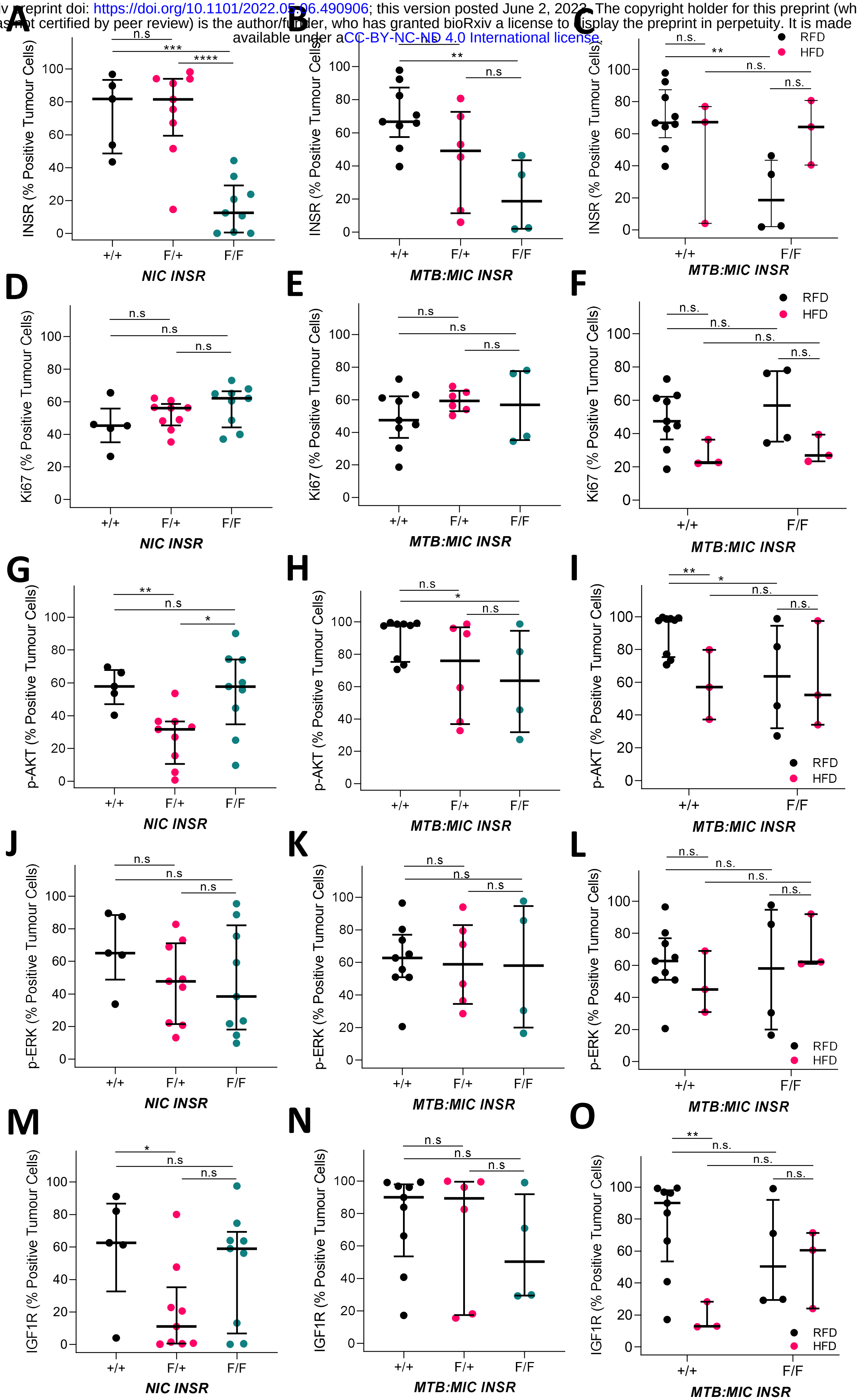

Supplementary Figure 10: ***Semi-automated digital image analysis of NIC and MTB:MIC tumour sections.***

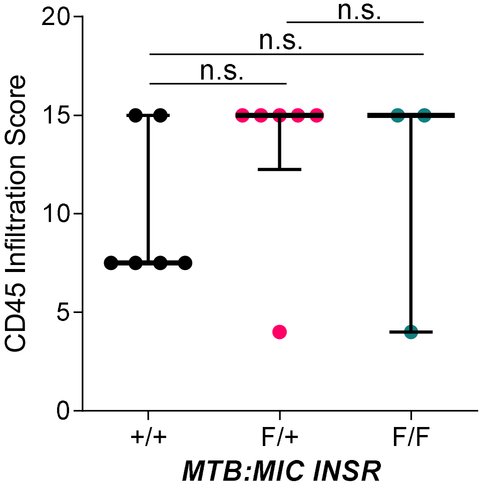

Supplementary Figure 11: ***INSR loss does not impact immune infiltration in progressing mammary tumours.***

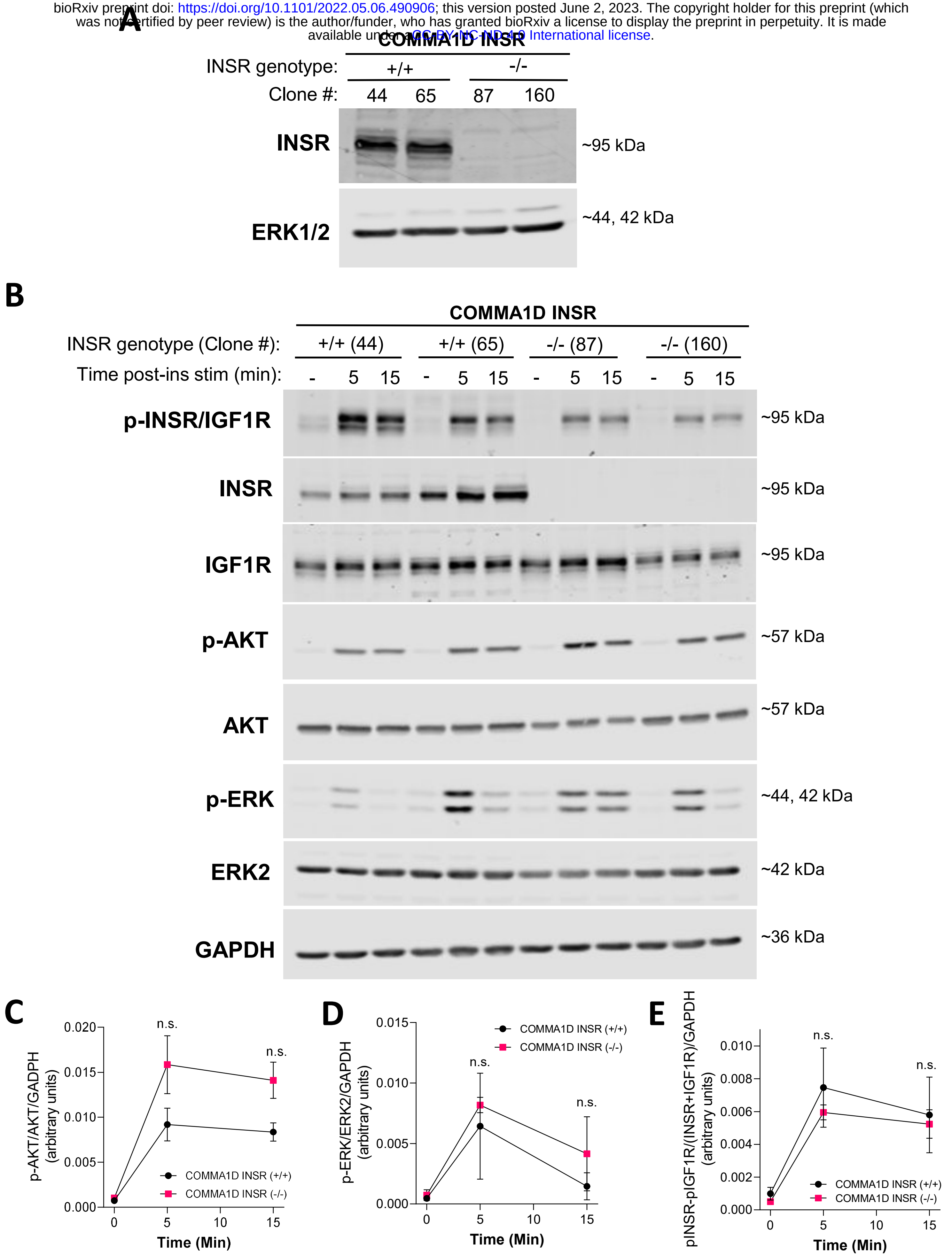

Supplementary Figure 12: ***INSR loss in murine mammary epithelial cells does not impact canonical INSR signaling.***

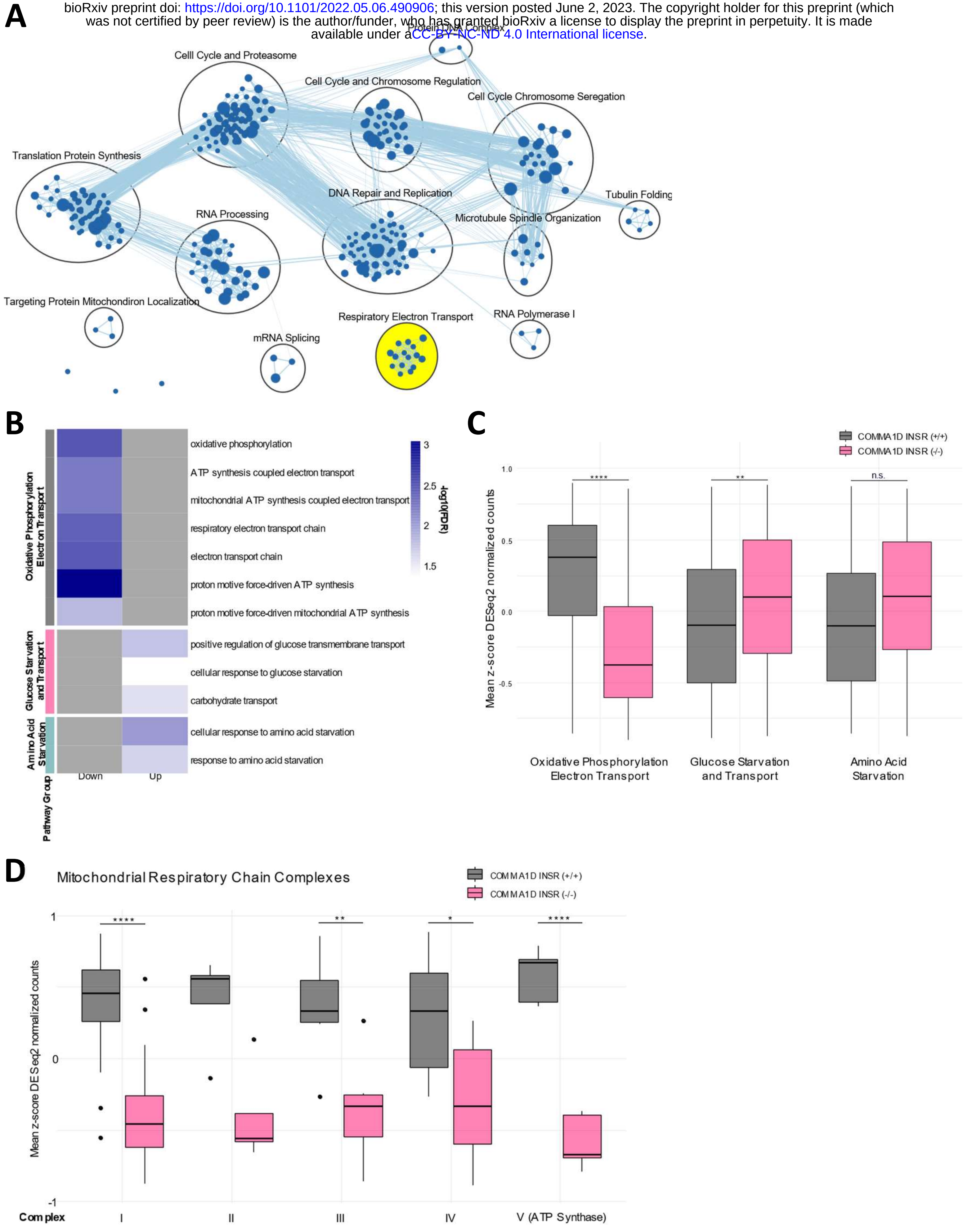

Supplementary Figure 13: ***Loss of INSR in mammary epithelial cells reduces expression of mitochondrial respiratory chain complex components.***

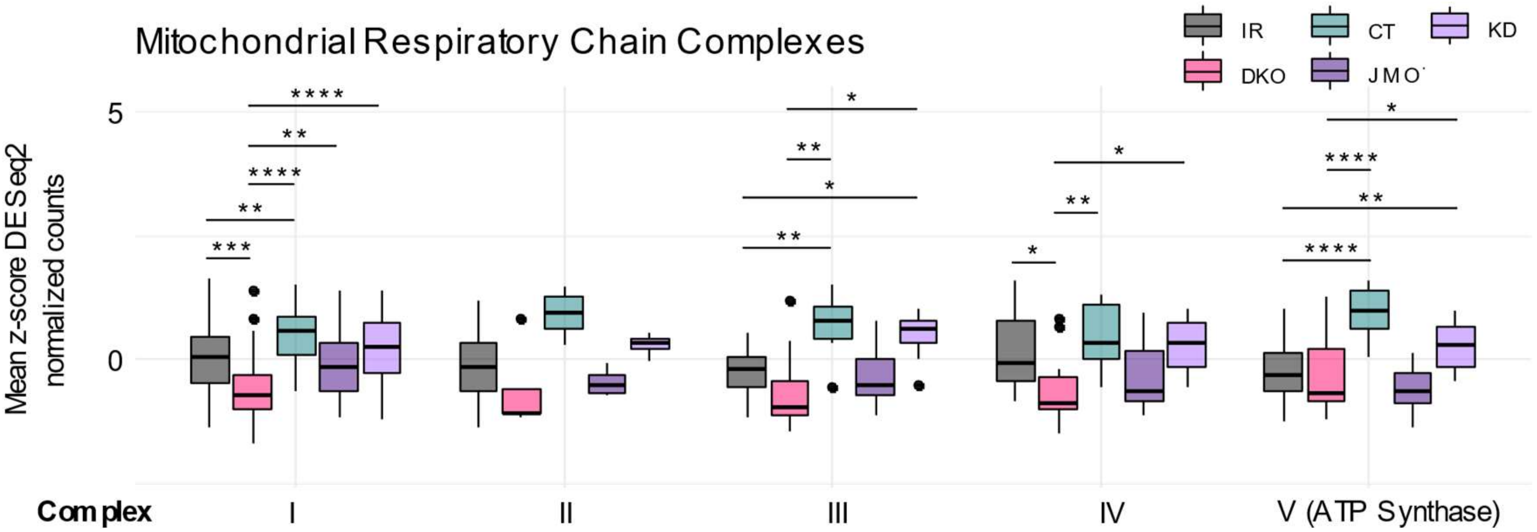

Supplementary Figure 14: ***Impact of INSR and IGF1R loss on mitochondrial respiratory chain subunit expression in mouse preadipocytes is rescued by kinase-dead INSR.***

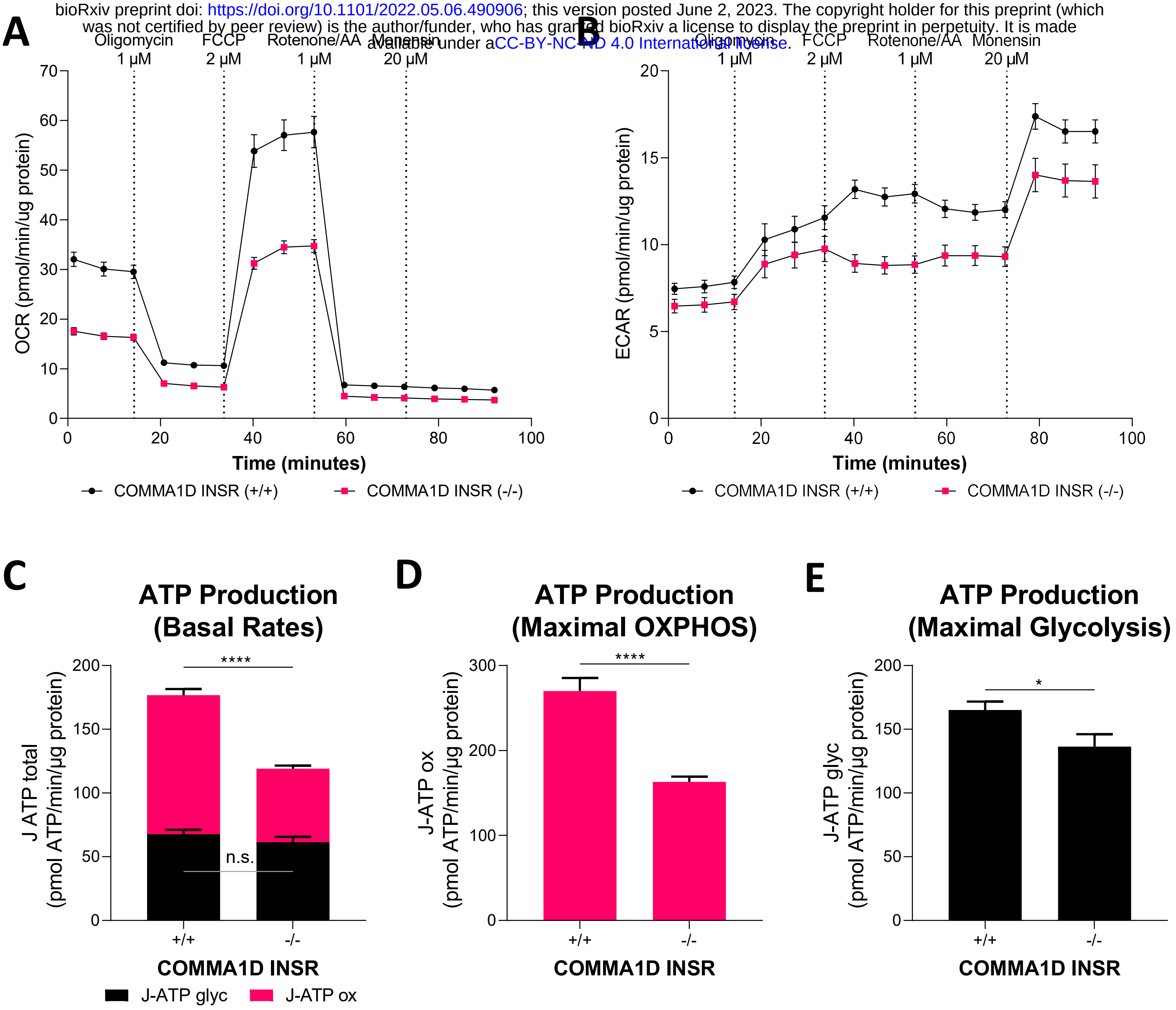

Supplementary Figure 15: ***Impact of INSR loss on bioenergetic fitness in mammary epithelial cells.***

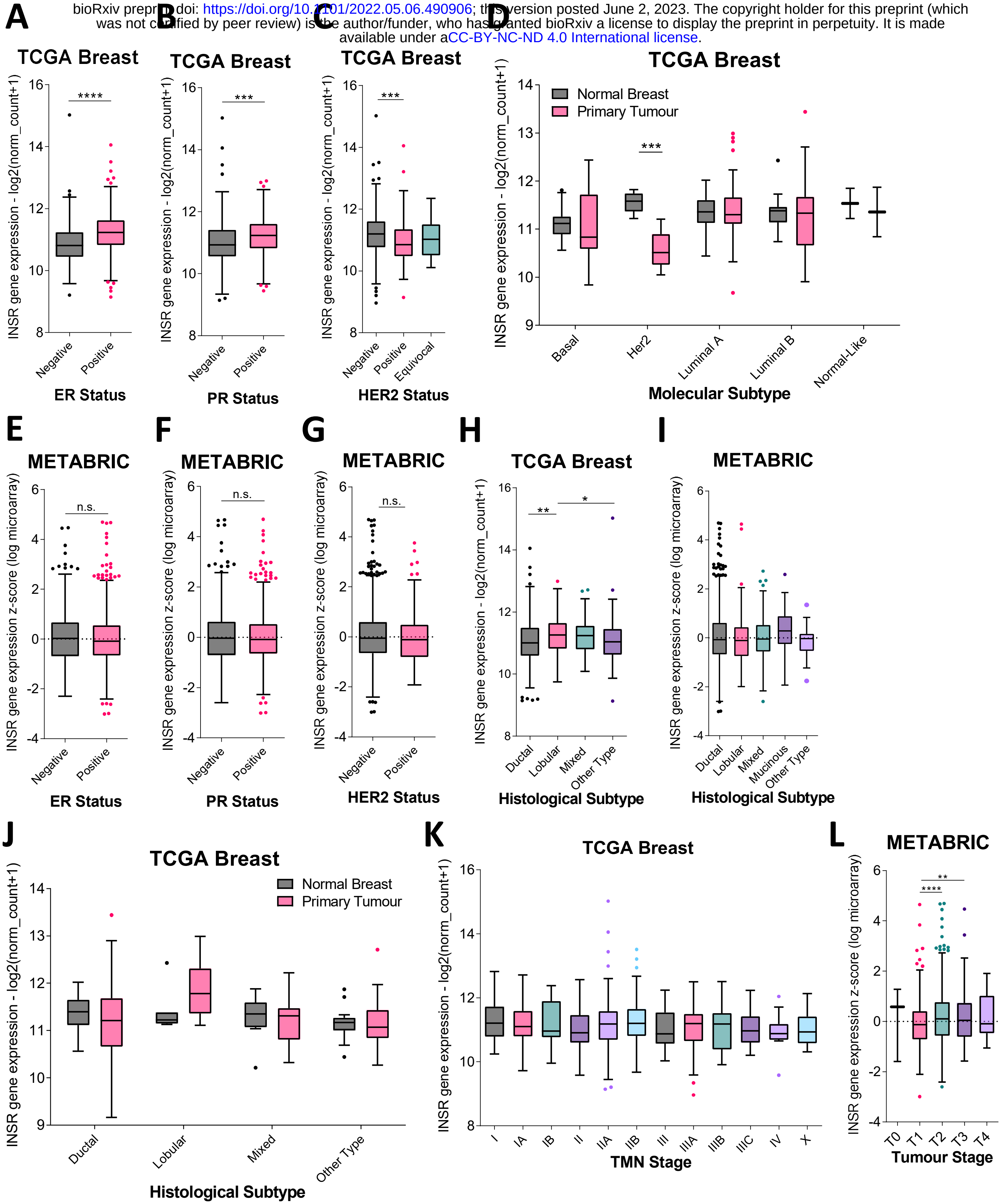

Supplementary Figure 16: ***INSR expression across breast cancer stage and subtypes.***